TABLE OF CONTENTS

NASA Contractor Report 3096

Vertical Motions in the Equatorial Middle Atmosphere

M. L. Weisman

CONTRACT NAS6-2726
APRIL 1979

NASA

NASA Contractor Report 3096

Vertical Motions in the Equatorial Middle Atmosphere

M. L. Weisman
The Pennsylvania State University
University Park, Pennsylvania

Prepared for
Wallops Flight Center
under Contract NAS6-2726

National Aeronautics
and Space Administration

Scientific and Technical
Information Office

1979

TABLE OF CONTENTS

LIST OF FIGURES

LIST OF FIGURES (Continued)

LIST OF TABLES

LIST OF SYMBOLS

A	amplitude of wave motion
C_p	specific heat at constant pressure
C_v	specific heat at constant volume
f	coriolis parameter = $2\ \Omega \sin \phi$
g	acceleration of gravity = 9.8 m/sec^2
h	height of constant pressure surface
$\hat{k}$	unit vector normal to earth's surface
k	wave number = $\frac{2\pi}{L}$
k_1	horizontal wave number
k_3	vertical wave number
L	wavelength or length scale, period
L_1	horizontal wavelength or length scale
L_3	vertical wavelength or length scale
$\hat{n}$	unit vector normal to flow
p	pressure
q	diabatic heating rate
R	gas constant for dry air = 2.87×10^6 erg g^{-1} k^{-1}
S	entropy
T	temperature: °K
t	time
$\hat{t}$	unit vector transverse to flow
u	magnitude of wind velocity in x direction
v	magnitude of wind velocity in y direction
$\underset{\sim}{V}$	velocity vector
$\underset{\sim H}{V}$	horizontal velocity vector

V_H	magnitude of horizontal velocity vector
w	magnitude of vertical velocity vector
w_p	$\equiv \frac{dp}{dt}$
x	position coordinate in east-west direction
y	position coordinate in north-south direction
z	position coordinate normal to earth's surface
α	specific volume $\equiv \frac{1}{\rho}$
γ	lapse rate $\equiv -\frac{\partial T}{\partial z}$
γ_{Ad}	adiabatic lapse rate $\equiv \frac{g}{C_p}$
$\Delta( )$	finite differencing interval; scaling amplitude for derivatives
$\delta( )$	magnitude of error estimate
∇_H	gradient, divergence operator on constant height surface
∇_p	gradient, divergence operator on constant pressure surface
π	= 3.14159...
ρ	density
τ	wave period or time scale
ϕ	latitude
Ω	angular velocity of earth's rotation = 7.292×10^{-5}/sec
ω	frequency = $\frac{2\pi}{\tau}$
ω_g	Brunt Väisalä frequency
ξ_p	relative vorticity in isobaric coordinates
$J( )$	Jacobian Operator
$(\dot{})$	$\equiv \frac{d}{dt}( )$

ACKNOWLEDGMENTS

The author would like to extend his sincere appreciation to Dr. John J. Olivero for the inspiration, guidance, and constructive criticism that he was always willing to provide. Thanks are also due to Dr. John H. E. Clark and Dr. John D. Lee for the many helpful discussions throughout the progress of this work. Additional thanks are due to Dr. John H. E. Clark for reviewing this manuscript.

Financial support and rocket data has been provided by NASA - Wallops Flight Center, Virginia under NASA Contract NAS6-2726.

1.0 INTRODUCTION

Throughout the history of meteorology, the atmosphere has been subdivided into various regions depending on the thought and observations of the times. These subdivisions have been based both on actual scientific properties (as in the troposphere, stratosphere, and mesosphere classifications) or merely on the proximity to man's influence or direct experience (such as the lower atmosphere, including the troposphere, and the upper atmosphere, including everything above the troposphere). The present is no exception for in the wake of new public and scientific concern over man's possible impact on the upper atmosphere, a new subdivision, the "middle atmosphere", has come into existence. This region includes the stratosphere and mesosphere (15-85 km in altitude) and is where ozone forms an important link between solar radiation and atmospheric dynamics. At the same time, it is a region relatively void of observations either of the ground based or satellite type, making all forms of analysis quite difficult.

The current study is concerned with an important but often times neglected part of the dynamics in the middle atmosphere, namely, vertical motions. Observational studies of vertical motions in this region are virtually non-existent yet observational studies of other parameters show many discrepencies with theory which point increasingly towards vertical motions as the chief culprit. Unfortunately, vertical motions cannot be measured directly and while they can be derived indirectly from other observed quantities, such techniques are subject to many restrictions which are especially evident in the

middle atmosphere. The goal of the present study is to devise a vertical velocity calculation and analysis scheme consistent with the middle atmospheric restrictions and apply this technique to an actual data set. The data to be used for this purpose was obtained from the Diurnal Experiment of March 19, 20, 1974 and covers equatorial regions. Before getting into the particulars of this experiment, however, it will be useful to review the concept of vertical motions in general and their relationship to current research efforts in the middle atmosphere.

1.1 IMPORTANCE OF VERTICAL MOTIONS

When one is first introduced to vertical motions in the atmosphere, it is usually in reference to tropospheric weather. Here, it is found that upward motion produces clouds and precipitation while downward motion produces clearer, drier weather. Researchers think of this in terms of vertical transports of moisture, heat, and momentum or as conversion processes in energetic studies, but however it is viewed, knowledge of the vertical component of the wind is essential to the understanding of tropospheric circulation. For this reason, tropospheric vertical motions have been the subject of many research efforts.

This important role of vertical motions does not stop at the tropopause, but until recently, studies of the vertical component of the wind above this level have been virtually nonexistent. To a large degree, this can be attributed to the lack of observational data from which such studies could be made, but to some degree, this

must also be attributed to the lack of understanding and concern of processes occurring above the tropopause. As an example, one informally accepted axiom of the recent past stated that the stratosphere was too stable to support significant vertical velocities and anything which occurred above the stratosphere was unimportant anyways.

Over the past decade, however, scientific interest in the middle atmosphere has increased dramatically, this in the wake of greatly improved observational networks as well as new understanding into the possible interactions between this region of the atmosphere and the more familiar troposphere. Indeed, one finds many of the same large and small scale features previously studied in the troposphere and along with these features come the same important questions concerning the vertical motions. In addition, many other interesting processes and phenomena are being isolated and studied which either are not found in the troposphere or only become significant above the troposphere. Some of these include sudden stratospheric warmings, quasibiennial oscillations, atmospheric tides and other forms of internal gravity waves, ozone and other minor constituent transport, and radiative transfer. While vertical motions are important in all of the above processes, particular attention will now be drawn towards the transport and radiative transfer problems.

Much of the new found interest in the middle atmosphere has been related in one form or another to the well publicized ozone problem. While only a minor atmospheric constituent, ozone essentially controls the dynamics of much of the stratosphere and mesosphere. Its absorption of ultraviolet radiation supplies much of the forcing for the atmospheric tides and at the same time shields the surface from

these potentially damaging rays. Recent concern has been that man is in the process of or, in fact, already has adversely affected the fragile balance which exists between ozone and the various other atmospheric constituents. Unfortunately, due to the lack of comprehensive observations covering many years, significant conclusions cannot yet be drawn as to the existence of such effects.

One of the major stumbling blocks to the type of scientific research which could solve this problem has been the lack of knowledge concerning the transport properties affecting the various trace constituents which make up the middle atmosphere. Although man's direct impact on the atmosphere occurs mainly in the troposphere, much of the attention has been on how the various chemical species are transported up to or down from the middle atmosphere. Without knowledge of the vertical motion field, the vertical transport must be approximated using parameterization schemes and so far, this approach has produced unsatisfactory and inconsistent results. Being able to characterize the vertical motion field in the middle atmosphere would be a vital step towards improving the above schemes and eventually solving the vertical transport problem.

Another aspect of middle atmospheric research which has received much attention recently has been the attempt to understand the inherent temperature structure of this region and its variations in space and time. To date, many results have been obtained by assuming that the observed temperature structure was a direct consequence of radiative transfer processes or even a state of radiative equilibrium. Under such an assumption, the observed temperatures could be used to calculate diabatic heating and cooling rates which would account for

the observed temperatures. This, in turn, would help determine the quantities of the various constituents taking part in the radiative process. The major drawback is that such an approach ignores horizontal advection of temperature or the adiabatic heating or cooling which accompanies vertical motions. Indeed, it has been noted over the past decade or so that vertical profiles and time cross sections of temperature for the middle atmosphere are full of "wiggles" which cannot be explained via radiative transfer or horizontal advection arguments. Another possibility is that the observed temperature structure is being significantly affected by vertical motions. Thus, knowledge of the vertical motion field would also be an important step towards understanding the radiative processes of the middle atmosphere.

Unfortunately, the determination of vertical motions is at best a difficult task. The problem is that their magnitude, usually only a few cm/sec, is too small to be measured directly. They must therefore be determined indirectly via the equations of motion. Several techniques are available for this purpose, but the limited data availability in the middle atmosphere puts restrictions even on the use of these methods. The role of vertical motions in the equations of motion, vertical velocity equations, and these restrictions will all be discussed in the next section.

1.2 VERTICAL VELOCITIES AND THE EQUATIONS OF MOTION

The most logical starting point for a discussion of vertical motions in the atmosphere is the complete set of meteorological equations given below (following Dutton, 1976).

$$\frac{\partial \underset{\sim}{V}_H}{\partial t} + \underset{\sim}{V} \cdot \nabla \underset{\sim}{V}_H = - \frac{1}{\rho} \nabla_H p + 2\underset{\sim}{\Omega} \times \underset{\sim}{V}_H \tag{1.1}$$

$$\frac{dw}{dt} = - \frac{1}{\rho} \frac{\partial p}{\partial z} - g \tag{1.2}$$

$$C_p \frac{dT}{dt} - \alpha \frac{dp}{dt} = q \tag{1.3}$$

$$\frac{\partial p}{\partial t} + \rho \nabla \cdot \underset{\sim}{V} = 0 \tag{1.4}$$

$$p = \rho RT \quad . \tag{1.5}$$

These represent the horizontal equation of motion, vertical equation of motion, first law of thermodynamics, equation of continuity, and the equation of state respectively. For most research applications, however, one finds that the acceleration term in equation (1.2) is much smaller than the remaining terms. Thus, equation (1.2) is usually replaced by the hydrostatic approximation:

$$\frac{\partial p}{\partial z} = - \rho g \quad . \tag{1.6}$$

This has the effect of eliminating a prognostic statement for w from the above system of equations. The vertical velocity must therefore be determined diagnostically through the remaining equations. Several standard techniques have been developed for this purpose, each one stressing different aspects of the link between vertical motions and the general circulation. These are briefly described below.

The link between the vertical motion field and the horizontal components of the wind can be expressed via the equation of mass continuity, equation (1.4). For this purpose, it is more convenient to use the isobaric form as in Dutton (1976).

$$\nabla_p \cdot \underset{\sim}{V} + \frac{\partial w_p}{\partial p} = 0 \tag{1.7}$$

where $w_p \cong \frac{dp}{dt}$ is related to w as follows:

$$w_p \simeq - \rho g w \quad . \tag{1.8}$$

Upon solving equation (1.7) for w_p, one obtains:

$$w_p = w_{p_o} + \int_{p}^{p_o} \nabla_p \cdot \underset{\sim}{V} \, dp \tag{1.9}$$

where w_{p_o} represents the surface value, usually taken to be 0. The above relation suggests that net horizontal divergence in a column will lead to negative vertical velocities at the top of the column while net horizontal convergence will lead to positive vertical velocities. Equation (1.9) is commonly referred to as the kinematic vertical velocity equation and produces vertical motions which will ensure that mass is being conserved in the atmosphere.

A second diagnostic equation can be derived from the first law of thermodynamics, equation 1.3. Upon expanding the time derivatives and making a few more approximations appropriate to atmospheric conditions, one obtains the following expression (see Chapter 2):

$$w = \frac{\frac{\partial T}{\partial t} + \underset{\sim}{V} \cdot \nabla_H T - \frac{q}{C_p}}{(\gamma - \gamma_{Ad})} \quad . \tag{1.10}$$

The equation demonstrates how the vertical motion field is linked to the temperature and heating fields. Since the stability term, $(\gamma - \gamma_{Ad})$, is usually negative under normal atmospheric conditions, one can see that local cooling, warm advection, and a positive diabatic heating rate all contribute positively to the vertical velocity as estimated by the above expression. Likewise, local heating, cold advection, and diabatic cooling contribute negatively in the above expression. If one neglects the diabatic heating term, then the above expression becomes the standard adiabatic vertical velocity equation.

Thus, vertical motions in the atmosphere are restricted by both the conditions of mass continuity and energy conservation. Both of these conditions along with the hydrostatic approximation can be included in one equation first derived by L. F. Richardson (Dutton, 1976):

$$w = \int_o^z \left[-\nabla_H \cdot \underset{\sim}{V} + \frac{C_v}{C_p} \frac{1}{p} \left(\left(\int_{z'}^{\infty} g\nabla \cdot \rho \underset{\sim}{V} \, dz'' \right. \right. \right.$$

$$\left. \left. \left. - \underset{\sim H}{V} \cdot \nabla p + \frac{p}{C_v} \frac{ds}{dt} \right) \right) \right] dz' \tag{1.11}$$

One will note, however, that this expression would be much more difficult to evaluate numerically then the two previous techniques.

Another expression for w can be derived using the isobaric vorticity equation along with the equation of continuity (Dutton, 1976).

$$w_p = (\xi_p + f) \left[\frac{w_{p_o}}{(\xi_p + f)_{p_o}} + \int_{p_o}^{p} \frac{1}{(\xi_p + f)^2} \left(\frac{\partial}{\partial t} + \underset{\sim}{V} \cdot \nabla p' \right) (\xi_{p'} + f)\, dp' \right] \quad (1.12)$$

Even though many terms had to be neglected to obtain the above form, it does portray one of the more useful properties of atmospheric motion, namely, that fields of vorticity can be directly related to fields of vertical motion. For forecasters, the above relation translates into the well known saying that an increase in vorticity advection with height leads to positive vertical velocities and vice versa. One could likewise make the statement that vertical motions tend to develop rotation in an otherwise smooth flow leading to the cyclones and anticyclones, troughs and ridges found on all synoptic maps.

Finally, using the complete set of meteorological equations along with the geostrophic approximation, one can derive the well known Omega Equation (Dutton, 1976).

$$\nabla_p^2 (w_p \sigma) + \frac{\partial^2 w_p}{\partial p^2} (\nabla_p^2 h + \frac{f^2}{g}) - w_p \nabla_p^2 \frac{\partial^2 h}{\partial p^2}$$

$$- \frac{\partial}{\partial p} (\nabla_p w_p \cdot \nabla_p \frac{\partial h}{\partial p}) = \frac{-g}{f} \nabla_p^2 J(h, \frac{\partial h}{\partial p})$$

$$+ \frac{\partial}{\partial p} J(h, \frac{g}{f} \nabla_p^2 h + f) - \frac{R}{g C_p p} \nabla_p 2 (\sigma, f_h) \quad . \qquad (1.13)$$

In principle, one could solve this expression for the vertical motion field, but this would imply using many approximate numerical schemes which could potentially induce much error into the results. For this reason, the omega equation is not commonly used in observational studies of vertical motions but rather is used along with the tendency equation for numerical weather prediction studies.

The critical factor in determining which if any of equations (1.9) through (1.13) can be used to study vertical motions for a particular case is obviously the data availability. In tropospheric studies, data is abundant enough to specify horizontal grids of data points, appropriate boundary conditions, and even local time derivatives so that any of the above techniques can be used. In high latitude regions of the lower stratosphere, this is still somewhat the case but for the mid-stratosphere and higher, one usually has only a handful of stations per hemisphere taking the required observations. This makes the formation of a horizontal grid of data points a difficult if not impossible task. For middle and high latitude regions this problem is alleviated somewhat by the 5, 2, 1, and 0.4 mb synoptic charts prepared weekly by the Upper Air Branch of the National Weather Service, but such information is not regularly available for

time periods less than a week and even if available, gives virtually no information concerning features in low latitude or equatorial regions. With the utility of the above techniques depending on the availability of horizontal grids of data, it initially appears unfeasible to calculate vertical velocities for short time scales and/or low latitudes in the middle atmosphere.

There is a way around this restriction, however, for through the use of the geostrophic approximation, one can derive a thermal wind relation which relates the horizontal advection of temperature to the vertical shear of the geostrophic wind. This relation can be used in equation (1.10) to create a single station technique for calculating vertical velocities.

$$w = \frac{\frac{\partial T}{\partial t} + \frac{fT}{g} \underset{\sim}{V} \times \frac{\partial \underset{\sim}{V}}{\partial z} - \frac{q}{C_p}}{(\gamma - \gamma_{Ad})} \quad . \tag{1.14}$$

Assuming one has a series of observations so that the local change of temperature term could be evaluated, equation (1.14) can be used with a single station supplied data set. Considering the potential data sparsity in the middle atmosphere, the above equation becomes a prime candidate for use in studying vertical motions in this region.

One important question which must be considered in using any of the above techniques is how one goes about verifying the results. The most obvious approach would be to compare the calculations to actually measured vertical velocities, but as has been previously suggested, vertical motions cannot be measured directly. One can get around this difficulty in the troposphere as vertical motions can be

correlated quite well with cloud and precipitation patterns. Through such studies, it has been determined that all of the above techniques can estimate the sign and order of magnitude of the vertical motions quite well. Unfortunately, no such correlation procedure exists for middle atmospheric regions. Thus when working in the middle atmosphere, one must either rely on the results obtained in the troposphere and assume the same for higher altitudes or one must rely on more indirect verification procedures. Such procedures will be discussed in Chapter 3.

By reviewing the equations of motion, we have seen how vertical motions link the many atmospheric variables together and have seen that several techniques are available for the actual calculation and study of vertical motions. In the next section, the focus will shift specifically to the middle atmosphere, considering in more detail the data limitations of this region as well as the results of vertical motion studies in this region to date.

1.3 VERTICAL MOTION STUDIES IN THE MIDDLE ATMOSPHERE

Over the years, observational studies of the stratosphere and mesosphere have been limited greatly by both the difficulty and expense of obtaining data from these regions. The relatively inexpensive balloon techniques used in the troposphere will supply data only as high as 25 or 30 km. To obtain observations higher than this, one must employ meteorological rockets. The Meteorological Rocket Network (MRN) encompasses only a handful of stations over the entire northern hemisphere, many of which are in middle and high latitude

regions. Except for special experiments, observations of wind and temperature are usually taken no more frequently than once a week, and sometimes even less. Once the observations have been taken, they must be subjected to correction and reduction procedures before the data can be used. Many times, these procedures differ from station to station producing very incoherent data sets.

In recent years, the data base has been enhanced somewhat by satellite derived thickness fields. With the help of this additional information, weekly northern hemispheric synoptic analysis are now produced for the 5, 2, 1, and 0.4 mb pressure levels by the Upper Air Branch of the National Weather Service. These maps depict features up to about wave number 10 for high latitude regions but still give virtually no information concerning features in the equatorial regions. Because of these restrictions, observational studies in the middle atmosphere have generally been limited to the middle and high latitudes and to large time and space scales. Thus, the majority of the research has been on middle and high latitude planetary waves.

One particular feature which has gained much attention recently has been the sudden stratospheric warmings which characterize many high latitude winters. These, along with the regular planetary waves, were the subject of several vertical motion studies during the mid 60's and early 70's. Because of the data limitations, all of these studies made use of the thermodynamic vertical velocity equation, either in the form of equation (1.10) or equation (1.14).

Kays and Craig (1965) used equation (1.14) to estimate the vertical motion field between 26 and 42 km for many of the middle and high latitude stations of the MRN. As far as is known, this was the

first attempt at applying the thermodynamic method above the 10 mb level (roughly, 31 km). Their results suggested large scale vertical motions ranging from a few mm/sec during the summer to a few cm/sec during the winter. Both the sign and magnitude of these results were found to rely on the horizontal advection of temperature term.

Equation (1.14) was used in another study by Quiroz (1969), this time to study the vertical motion field associated with a major stratospheric warming event. These calculations ranged between 20 and 44 km in height and again were limited to middle and high latitude regions. The magnitudes suggested, however, were much larger than the previous study, ranging up to 60 cm/sec.

Miller (1970) calculated vertical velocities using equation (1.10) directly. In order to form the necessary horizontal grid of data points, he made use of the stratospheric height fields described above. The calculations ran in latitude from 25°N to 65°N in the western hemisphere and suggested vertical motions on the order of 3-9 cm/sec. As with Kays and Craig, Miller found that the sign and order of magnitude of the derived vertical motions was essentially determined by the horizontal advection of temperature term.

The important observation which was drawn from these studies, however, was that the results were consistent with our knowledge of large scale synoptics and dynamics in this region. This implied that the thermodynamic technique could be used in middle and high latitudes to determine at least the sign and order of magnitude of large scale vertical motions for the middle atmosphere. This result can now be used as a stepping stone from which to attack the problem of concern

in this thesis, namely, the study of vertical motions in the equatorial middle atmosphere.

Observational studies in the equatorial middle atmosphere have been even more limited than for the higher latitudes. Due to the scarcity of data sets from which proper analysis could be made, theoretical results seem to be more abundant than observational results. Much attention has been devoted to studying large time and space scale features such as Kelvin waves, Rossby-gravity waves, and the quasibiennial oscillation. Theoretical results, however, suggest that small time scale features become quite significant in this region, taking the form of tidal motions and internal gravity waves. Several special data sets have been obtained for the purpose of studying these features, especially the tidal motions, but to date, no results have been presented for vertical motions. One reason for this has been the lack of sufficient data from which such calculations could be made, but perhaps just as importantly, working in the vicinity of the equator puts an additional restriction on the use of equation (1.14). With the loss of geostrophy near the equator, one apparently loses the single station technique for calculating the vertical motions.

A special Diurnal Experiment has solved at least the data aspects of the above problem. This data set and the additional restriction of the use of equation (1.14) will be the topic of discussion in the next section.

1.4 THE DIURNAL EXPERIMENT AND EQUATORIAL VERTICAL MOTIONS

In 1974, NASA attempted to obtain a more comprehensive equatorial data set by organizing and running the Diurnal Experiment. This experiment covered the equinoctial period of March 19, 20 and consisted of a series of measurements of both horizontal winds and temperatures taken roughly every three hours for an entire diurnal period. The observations were taken through the use of meteorological sounding rockets and reduced values were obtained at 1 km intervals within the altitude range of 25 to 65 km. In all, eight stations were involved in the experiment, five of which were located in the vicinity of the equator (see figure 1). The stations of interest in this particular study are Kourou (French Guiana), Fort Sherman (Panama Canal Zone), Ascension Island, Antigua (British West Indies), and Natai (Brazil).

Besides being the most extensive data set ever compiled for studying short time scale motions in this region, the Diurnal Experiment was unique in many other ways. Not only did each station use the same measuring device, the Datasonde, but all the data was subjected to the same correction and reduction procedure. This led to an unusually coherent data set for studying the middle atmosphere.

The size of the present data set limits the range of time scales which can be studied from several hours to one day. But fortunately, theory suggests that these are the scales which should dominate the motion in this region, taking the form of tidal and other internal gravity waves. One would thus expect evidence of these waves in the observed temperature and wind fields. To see that this is the case, time series cross sections of zonal and meridional winds and

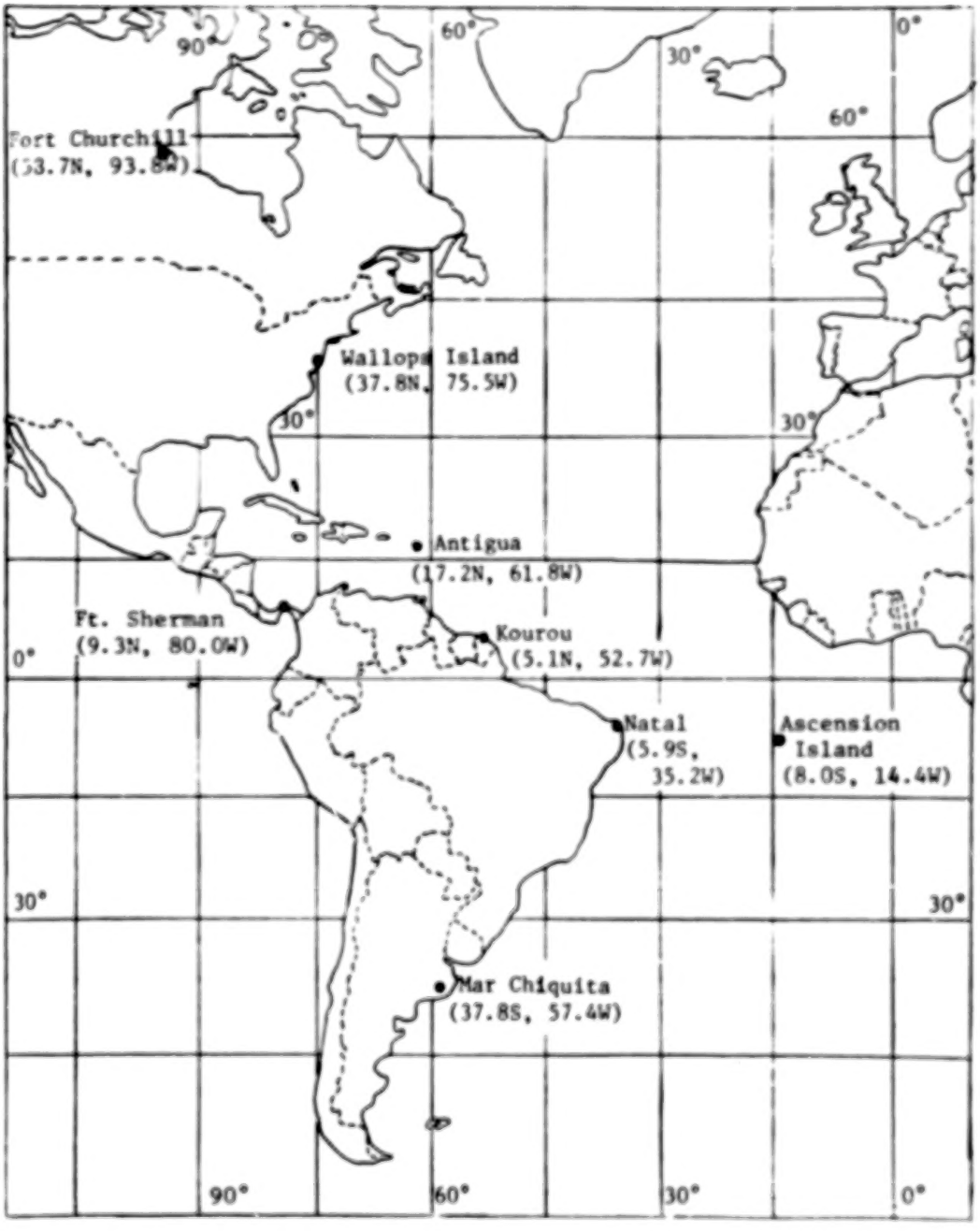

FIGURE 1. Diurnal Experiment Stations, March 19, 20, 1974.

temperature for Kourou are presented in figures 2A, 2B, and 2C. Perturbations about the diurnal mean are used here to properly depict the possible wave type features. Regions of positive perturbations have been shaded in. One will note that continuous features of diurnal period and less are evident in both the wind and temperature cross sections with even a tendency towards a downward phase progression. It also appears as if the amplitudes of the variations increases steadily with height.

All of the above mentioned features are characteristics of tidal type motions and the results for Kourou are quite representative of the other stations as well. Schmidlin (1976) and Kao and Lordi (1977) analyzed the horizontal winds and temperatures for this data set in an attempt to discern the amplitudes and phases of the various tidal components. Their results suggested that tidal motions were indeed the major contributor to the features evident in the above cross sections.

The question which is now posed in this thesis is whether the above data set can be used to calculate and analyse vertical motions in the equatorial middle atmosphere. We have already seen that several techniques are available for this purpose but we have also noted that the data limitations of this region restrict one to using a single station calculation scheme. One such scheme is available as in equation (1.14) but this relies on the use of the geostrophic approximation which does not necessarily hold in equatorial regions. The first task of this study will thus be to derive a single station vertical velocity calculation scheme which can be used with an equatorial data set. Perhaps fortuitously, it will be shown in Chapter 2 that

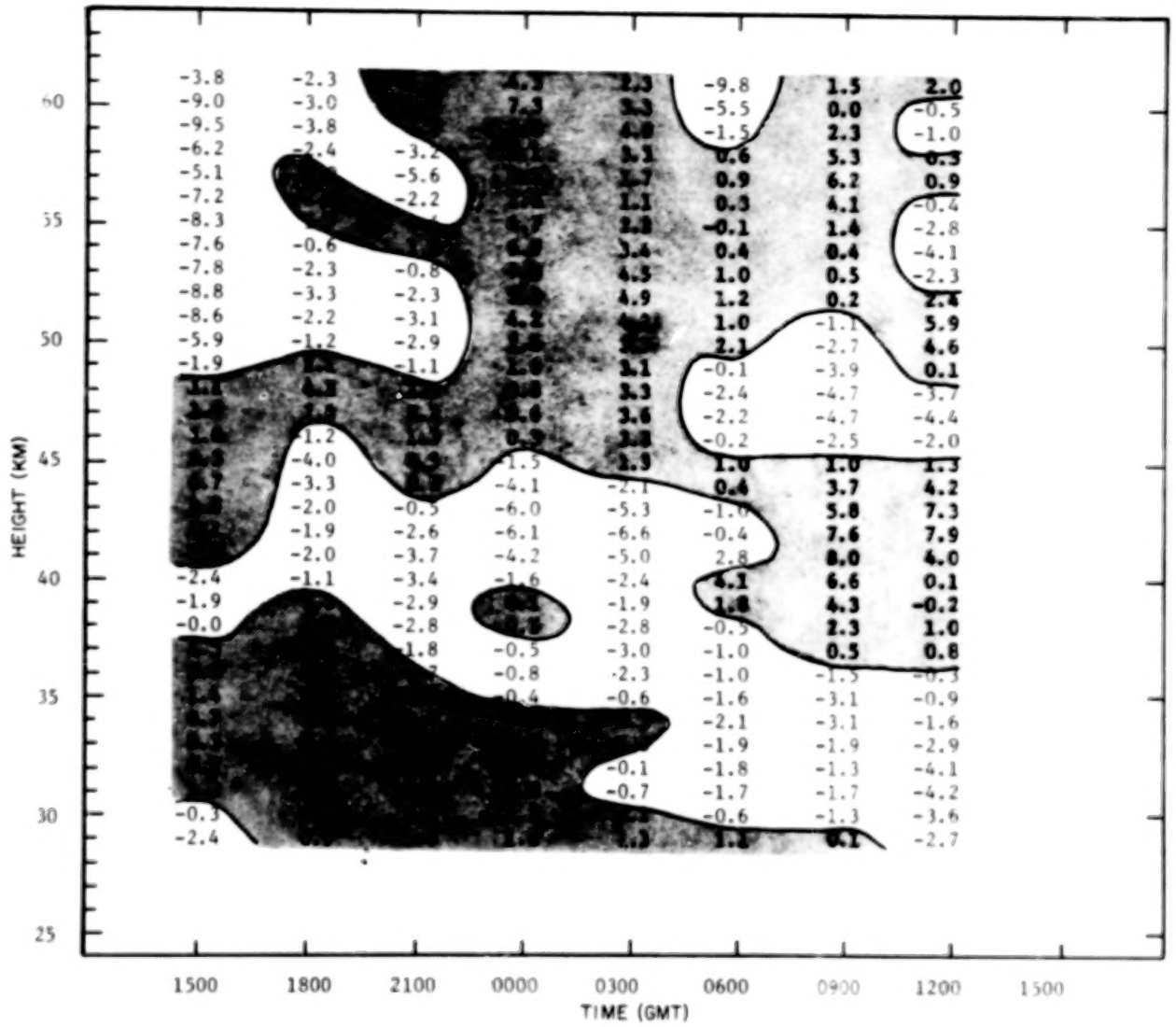

FIGURE 2A. Perturbations in zonal winds at Kourou, March 19-20, 1974.

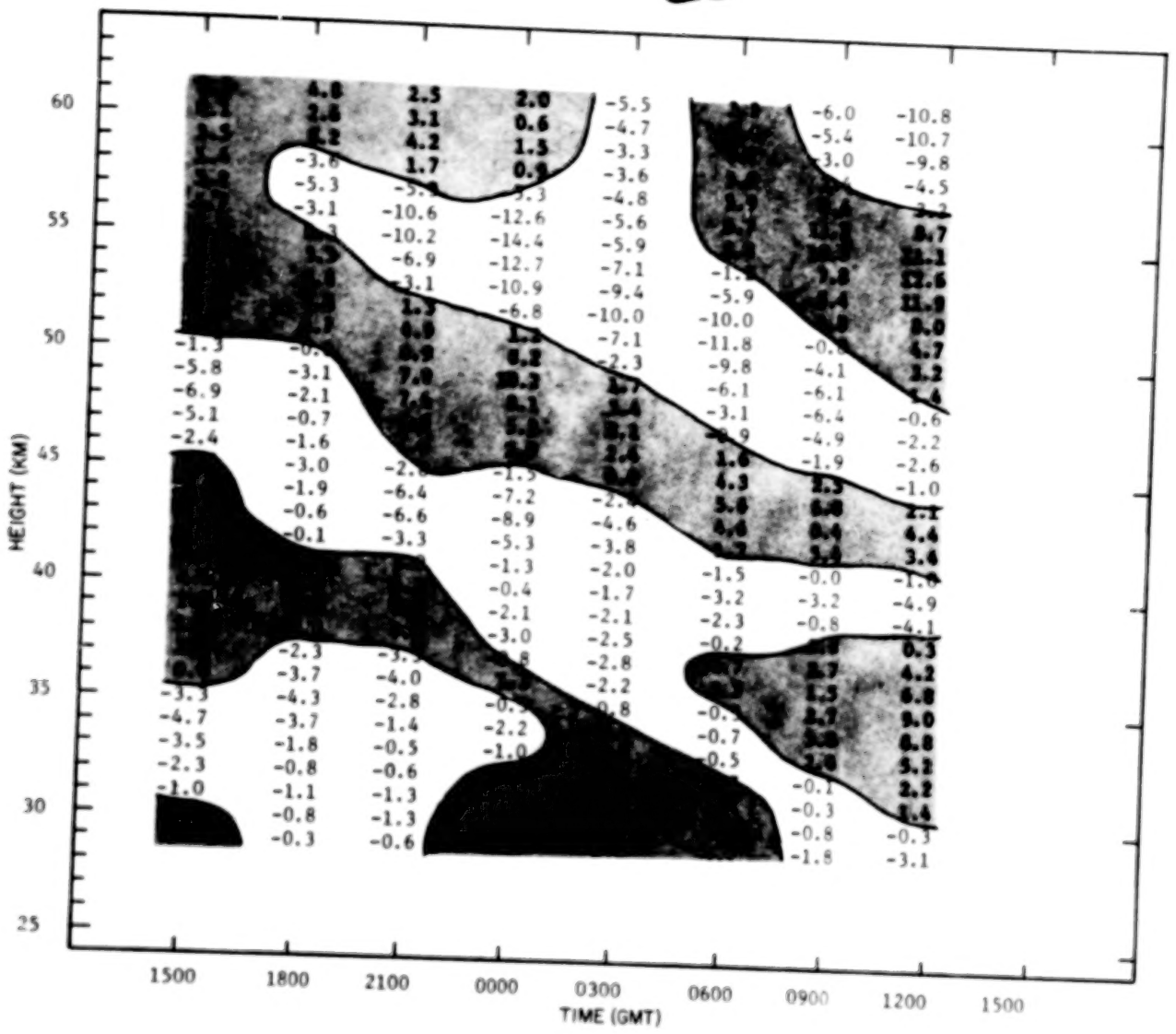

FIGURE 2B. Perturbations in meridional winds at Kourou, March 19-20, 1974.

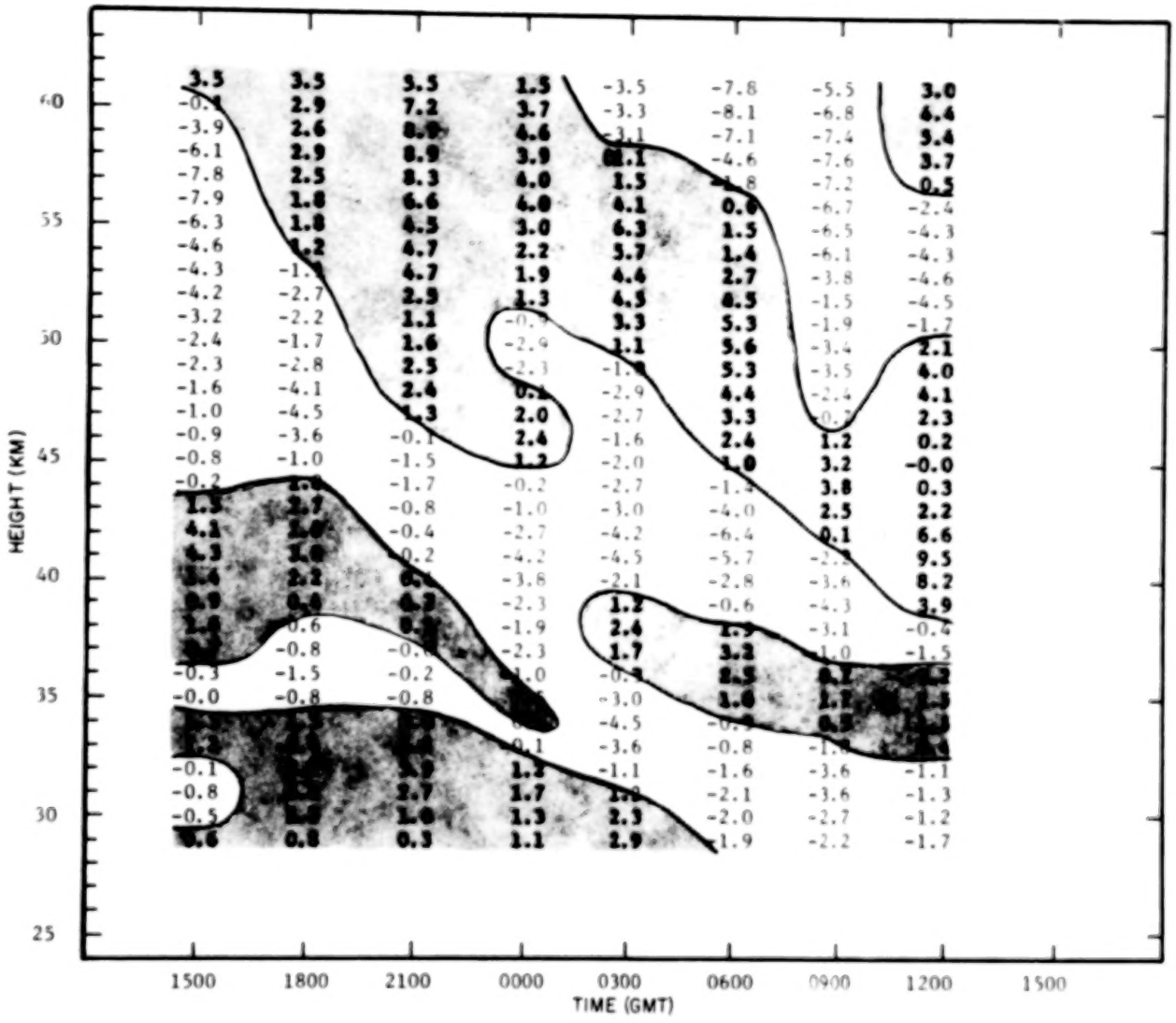

FIGURE 2C. Perturbations in temperatures at Kourou, March 19-20, 1974.

such a scheme can be derived for the scales of motion depicted in the Diurnal Experiment data set.

The second task of the study will be to devise an analysis scheme by which the results can properly be judged. As will be discussed in Chapter 3, this entails considering the potential numerical error and numerical stability of the results as well as comparing the results to the predictions of atmospheric wave theory. In particular, reference will be made to the theoretical calculations for atmospheric tides presented by Lindzen (1967), Chapman and Lindzen (1970), and Lindzen and Hong (1974). The fact that atmospheric tides played a major contributory role in the horizontal winds and temperatures fields suggests that this role should also be evident in the derived vertical motion field.

Finally, the results will be presented and discussed in Chapter 4 and summarized in Chapter 5. Also included in Chapter 5 will be a discussion of implications of the current findings for middle atmospheric research along with suggestions for further research.

2.0 DERIVATION OF THE VERTICAL VELOCITY EQUATION

Several techniques for calculating vertical velocities have been reviewed in the Introduction and it is found that their utility depends highly on the characteristics of the available data. In particular, for the Diurnal Experiment, it is suggested that a single station technique is necessary to derive vertical motions. One such technique has been discussed and consists of the thermodynamic equation along with a geostrophic thermal wind relation. Since the present data set covers equatorial regions, however, the geostrophic thermal wind relation may not hold and one is forced to use a more generalized form. Such a form will be derived in section 2.1. Since the data set covers a relatively short time period and an altitude range where radiative effects are quite important, one must also account for possible contributions to the resultant vertical motions via diabatic heating or cooling. This topic is discussed in section 2.2. Finally, consideration of scaling arguments in section 2.3 suggest that this more general vertical velocity equation can be reduced for the purposes of this study to a single station technique. This technique is then used in the subsequent chapters to analyze the vertical motions for the Diurnal Experiment data set.

2.1 A GENERALIZED THERMODYNAMIC VERTICAL VELOCITY EQUATION

The expression for calculating vertical velocities will be derived using the first law of thermodynamics:

$$C_p \frac{dT}{dt} = \alpha \frac{dp}{dt} + q \quad . \tag{2.1}$$

where the explicit form of the diabatic terms will be discussed later. Upon expanding the total derivatives, one obtains:

$$C_p \left[\frac{\partial T}{\partial t} + \underset{\sim}{V}_H \cdot \nabla_H T + w \frac{\partial T}{\partial z} \right] = \alpha \left[\frac{\partial p}{\partial t} + \underset{\sim}{V}_H \cdot \nabla_H p + w \frac{\partial p}{\partial z} \right] + q \quad . \tag{2.2}$$

The first two terms on the right are generally much smaller than the third term and will be neglected at this point. With one use of the hydrostatic approximation, equation (2.2) can be solved for w, revealing the following:

$$w = \frac{- \frac{\partial T}{\partial t} - \underset{\sim}{V}_H \cdot \nabla_H T + \frac{q}{C_p}}{\frac{\partial T}{\partial z} - \frac{g}{C_p}} \quad . \tag{2.3}$$

Upon defining $\gamma \equiv - \frac{\partial T}{\partial z}$ and $\gamma_{Ad} \equiv \frac{g}{C_p}$, equation (2.3) becomes:

$$w = \frac{\frac{\partial T}{\partial t} + \underset{\sim}{V}_H \cdot \nabla_H T - \frac{q}{C_p}}{(\gamma - \gamma_{Ad})} \quad . \tag{2.4}$$

If one neglects the diabatic terms, equation (2.4) becomes the standard adiabatic vertical velocity equation.

Assuming that the proper data is available, equation (2.4) can now be used to calculate vertical velocities. The observing stations

for the Diurnal Experiment, however, are too sparse to allow a direct calculation of the horizontal advection of temperature term. For middle and high latitudes, this problem is easily solved by applying the geostrophic thermal wind relations, but again, since the current data set covers equatorial regions, geostrophy may not hold and a generalized thermal wind relation must be used. In that this expression is not commonly seen in the literature, its derivation will be outlined below following Forsythe (1945).

First, consider the horizontal equation of motion in the absence of friction:

$$\frac{d\underset{\sim}{V}_H}{dt} = -2\underset{\sim}{\Omega} \times \underset{\sim}{V}_H - \frac{1}{\rho}\nabla_H p \quad . \tag{2.5}$$

Rewritten in terms of natural coordinates, the Coriolis term becomes

$$-2\underset{\sim}{\Omega} \times \underset{\sim}{V}_H \simeq 2\Omega \sin\phi V_H \hat{n} = f\hat{Vn} \tag{2.6}$$

and the acceleration term becomes

$$\frac{d\underset{\sim}{V}_H}{dt} \equiv \dot{\underset{\sim}{V}}_H = \dot{V}_H \hat{t} + \frac{V_H^2}{R}\hat{n} \quad . \tag{2.7}$$

After taking a cross product with the unit vector, $\hat{k}$, equation (2.5) may be rewritten as

$$-\dot{V}_H \hat{n} + (f + \frac{V_H}{R})\underset{\sim}{V}_H = -\frac{1}{\rho}\nabla_H p \times \hat{k} \quad . \tag{2.8}$$

Now, taking the partial derivative with respect to height, one obtains

$$- \left(\frac{\partial \dot{\underset{\sim}{V}}_H}{\partial z}\right)\hat{n} - \dot{V}_H \frac{\partial \hat{n}}{\partial z} + \left(f + \frac{V_H}{R}\right) \frac{\partial \underset{\sim}{V}_H}{\partial z} + \underset{\sim}{V}_H \frac{\partial \left(\frac{V_H}{R}\right)}{\partial z} =$$

$$\frac{\partial}{\partial z} \left(- \frac{1}{\rho} \nabla_H p\right) \times \hat{k} \quad . \tag{2.9}$$

It is shown in Appendix A that for the present data set, the following approximation can be made:

$$\frac{\partial}{\partial z} \left(- \frac{1}{\rho} \nabla_H p\right) \simeq \frac{-g}{T} \nabla_H T \quad . \tag{2.10}$$

Finally, using equation (2.10), another cross product with $\hat{k}$, a dot product with $\underset{\sim}{V}_H$, and some vector identities, equation (2.9) becomes

$$- \underset{\sim}{V}_H \cdot \nabla_H T = \frac{-T}{g} \left(f + \frac{V_H}{R}\right) \left(\underset{\sim}{V}_H \times \frac{\partial \underset{\sim}{V}_H}{\partial z}\right) \cdot \hat{k}$$

$$+ \frac{T}{g} \left(\underset{\sim}{V}_H \times \frac{\partial \dot{\underset{\sim}{V}}_H}{\partial z} \hat{n}\right) \cdot \hat{k} \quad . \tag{2.11}$$

In the stratosphere and mesosphere, the term involving the radius of curvature is usually considered small and will be neglected at this point with little hesitation. The above equation can now be used to replace the advection term in equation (2.4), yielding

$$w = \frac{\frac{\partial T}{\partial t} + \frac{fT}{g} \left(\underset{\sim}{V}_H \times \frac{\partial \underset{\sim}{V}_H}{\partial z}\right) \cdot \hat{k} - \frac{T}{g} \underset{\sim}{V}_H \frac{\partial \dot{\underset{\sim}{V}}_H}{\partial z} - \frac{q}{C_p}}{(\gamma - \gamma_{Ad})} \quad . \tag{2.12}$$

The only term in this equation which cannot be calculated from data collected at a single station is $-\frac{T}{g} V_H \frac{\partial V_H}{\partial z}$ for expansion of the time derivative reveals another advection term:

$$\dot{V}_H \equiv \frac{\partial V_H}{\partial t} + \underset{\sim}{V} \cdot \nabla V_H \tag{2.13}$$

Fortunately, scaling arguments will show this term to be small enough to neglect. Considering this, all the terms in equation (2.12) can be calculated from data available at a single station, assuming that one specifies the appropriate diabatic contributions. The specification of the diabatic term will be the subject of the next section.

2.2 DIABATIC PROCESSES

When formulating a diabatic term for use in middle atmospheric studies, many of the common forms of diabatic heating such as latent heat release, friction, and molecular viscosity can be considered negligible. The heating and cooling rates associated with radiative processes, however, can become significant depending on which time scales are being studied. For very long time scales (> 100 days), the circulation features and temperature structure in middle and low latitudes is almost entirely a function of radiative effects and the atmosphere is said to be in a state of radiative equilibrium. For medium time scales (1 day - several weeks), temperature changes due to radiative processes can be overwhelmed by the changes caused by large scale dynamical features such as planetary waves. For this reason, radiative processes are often neglected in studying systems

of these time scales. For short time scales (< 1 day), however, radiative processes can again become significant. Diabatic heating due to absorption of ultraviolet radiation ranges from relatively large positive values during the daylight hours to zero at night while infrared cooling rates remain fairly constant the entire day. If dynamical effects are small, relatively large heating rates can be realized during the day followed by relatively large cooling rates at night, both interacting significantly with the short term circulations. This, in fact, describes the main driving mechanism for atmospheric thermal tides.

The time scales of interest in this study range from several hours to one day. With evidence suggesting that medium time scale dynamical features have an insignificant effect on the hourly temperature structure at low latitudes, it appears conceivable that diabatic processes could become significant. For this region, however, dynamical heating as a result of tidal motions can also become significant. The magnitudes of the diabatic heating rates and these dynamical heating rates must therefore be compared to properly judge the possible significance of the diabatic term in the present calculations. This will be accomplished in the next section but first, one must assign an appropriate magnitude and form to the diabatic term. For this purpose, one must look to theoretical results.

The theory of diabatic heating and cooling in the upper atmosphere has been fairly well developed for many years. In order to put the theory into practice, however, one must accurately know the horizontal and vertical profiles of the various constituents which contribute to the radiative exchanges. The most important of these

include O_3 and H_2O. Unfortunately, measurements of these constituents are unavailable for the present data set so that one must rely on results obtained from averaged data.

Murgatroyd and Goody (1958) presented such results as obtained from a fairly detailed calculation of the various heating and cooling rates and their latitudinal variation. Some of the more pertinent features of their analysis for equatorial regions is suggested in figures 3A and 3B. First from figure 3A, one will note that the net heating over a period of a day differs from a condition of radiative balance by at most $\pm$ 1°K/day over the latitude range for the present study (30-60 km). This implies that the ultraviolet heating comes close to cancelling the infrared cooling for the diurnal period. Figure 3B represents the contributions to the diabatic term over the diurnal period by absorption of solar radiation and suggests that the maximum heating rate (and subsequently, the maximum cooling rate to ensure radiative balance) occurs at about 50 km, corresponding closely to the stratopause. Since 1958, much work has been done to refine many of the particular features of Murgatroyd and Goody's analysis, but to date, the general features and magnitudes suggested above have still remained intact. These results will thus be used as guidance in choosing an appropriate diabatic term for this study.

The following scheme has been adopted assuming a condition of radiative balance over the diurnal period and a height dependence of the heating - cooling rates as suggested above. The variation of the heating rate over the diurnal period has been approximated by a square wave (see figure 4A) and the variation of heating rate with height has been approximated by a sine wave (see figure 4B). Thus, this

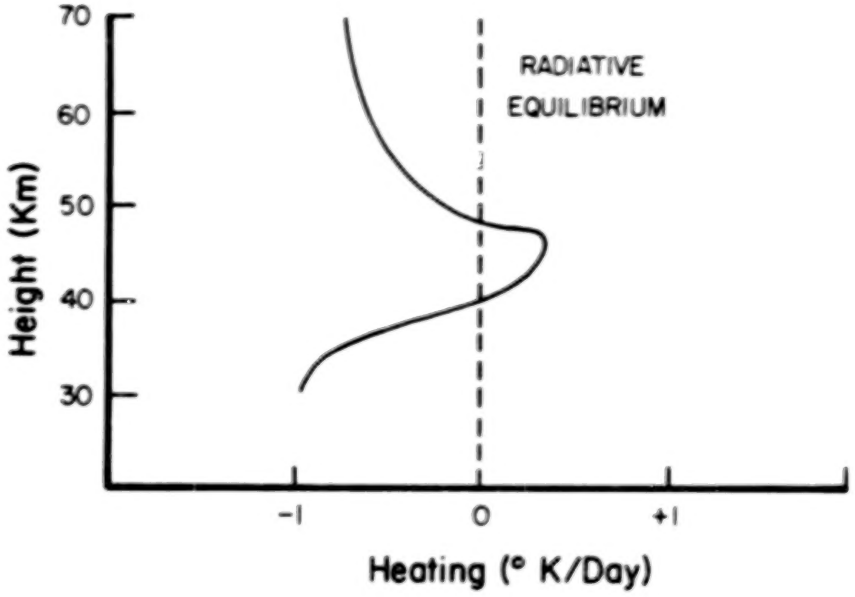

Figure 3A. Net Radiative Heating Over Diurnal Period for Equatorial Regions (Solstice).

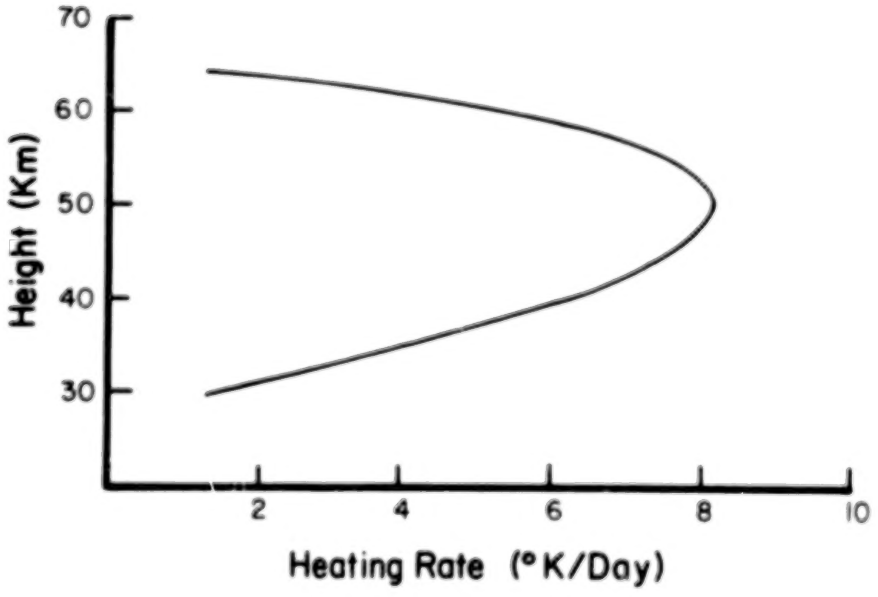

Figure 3B. Temperature Change Caused by Solar Radiation Over a Diurnal Period for Equatorial Regions.

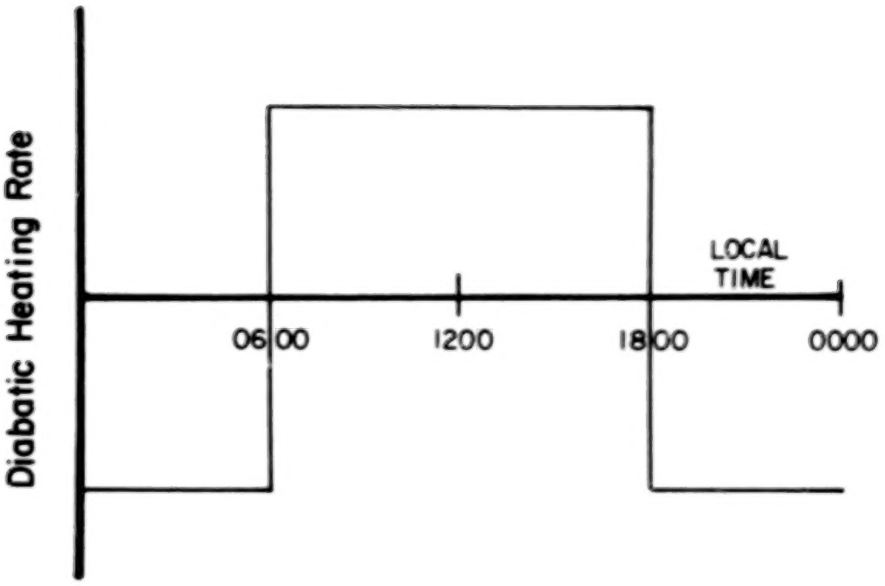

Figure 4A. Time Dependence of Proposed Diabatic Function.

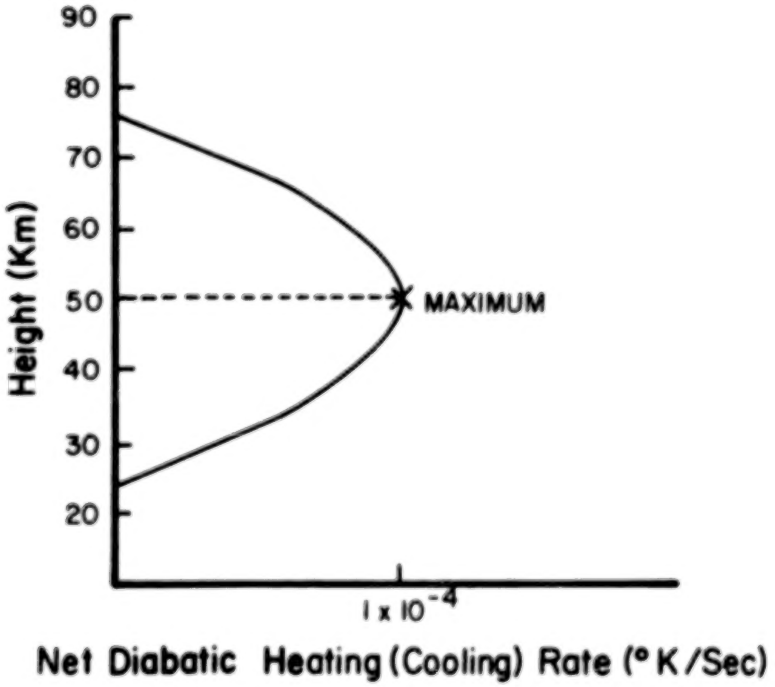

Figure 4B. Height Dependence of Proposed Diabatic Function.

scheme assumes zero net heating over the diurnal period and a maximum instantaneous heating or cooling rate at 50 km. This maximum magnitude has been taken to be 1×10^{-4}°K/sec, which corresponds to 8.6°K/day. This value decays to zero at 25 km and 75 km.

The diabatic term, $\frac{q}{C_p}$, can be expressed analytically as follows:

$$\frac{q}{C_p} = \text{DAMP} \times \sin\left(\frac{2\pi}{100}(z - 25)\right), \tag{2.14A}$$

where

$$\text{DAMP} = \begin{cases} 1 \times 10^{-4}\text{°K/sec} & 0600 < \text{Local time} < 1800 \\ -1 \times 10^{-4}\text{°K/sec} & 1800 < \text{Local time} < 0600 \end{cases} \tag{2.14B}$$

The above form of the diabatic term is considered to be only a first approximation to the results suggested by Murgatroyd and Goody. It is felt, however, that these magnitudes are accurate at least to within $\pm$ 20% and that a more accurate formulation could be obtained only from a direct calculation of the diabatic heating rates.

2.3 SCALE ANALYSIS AND THE FINAL EQUATION

With all the terms in equation (2.12) now assigned, the next step is to compare the magnitudes of the various contributing terms. Through this procedure, one will be able to determine whether any additional terms in the equation can be neglected in subsequent calculations. For the Diurnal Experiment data, it is hoped that the advection of velocity term can be neglected, yielding a single station

technique for calculating the vertical velocities. For this purpose, use will be made of the techniques of scale analysis.

Scale analysis can be approached in many ways. In theoretical studies, the assigned scales are those which correspond to the particular problem being studied. In practical studies, however, the scales which can be used are limited to a great degree by the characteristics of the available data. This is largely the case for the Diurnal Experiment data, with only one exception. The current data set cannot produce an appropriate horizontal length scale, much in the same way that it can't produce horizontal advection terms directly. But, as it turns out, this scale can be assigned by referring to theoretical results.

It will be assumed that the motions which are being studied can be represented as some type of wave form. The potential for this has already been noted in the Introduction. Approximate time and vertical length scales are now easily assigned by considering the time and vertical space coverage of the Diurnal Experiment data.

First, considering a time scale, one will note that the data covers one diurnal period. Thus, one cannot expect to properly observe time scales much greater than a day. Likewise, observations are reported every three hours implying that time scales less than three hours also cannot be properly observed. In fact, one really needs two consecutive observations, corresponding to six hours in this case, to begin to observe possible wave forms. A mean observable time scale for this data will fall somewhere between 6 hours and 24 hours and will be taken at 12 hours, or roughly 4×10^4 sec.

For the vertical length scale, observations cover roughly 30 km of altitude and are reported at every km. Again, assuming a wave nature to the data, one cannot expect to properly observe vertical scales of motion greater than 30 km or less than 2 km. A mean observable vertical scale will be taken to be about 15 km.

As previously suggested, assigning an appropriate horizontal length scale for the present data set is not as straightforward. Normally, one would be tempted to follow the same reasoning used above and consider the total number of reporting stations along with the horizontal distances between them. This would be the proper approach if the data were sufficiently dense, i.e., dense enough to calculate horizontal advection terms, but this possibility has already been discounted. A more viable approach for this case is to assign a horizontal length scale which is consistent through theoretical results with the time and vertical length scales already derived. For example, the above time scale would suggest that Kelvin waves with a period of 12-24 days and Rossby gravity waves with a period of 4-5 days need not be considered. On the other hand, thermally forced solar tides and other forms of internal gravity waves which have time scales of a day or less will be considered.

An appropriate horizontal length scale for internal gravity waves can easily be derived from the well known dispersion relation (Dutton, 1976):

$$\omega^2 = \omega_g^2 \frac{k_1^2}{k_1^2 + k_3^2} \quad , \tag{2.15}$$

where ω represents the frequency of the wave, ω_g represents the Brunt Väisalä frequency, and k_1 and k_3 represent the horizontal and vertical wave numbers respectively. Expressed in terms of horizontal wavelength (L_1), vertical wavelength (L_3), and wave period (τ), this becomes

$$L_1 = L_3\left[\frac{\tau^2 \omega_g^2}{4\pi^2} - 1\right]^{1/2} . \qquad (2.16)$$

By setting $\tau = 4 \times 10^4$ sec, $L_3 = 5$ km, and $\omega_g = 2 \times 10^{-2}$/sec, one obtains an estimate for L_1 of $\sim$ 1800 km.

Now considering thermal tides, the dominant modes include the diurnal and semidiurnal waves, both of which are acceptable within the time scale requirement. One, however, must also take into account the vertical scale requirements. The dominant diurnal component has a theoretical vertical wavelength of about 28 km, which is within the observing range, but the dominant semidiurnal component has a theoretical vertical wavelength on the order of 100 km, which is outside the proposed observing range. Thus, if a significant semidiurnal tidal component exists in the current data, it should appear as a wave with semidiurnal period but little or no vertical structure.

The diurnal and semidiurnal tidal modes have horizontal wavelengths of roughly 40,000 and 20,000 km respectively. Along with the 1800 km wavelength estimate for an internal gravity wave, this represents quite a spread of possible scales from which to choose. Since tides are usually considered to dominate the short time period motions in equatorial regions, the horizontal length scale will be

chosen to be about 10^4 km. The implications of choosing a smaller scale more appropriate to internal gravity waves, however, will still be considered qualitatively in the discussion which follows.

Using standard techniques, equation (2.12) may be rewritten in terms of scaling quantities (see Appendix B):

$$w = \frac{\dfrac{|\Delta T|4}{\tau} + \dfrac{|f||T|V_H|\Delta V_3|4}{|g|\,L_3} + \dfrac{|T|V_H|\Delta V_3|16}{|g|\,\tau\,L_3}}{|\gamma - \gamma_{Ad}|}$$

$$+ \frac{\dfrac{|T|V_H^2|\Delta V_1|16}{g\,L_1L_3} + \left|\dfrac{q}{C_p}\right|}{|\gamma - \gamma_{Ad}|} \qquad (2.17)$$

Appropriate values for τ, L_1, and L_3 were derived above and the magnitude of $\frac{q}{C_p}$ was assigned in the previous section. Magnitudes for the other quantities in the above equation were determined from the Diurnal Experiment data set and represent characteristic values at an altitude of about 45 km. A complete list of the actual values used is given in Table 1. Substituting these values into equation (2.17) and dividing through by $(\gamma - \gamma_{Ad})$, one obtains for the various terms:

$$\begin{matrix} & A & & B & & C & & D & & E & \\ w & \simeq & 10 & + & 10^{-1} & + & 1 & + & 5 \times 10^{-2} & + & 1 \simeq 10 \text{ cm/sec} \end{matrix} \qquad (2.17A)$$

where term A represents the local temperature change, term B represents the geostrophic contribution to the horizontal temperature advection, term C and D represent the ageostrophic contribution to the horizontal temperature advection, and term E represents the

TABLE 1. Scaling Magnitudes at 45 km for the Diurnal Experiment.

Variable	Scaling Magnitude
τ	4×10^{4} sec
L_1	10^{4} km
L_3	15 km
$\left\|\frac{(q)}{C_p}\right\|$	1×10^{-4} °K/sec
$\|f\|$	10^{-5}/sec
$\|g\|$	10^{-2} km/sec
$\|T\|$	2.5×10^{2} °K
V_H	3×10^{-2} km/sec
$\|\Delta T\|$	10°K
$\|\Delta V_3\|$	5×10^{-3} km/sec
$\|\Delta V_1\|$	3×10^{-3} km/sec
$\|\gamma - \gamma_{Ad}\|$	10°K/km

diabatic contributions. From this analysis, one would expect to calculate vertical velocities on the order of 10 cm/sec at 45 km assuming that all the terms contributed positively. The major contributions would come from term A and the least from term D. One will recall that term D is the only term which could not be calculated from a single station supplied data set. Here, one notes that this term is scaled about 2 orders of magnitude smaller than the other major contributing terms, and thus it would appear quite safe to neglect it entirely. Now, if a shorter horizontal wavelength had been used instead, say 10^3km, corresponding more closely to the scale suggested for internal gravity waves, then term D would increase in magnitude by a factor of ten. It would still, however, be an order of magnitude smaller than the major contributing terms and could still be neglected with little hesitation.

Equation (2.12) can now be written in the final form used in this study:

$$w = \frac{\frac{\partial T}{\partial t} + \frac{fT}{g}\left(\underset{\sim}{V}_H \times \frac{\partial \underset{\sim}{V}_H}{\partial z}\right) \cdot \hat{k} - \frac{T}{g} \underset{\sim}{V}_H \frac{\partial}{\partial z} \frac{\partial \underset{\sim}{V}_H}{\partial t} - \frac{q}{C_p}}{(\gamma - \gamma_{Ad})} \qquad (2.18)$$

where $\frac{q}{C_p}$ is defined as in equation (2.14). The important point is that this equation represents a single station technique for calculating vertical velocities in equatorial regions where both data is sparse and geostrophy does not necessarily hold.

3.0 VERTICAL VELOCITY ANALYSIS

In the previous chapter, an expression for calculating vertical velocities was derived which could be used with equatorial data sets in general and the Diurnal Experiment data set in particular. The goal of this chapter is to develop the practical framework by which the vertical velocity analysis will be made. This will be achieved in two steps. First, a finite difference scheme will be constructed by considering the practical limitations of the data set along with the scaling arguments of the previous chapter. This will include a discussion of time and space smoothing and the ever present problem of missing data. Secondly, a scheme will be developed by which the validity of the results can properly be judged. This will include a discussion of inherent calculation errors as well as physical interpretation techniques. This approach will then be applied to the actual data set, the results of which will be presented and discussed in Chapter 4.

3.1 CALCULATION SCHEME

In order to apply equation (2.18) to an actual data set, a scheme must be developed by which the time and height derivatives can be approximated. The standard technique is to use finite differences but in choosing such a scheme, two conditions must be met to ensure that significant errors do not propagate into the calculations. First, the finite difference interval chosen must be consistent with the actual interval between the data points. (One should not choose a finite difference interval of one hour if data points are separated

by several hours.) Secondly, the finite difference interval chosen must be consistent with the scales of motion which one desires to see. (One cannot choose a finite difference interval of several hours and hope to see scales of motion on the order of one hour.)

Both of these conditions can be accounted for quantitatively by considering the finite difference form for a function of an arbitrary variable, x.

$$f'(x) = \frac{f(x + \Delta x) - f(x - \Delta x)}{2\Delta x} \tag{3.1}$$

Assuming the motion to be wavelike, f(x) can be approximated as

$$f(x) = A \sin \frac{2\pi}{L} x \tag{3.2}$$

where A represents the amplitude of the wave motion and L represents the wavelength (or period). By substituting equation (3.2) into equation (3.1) and using some trigonometric identities, one obtains

$$f'(x) \simeq A \frac{2\pi}{L} \cos \frac{2\pi x}{L} \left(\frac{\sin \frac{2\pi}{L} \Delta x}{\frac{2\pi}{L} \Delta x}\right) \quad , \tag{3.3A}$$

while simply taking the derivative of equation (3.2) reveals

$$f'(x) = A \frac{2\pi}{L} \cos \frac{2\pi}{L} x \quad . \tag{3.3B}$$

The degree of approximation in the finite difference scheme is thus suggested by the factor in parentheses in equation (3.3A). Clearly,

the approximation improves as this factor approaches a value of 1. This implies that $\frac{\Delta x}{L}$ should be very small. A graph of the various values of $\frac{\Delta x}{L}$ and the resulting error is shown in figure 5. It is obvious that any value of $\frac{\Delta x}{L}$ greater than $\frac{1}{4}$ would portray the wave motion very poorly. Thus, one would not want the finite differencing interval, Δx, to be any larger than $\frac{1}{4}$ the wavelength or period of the motion, L, and should preferably be much smaller. This criteria can now be used as an aid in assigning proper differencing intervals for the Diurnal Experiment data.

First consider the vertical derivatives. Horizontal winds and temperature are reported at every km roughly between 30 and 60 km. From the scaling arguments of the previous chapter, a mean observable vertical wavelength was chosen at 15 km. Considering the above criteria, the largest advisable vertical differencing interval would be 4 km, but preferably much smaller. However, the possibility also exists for seeing features of smaller vertical scale in the data, for example, 8 km features. This would then suggest a differencing interval of 2 km or smaller. From the point of view of scaling and potential induced errors, it would not be unreasonable to choose a vertical differencing interval of 1 km.

For the time derivative, the data covers a 24 hour period and is reported approximately every 3 hours. From the scaling arguments, a time period of 12 hours was chosen as the mean observable feature. Reference to the above criteria, however, immediately suggests that the time period suggested by scaling is perhaps too ambitious for this particular data set with only 4 observations comprising any given 12 hour period. At best, this data set must be considered minimal for

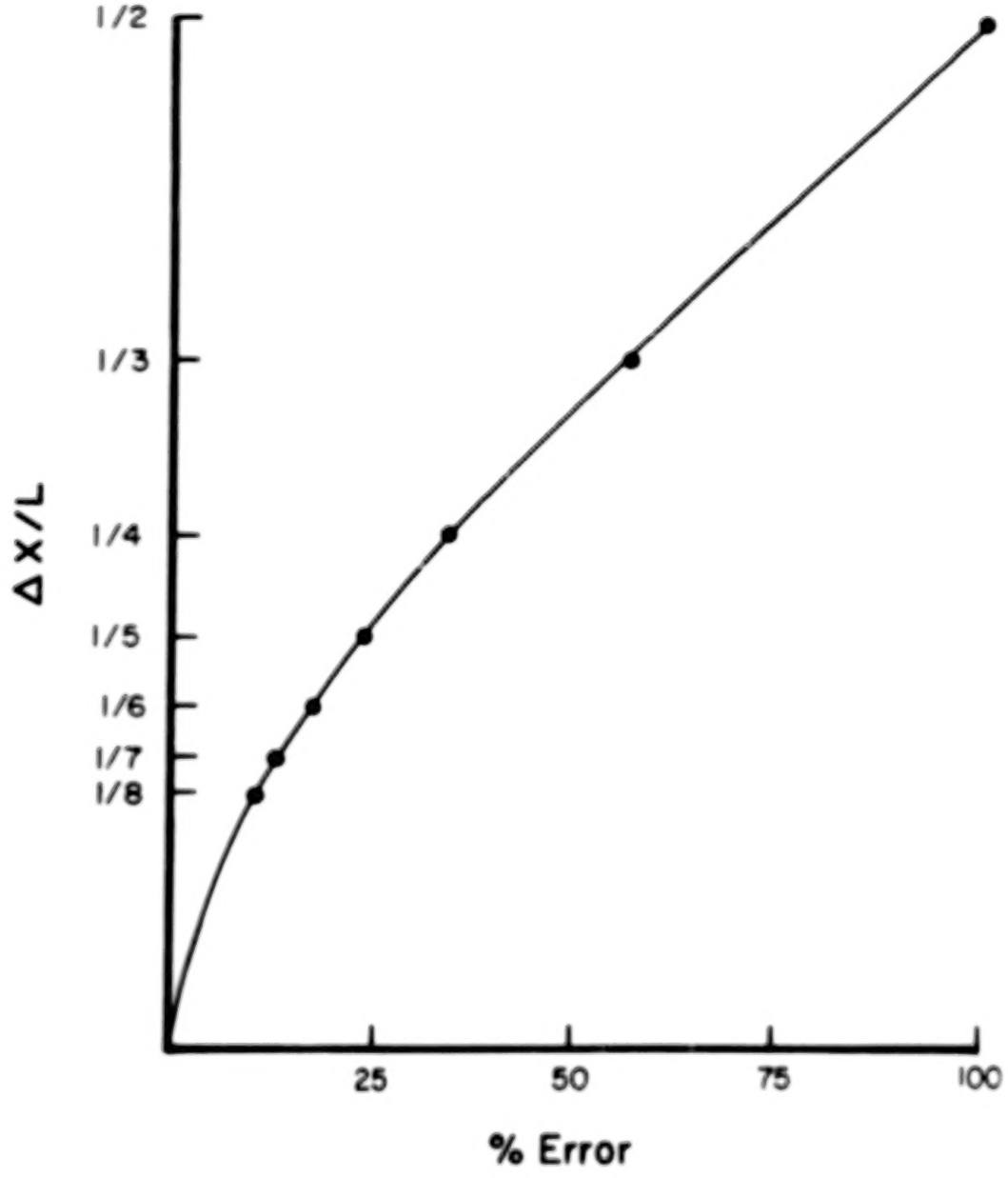

Figure 5. Finite Differencing Errors for Derivative Approximation.

accurately observing a semidiurnal period wave. On the other hand, theory suggests that the semidiurnal tidal component should be a significant part of the motion in the region of the atmosphere being studied. One has little choice under these circumstances but to choose 3 hours as the time differencing interval if one has any intentions of depicting the 12 hour time period waves.

At this point, one must take into account another aspect of the calculation problem. Measurement techniques for atmospheric variables such as wind and temperature are subject to many random errors, especially for the middle atmosphere. These errors show up in the data as high frequency noise which can contaminate any subsequent results. Since 1 km in the vertical and 3 hours in time represent the highest frequencies available from the present data set, one might suggest that the magnitudes of derivatives calculated over such intervals could be contaminated with noise. This, indeed, is a possibility but the potential problem can be alleviated somewhat by either smoothing the data before it is used in the calculations or by increasing the size of the finite differencing interval. Both of these operations could have serious drawbacks, though, when the number of data points is small. While smoothing or differencing over a few kms in the vertical would affect only a small proportion of the observable wavelengths for the present data set, any smoothing or differencing over more than a 3 hour interval in time could seriously affect all the possibly observable wave periods. Thus, for this particular data set, any such operation in the time domain must be used very sparingly or not at all.

Considering the above discussion, the following two calculation schemes have been adopted for use with the Diurnal Experiment data. The first, referred to as scheme A, attempts to get as much information concerning the smaller time and space scale features as possible. For this purpose, vertical derivatives have been approximated over a 1 km interval ($2\Delta z$ = 1 km; see equation (3.1)) and time derivatives have been approximated over a 3 hour interval ($2\Delta t$ = 3 hours). All calculated quantities are assigned to the center point of the given time or space interval (see figure 6). Also, in an attempt to filter out some of the potential high frequency noise, the input data has been smoothed over 3 points (2 km) in the vertical using a 1-2-1 filter.

The second scheme, referred to as scheme B, approximates the vertical derivatives over a 2 km interval ($2\Delta z$ = 2 km) and the time derivatives over a 6 hour interval ($2\Delta t$ = 6 hours), the only exception being the end intervals in both the time and space domain where the 1 km and 3 hour intervals are again used. This is necessary, especially in the time domain, to ensure sufficient results to analyze. Again, all calculated quantities are assigned to the center of the space or time interval (see figure 6). The input data is smoothed in the vertical as above. Besides filtering out more of the potential noise, scheme B should filter out some of the higher frequency information leaving larger time period motions and larger vertical wavelengths more prevalent in the results. By comparing the results from the two schemes, one should obtain information concerning the sensitivity of the results to changes in finite differencing intervals as well as information as to which scales of motion are dominant. As

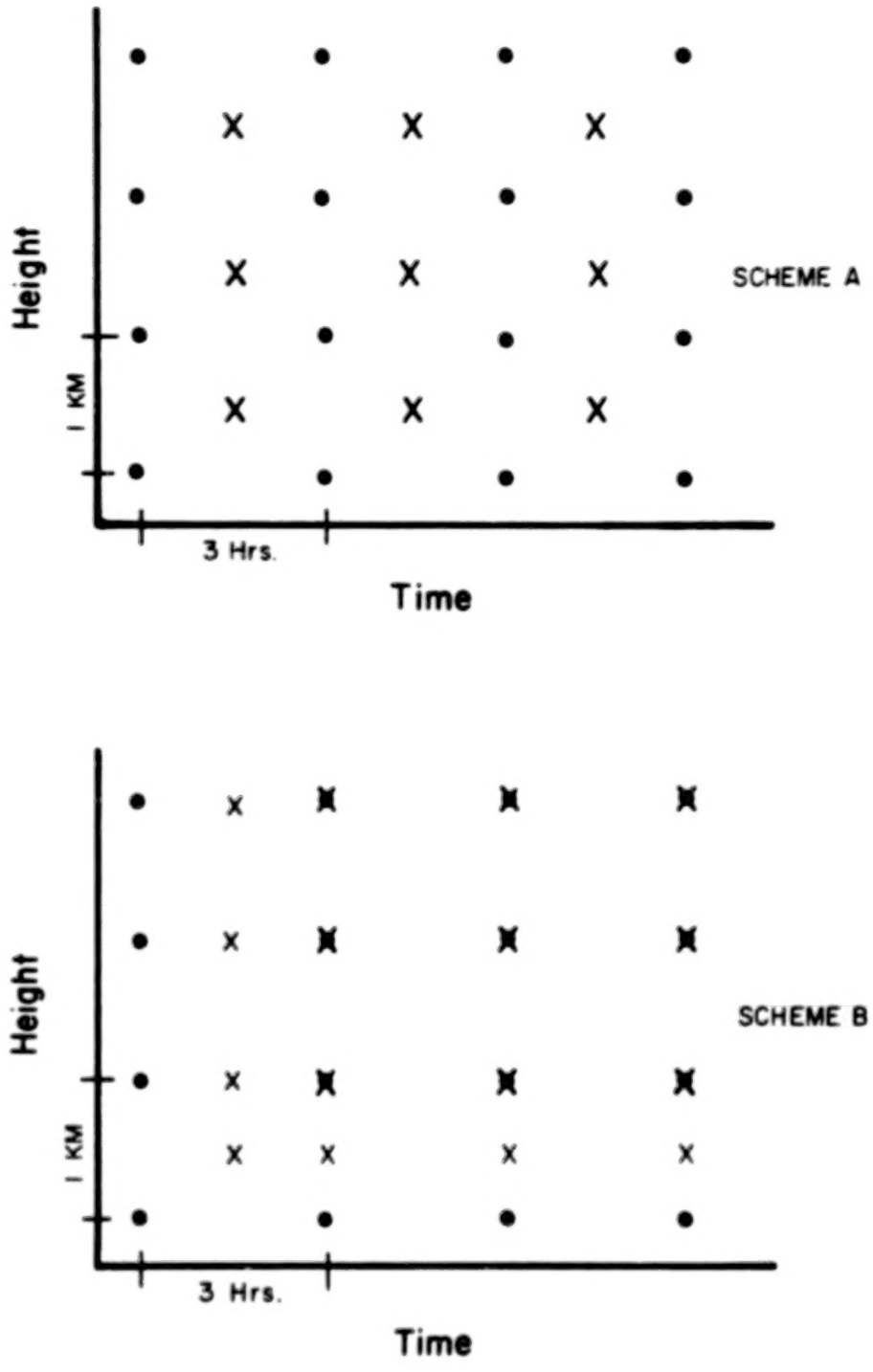

Figure 6. Finite Difference Schemes: Dots Represent Data Points, X Represents Assigned Position of Calculated Quantities, X Represents Assigned Position of Calculated Quantities on the Boundaries.

discussed in the next section, this will aid in the process of judging how good the results actually are.

One additional consideration in the application of these calculation schemes is the handling of missing data. While observations of wind and temperature were to be taken about every three hours for an entire diurnal period at each station, the usual problems such as bad weather or payload failure deemed this goal unrealizable. The result was that all stations except for Kourou missed at least one temperature measurement and a few stations missed both temperatures and wind measurements for the given observation period. In such cases, the following rules were adhered to. If only a temperature observation was found missing, values were linearly interpolated from the neighboring values in time and calculations proceeded as normal. If both temperatures and winds were missing for the same observation period, no interpolated values were assigned but the finite difference interval in time was increased over the affected time periods. This, in essence, served as a linear interpolation of the time derivatives. It was felt that these rules would subject the data set to the least amount of manipulation while still ensuring a reasonable amount of continuity in the calculations over the affected time periods. A list of those time periods affected at each station is given in Table 2.

TABLE 2. Missing Data Log

Station	Time Period of Interpolated Temperatures (GMT)	Time Periods of Missing Temperatures and Wind (GMT)
Kourou	-	-
Fort Sherman	2200	-
Ascension	1900	2200
Antigua	2100	0000
Natal	2218	0400

3.2 VERIFICATION SCHEME

Up to this point, much of the emphasis has been placed upon deriving a single station technique for calculating vertical velocities. While this has been achieved, an equally important aspect of the problem has been neglected, namely, how does one determine whether the results are valid? One obvious approach would be to compare the derived vertical velocities to actually observed values, but this possibility has already been discounted. Another approach would be to compare the results to those derived via an alternate vertical velocity equation, but the characteristics of the present data set preclude this possibility.

One method which can be used for this study is to compare the derived vertical velocities to results suggested by theory. Along this line, two questions must be considered:

1) Are the results physically reasonable?

2) Do the results match current models?

The first question can be approached in several ways. For example, it is generally accepted that real atmospheric features should show some continuity in time and space. If the derived vertical motion fields do not show this continuity, the validity of the results might be questioned. Another approach deals with the assumption that the results resemble some form of internal gravity wave motion. It is generally accepted that the magnitude of upward propagating wave type motion should increase with height as $\rho^{-1/2}$ where ρ is the density. Thus, one would expect the derived vertical motions to verify this relation.

To answer the second question, one must have a model to which the results can be compared. Such a model is available in the theory of atmospheric tides but the limitations of the present data set subject this type of analysis to much uncertainty. In order to directly compare the derived vertical motions to the tidal predictions, the vertical motion fields must be decomposed into their diurnal and semi-diurnal components, a procedure which can create much error with only eight data points covering the entire diurnal period. Still, this analysis will enable one to draw many general conclusions concerning the derived vs. predicted vertical motions.

The scaling arguments of the previous chapter afford an indirect means of comparing the derived vertical velocities to tidal predictions. Since the time and length scales chosen for the analysis were those suggested by tidal theory, one could compare the calculated magnitudes of the various terms in equation (2.18) to those suggested by

the scaling arguments. A necessary condition for the observed motions to be tidal would then be that the various terms agree at least in order of magnitude. If they do not, then one must question either whether tidal type motions are being observed or whether the vertical velocity equation is in the proper form for this particular study. This internal consistency check, however, can only serve as a necessary and not a sufficient condition for the observed motions to be classified as tidal, etc., since the time and length scales used could represent other types of motion as well.

The next step in the verification process is to consider the numerical aspects of the calculations. Two more questions arise:

3) Are the results numerically stable?

4) Are the results significant with respect to the errors of measurement?

In reference to the third question, one would expect good results to be relatively insensitive to changes in the calculation scheme. For example, change in the data smoothing procedure or finite differencing interval should not greatly affect the overall results. For the present study, this criteria will be checked by comparing the results obtained via the scheme A and scheme B calculation procedures discussed earlier in this chapter.

In many ways, the fourth question serves as the final judge of the validity of any results, for if the magnitudes of the results are smaller than the magnitudes of the numerical errors, then the results must be invalidated despite any previous conclusions. The next step in the methodology is thus to derive a scheme by which these numerical errors can be accounted for.

Numerical errors can come from three distinct sources:

1) Errors inherent in the data set, usually referred to as noise.

2) Errors introduced by neglecting terms in the generalized equation.

3) Errors inherent in the finite differencing scheme used.

The first type of error can be accounted for by considering the characteristics of the measuring devices and procedures. In this case, the measured winds and temperatures are considered repeatable to within $\pm$ 3 m/sec and $\pm$ 1°K respectively. Errors derived from neglecting terms in an equation are accountable by referring to scaling arguments. Both of these forms can be included in a single expression which will be derived below. Errors inherent in using a given finite difference scheme must be considered subjectively, however, as one is never quite sure what scales of motion are being observed.

The expression for estimating the error can be derived by taking the vertical velocity, w, to be a function of four independent variables; the local time derivative of temperature (DTDT), the horizontal derivative of temperature (ADVT), diabatic heating (DIAB), and stability (STAB):

$$w = \frac{DTDT + ADVT + DIAB}{STAB} \quad . \tag{3.4}$$

By forming the total differential of w, δw, the error expression becomes:

$$\delta w = \frac{1}{STAB} \left[\delta(DTDT + \delta(ADVT) + \delta(DIAB)\right] - \frac{(DTDT + ADVT + DIAB)\ \delta STAB}{(STAB)^2} \tag{3.5}$$

One is usually interested in the maximum error obtainable. Thus, each term in the above expression should contribute positively to the whole. To ensure that this happens, the expression is usually squared. Then, assuming that the errors are random, cross terms drop out, leaving:

$$\delta w = \left[\frac{(\delta DTDT)^2 + (\delta ADVT)^2 + (\delta DIAB)^2}{(STAB)^2} + \frac{(\delta STAB)^2 \, (DTDT + ADVT + DIAB)^2}{(STAB)^4} \right]^{1/2} . \qquad (3.6)$$

Equation (3.6) is the expression for the absolute error. Relative error may be calculated by dividing the above expression by w. A more representative value to use, however, is the root mean square of the error:

$$\delta w_{ST} = \left(\frac{\sum_{i=1}^{N} \delta w_i^2}{N} \right)^{1/2} , \qquad (3.7)$$

where N represents the number of points being summed over.

Using the $\pm$ 1°k and $\pm$ 3 m/sec accuracy estimates previously stated, one can now assign specific values to each error term in equation (3.6). The details of this procedure are reviewed in Appendix C, the results of which are suggested below.

$$\begin{aligned} &\delta(DTDT) = 1°K/3 \text{ hours} \\ &\delta(ADVT) = 0.3 \ (ADVT) \\ &\delta(DIAB) = 0.2 \ (DIAB) \\ &\delta(STAB) = 0.5°K/km \end{aligned} \qquad (3.8)$$

Substitution of these values in equation (3.6) yields the final form of the error equation used for this study:

$$\delta w = \left[\frac{10^{-8} \text{ k/sec} + 0.09\ (\text{ADVT})^2 + 0.04\ (\text{DIAB})^2}{\text{STAB}^2} + \frac{0.25(w)^2}{\text{STAB}^4} \right]^{1/2} . \qquad (3.9)$$

At each altitude, the above calculated values are summed over time as in equation (3.7). This yields a vertical profile of error estimates to which the actual vertical velocities can be compared.

Since direct measurements of vertical velocities are unavailable for comparison with the derived values, the verification procedure developed over the last several pages cannot be expected to give the final judgment over the results. It is felt, however, that if the above four questions are considered carefully and all the evidence is collectively weighed, some fairly definite conclusions can be drawn concerning the vertical motion fields for the Diurnal Experiment.

4.0 RESULTS AND DISCUSSION

Over the past two chapters, a scheme has been developed to both calculate and analyze vertical motions in the equatorial middle atmosphere. This scheme has been used along with the Diurnal Experiment data set to calculate vertical motions at Kourou (French Guiana), Ft. Sherman (PCZ), Natal (Brazil), Antigua (BWI), and Ascension Island. The purpose of this chapter is to present and discuss these results. This will be accomplished in three steps. First, time series cross sections will be presented and discussed with respect to the numerical stability and error criteria of the previous chapter as well as to the identification of prominent features continuous in space and/or time. The next step will be to check the internal consistency between the calculated magnitudes of terms and those suggested by the scaling arguments of Chapter 2. Finally, the results will be compared to the predictions of atmospheric wave theory, specific reference being made to the predictions of atmospheric tides.

4.1 TIME SERIES CROSS SECTIONAL ANALYSIS

Time series cross sectional analysis is perhaps the most straightforward means of depicting continuous features in a given data set. If the data is made up of various wave forms, however, one must be sure that it is properly presented on the cross sections to depict these features. The following considerations are especially important. First, wave motion almost always appears as perturbations on a mean flow. Thus, in cases where the mean varies over the study range, perturbation values of the derived field quantity should be used.

Secondly, if waves with periods larger than can be depicted by the data set form a significant part of the motion, they can appear as linear trends in the data. If one is interested only in those particular waves which can be completely depicted by the data, then these linear trends must also be removed.

The diurnal means of the derived vertical motions at each altitude are presented for scheme A in Table 3. One will note that the magnitudes vary irregularly over the altitude range but do show a tendency to increase with height. The magnitudes as calculated for scheme B are slightly smaller but the tendencies are roughly the same. Since wave forms are expected in the data it therefore does appear advisable to use perturbation values in the cross sections. These will be defined relative to the diurnal mean as follows:

$$w' = w - \bar{w} \tag{4.1}$$

where w' represents the perturbation quantity and $\bar{w}$ represents the diurnal mean.

At this point in the analysis, interest will not be limited only to wave features which can be completely depicted by the data set, for evidence of wave periods greater than 24 hours would be as significant a result as the depiction of the tidal fields. Therefore, linear trends are not removed from the cross sectional data. This subject will again be brought up later in the chapter when an attempt is made to decompose the results into the various tidal components.

The time series cross sections of the perturbation vertical motions for Kourou, Ascension Island, Ft. Sherman, Antigua and Natal

TABLE 3. Diurnal Means of Vertical Velocity, Scheme A (cm/sec).

Height (km)	Kourou	Ft. Sherman	Ascension	Antigua	Natal
63					
62					
61	2.5				
60	2.4			1.3	
59	1.1			2.8	
58	0.3		0.3	3.0	
57	0.1		1.0	1.8	1.0
56	-1.1	-0.2	2.4	1.7	-1.5
55	-1.4	-0.9	2.2	1.4	-0.6
54	-1.0	-1.4	0.2	0.4	-0.3
53	-0.3	-1.5	-0.3	-0.4	0.1
52	-0.1	-0.9	-0.9	-1.0	1.0
51	-0.1	-0.3	-0.2	-0.3	0.8
50	0.4	0.4	0.3	0.5	0.4
49	0.4	0.4	0.5	0.8	0.1
48	0.6	0.4	1.6	0.1	0.2
47	0.4	0.4	1.6	-0.5	0.6
46	0.4	0.3	1.0	-0.1	0.9
45	0.4	0.4	0.3	-0.3	0.9
44	0.4	0.3	-1.0	-0.2	0.5
43	0.1	-0.1	-1.2	-0.2	0.1
42	0.5	-0.8	-1.0	-0.1	-0.1
41	0.5	-0.8	-0.5	0.1	0.4
40	0.1	-0.1	0.4	-0.1	0.3
39	-0.1	-0.2	-0.1	-0.1	0.6
38	-0.1	-0.1	-0.1	0.0	0.8
37	0.0	0.2	0.3	-0.2	0.7
36	-0.5	0.2	0.8	0.2	0.7
35	-0.0	-0.7	1.3	0.4	0.1
34	0.0	-0.9	1.3	0.2	0.1
33	-0.1	0.4	0.7	-0.5	0.7
32	0.3	1.7	0.1	-0.3	0.3
31	0.1	0.8	0.1	-0.1	0.5
30	0.2	0.1	0.2	-0.0	0.7
29	0.3	0.1	0.6	-0.3	-0.0
28		0.2	0.5	-0.2	-0.1
27			-0.0		-0.1
26			-0.2		0.0
25			-0.0		

are presented in figures 7 through 11. In each of these figures, the A part corresponds to the results for scheme A and the B part corresponds to the results for scheme A and the B part corresponds to the results for scheme B. The cross sections have been analyzed to depict the positive (shaded) and negative (unshaded) areas of vertical motion.

An inspection of the cross sections suggests that some sort of gravity wave type motion is being depicted. In general, the waves seem to have diurnal, semidiurnal, and even shorter time periods with amplitudes increasing from 1 or 2 cm/sec at 30 km to as large as 15 cm/sec near 60 km. In addition, it appears as if the cross sections can be classified into two distinct groups. In group I, including Kourou, Ft. Sherman, and Ascension, the dominant wave features are characterized by relatively short vertical wavelengths (15-20 km) and an evident downward phase progression (20-50 km/day). In group II, including Natal and Antigua, the dominant wave features are characterized by relatively long vertical wavelengths (> 20 km), a mainly diurnal period, and little or no evident phase progression. These group designations prove to be an unexpected but interesting feature in the results and will be discussed further below.

The fact that features as suggested above can clearly be seen in the cross sections gives some initial credence to the results. These features must be compared to atmospheric wave theory in a more quantitative fashion, though, before one classifies the results as physically acceptable. This will be done later in the chapter, but first it is advisable to check the numerical stability and error criteria suggested in section 3.2.

BLANK PAGE

BLANK PAGE

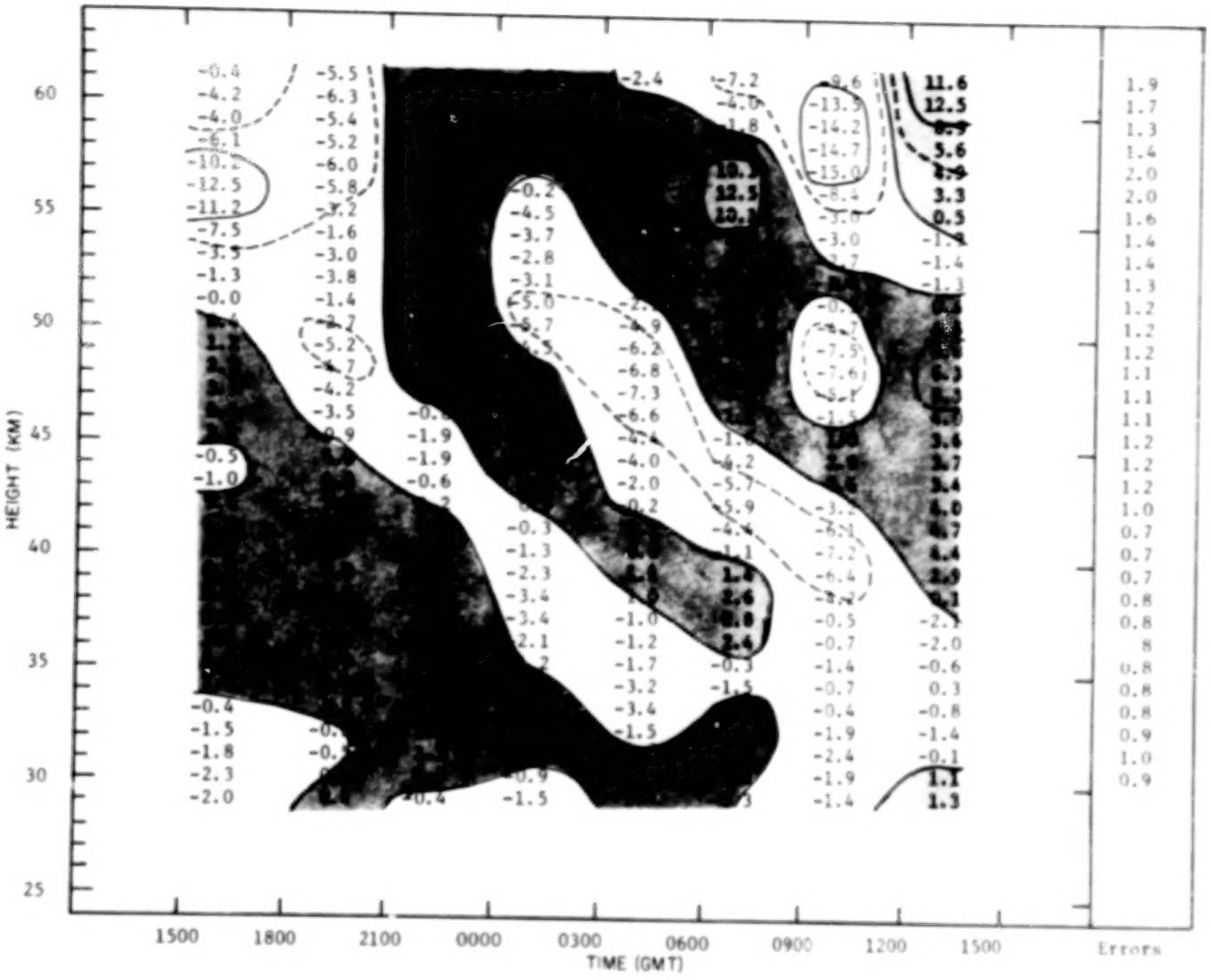

FIGURE 7A. Vertical velocities and error estimates for Kourou, scheme A (cm/sec).

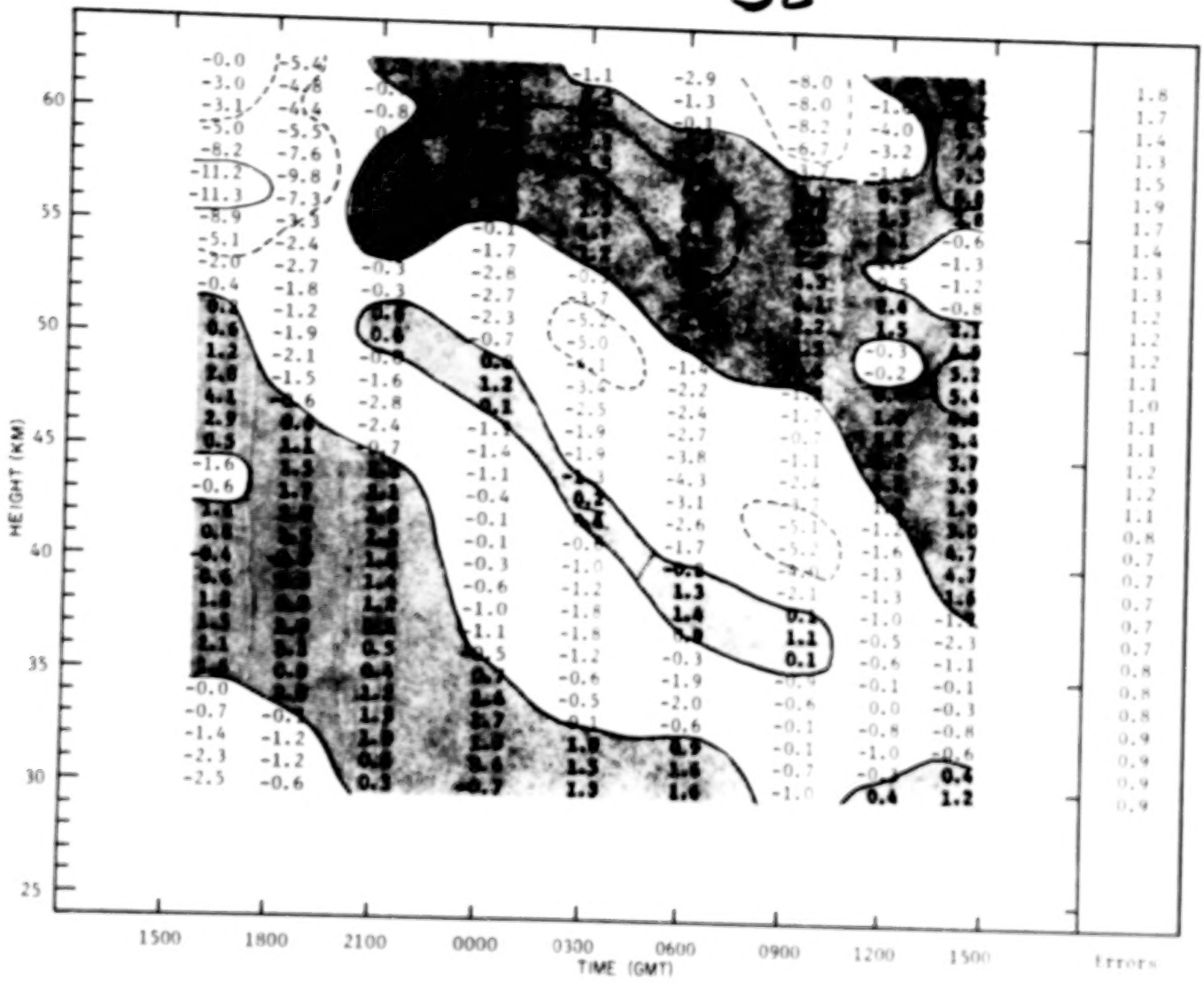

FIGURE 7B. Vertical velocities and error estimates for Kourou, scheme B (cm/sec).

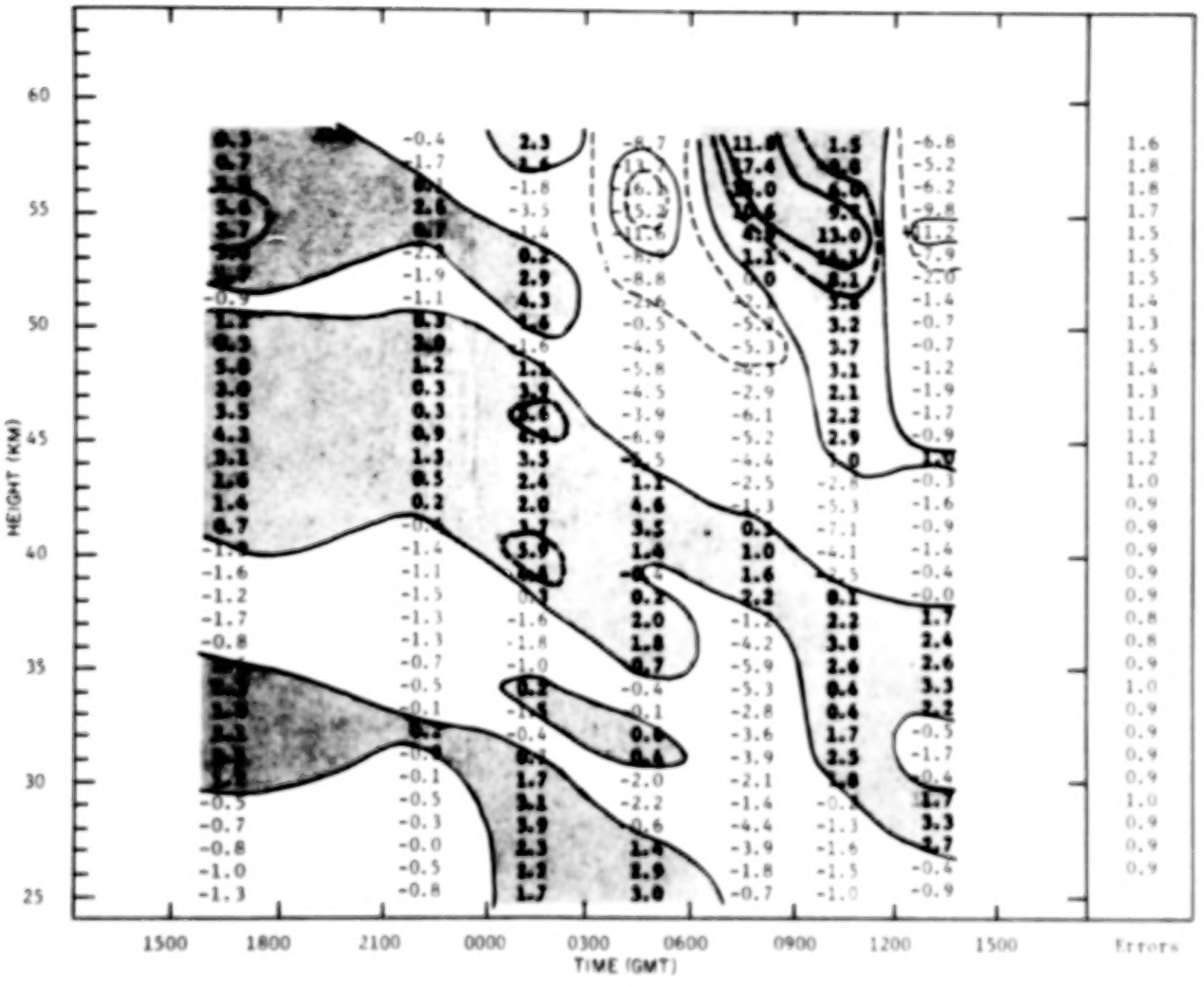

FIGURE 8A. Vertical velocities and error estimates for Ascension Island, scheme A (cm/sec).

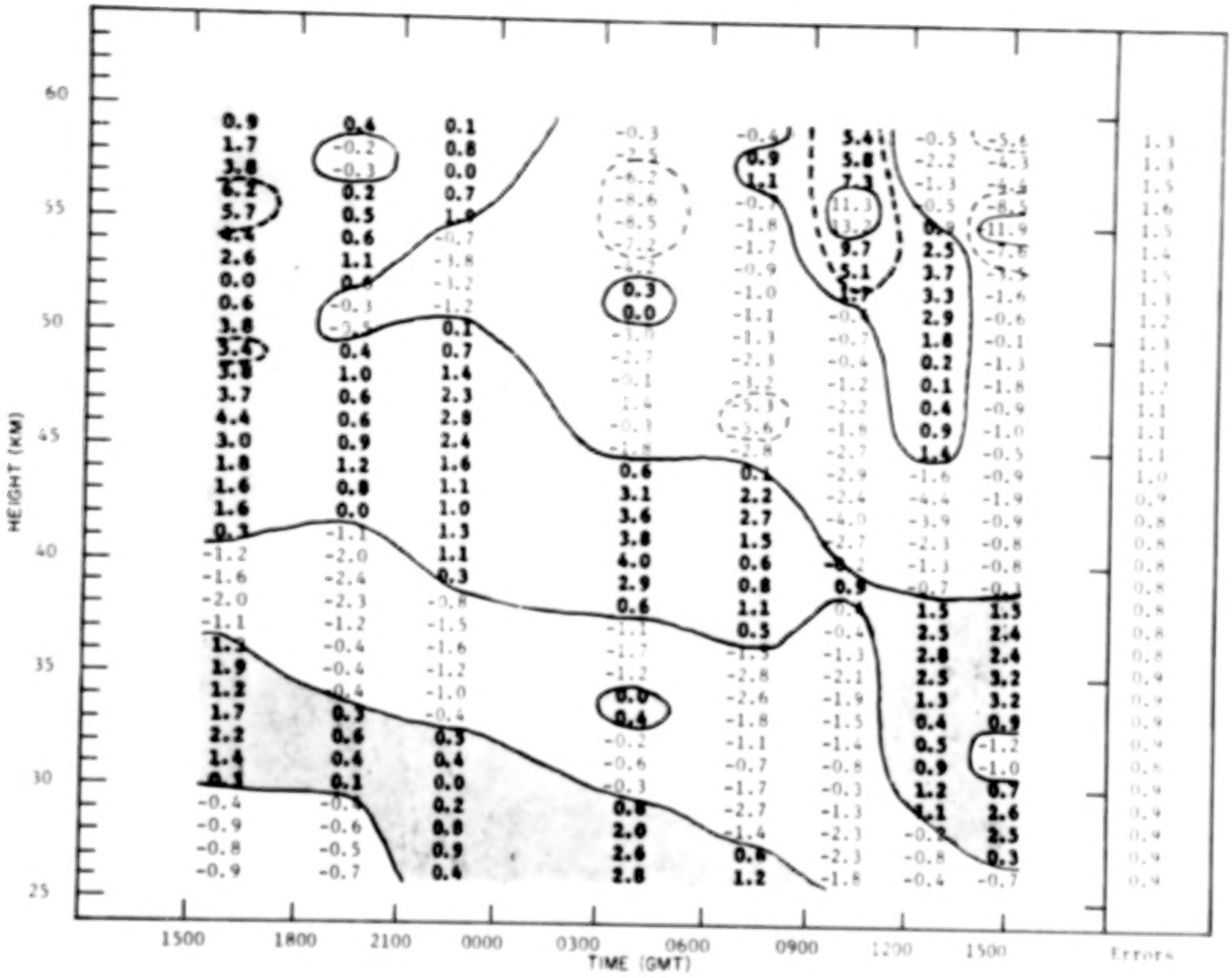

FIGURE 8B. Vertical velocities and error estimates for Ascension Island, scheme B (cm/sec).

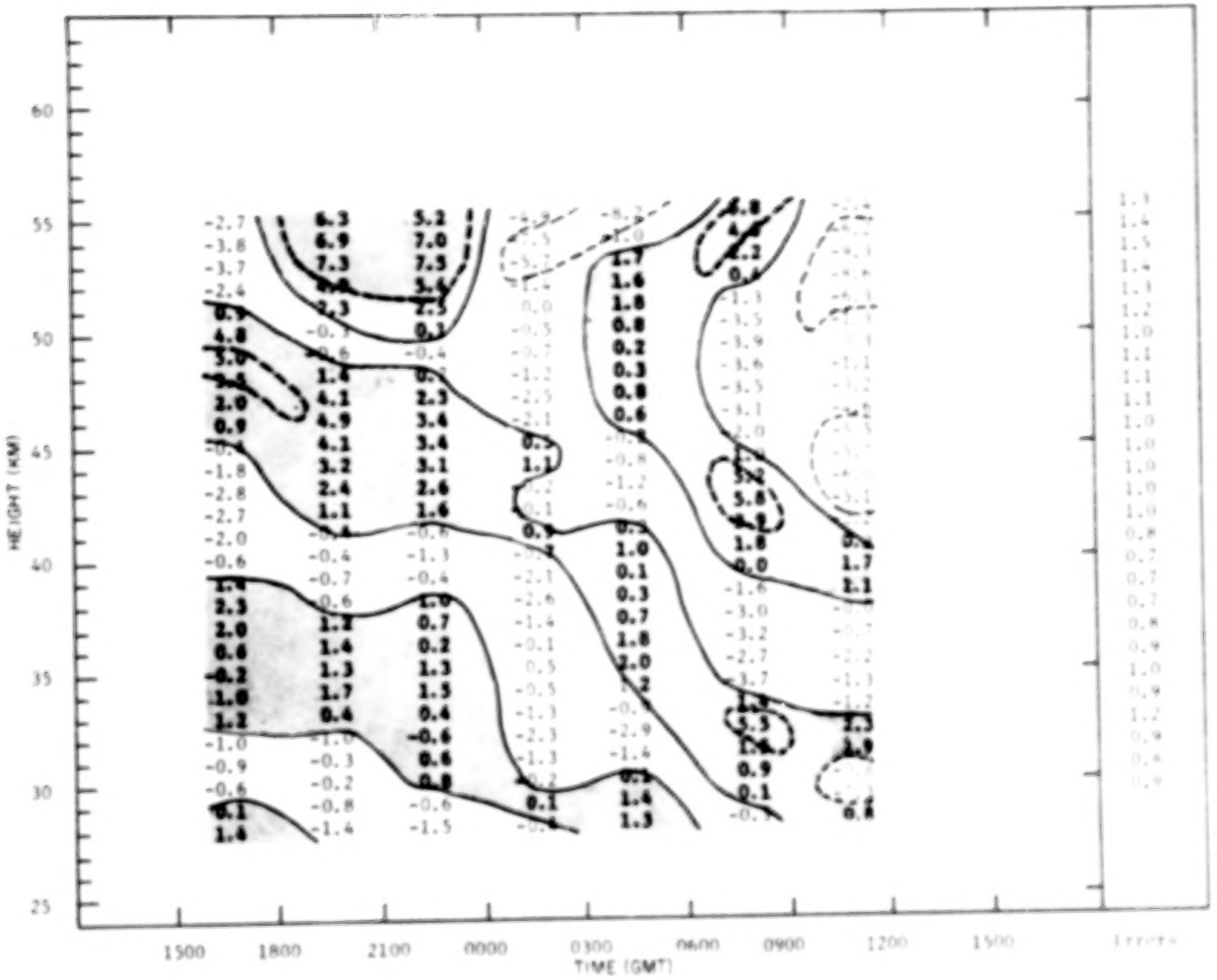

FIGURE 9A. Vertical velocities and error estimates for Ft. Sherman, scheme A (cm/sec).

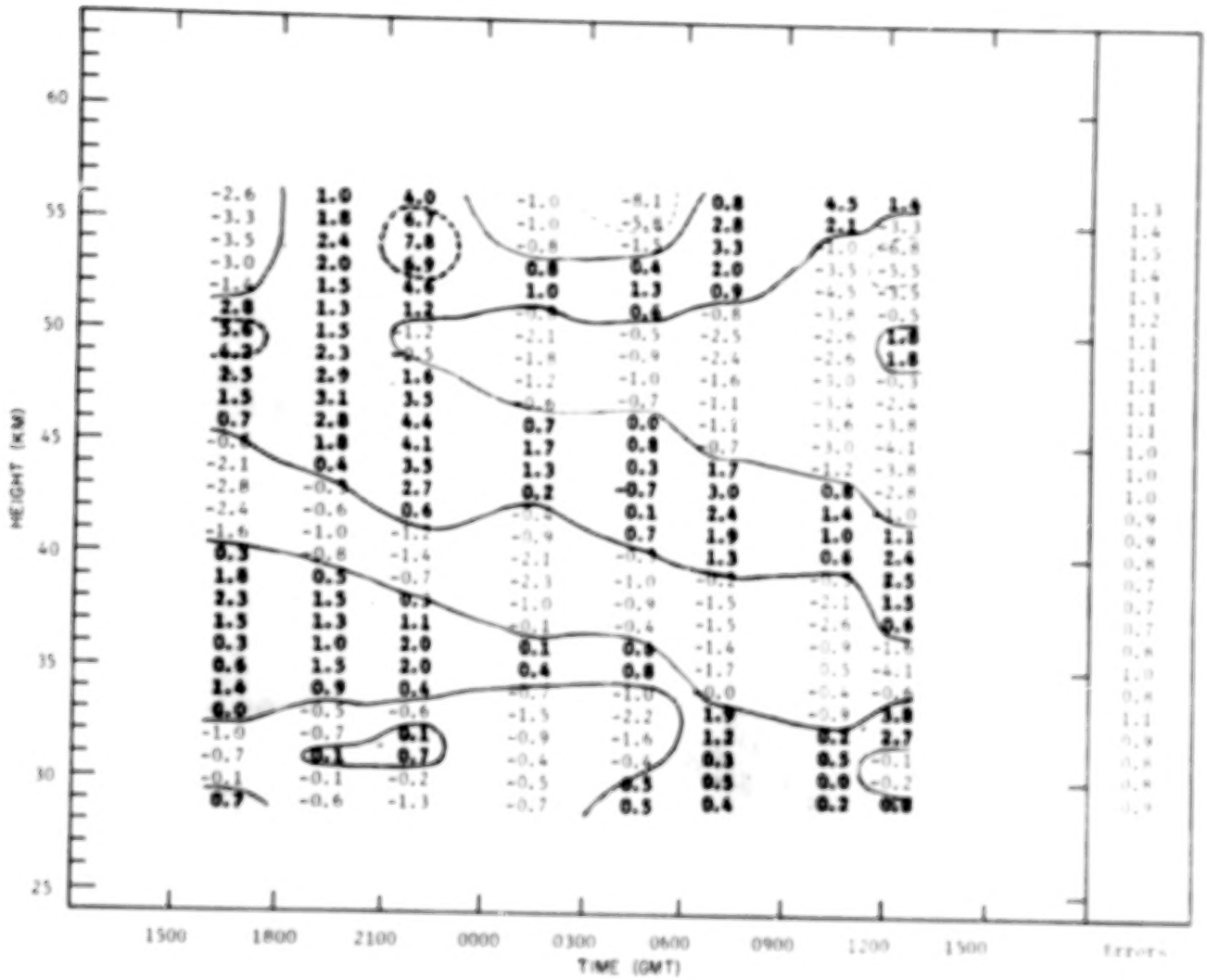

FIGURE 9B. Vertical velocities and error estimates for Ft. Sherman, scheme B (cm/sec).

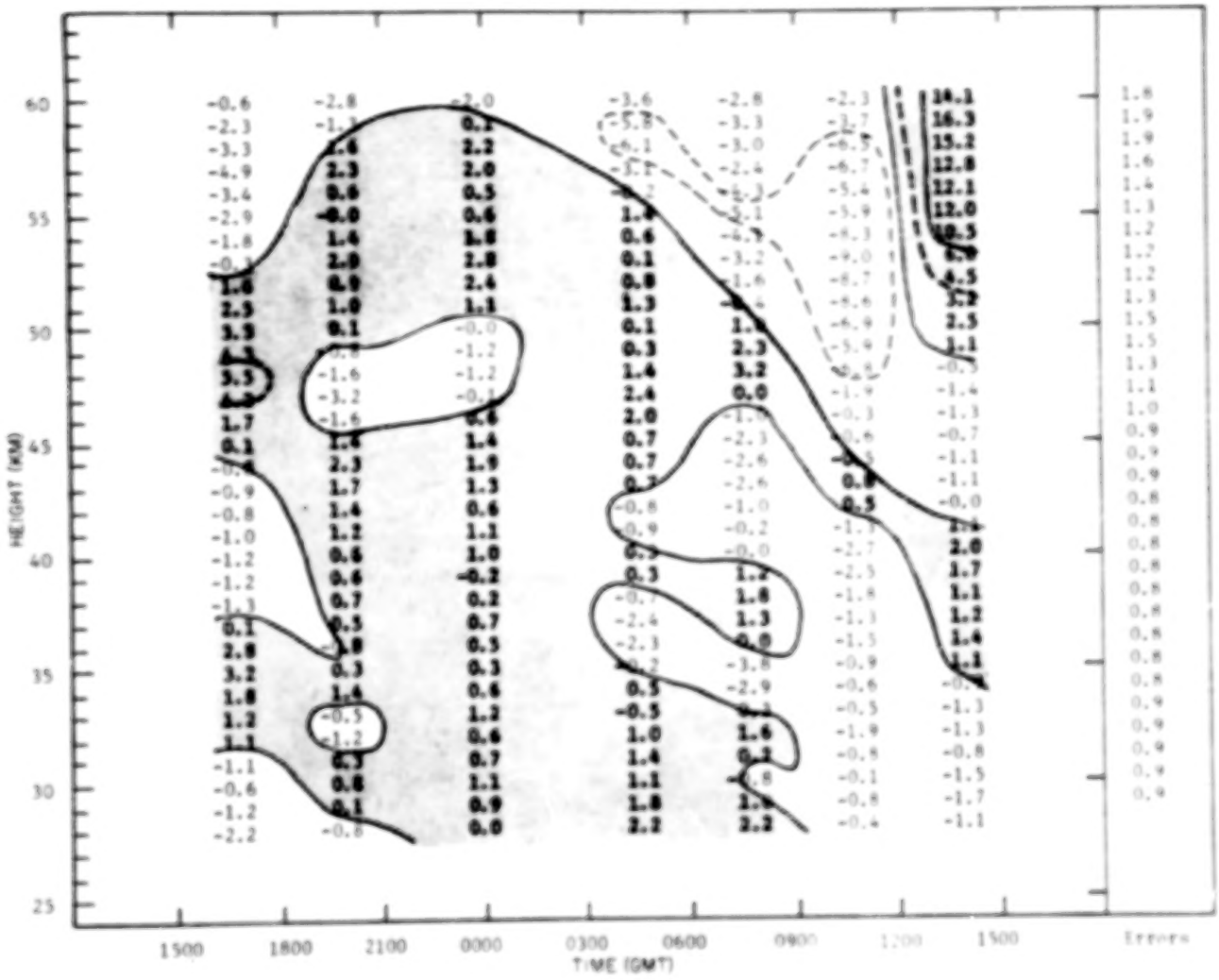

FIGURE 10A. Vertical velocities and error estimates for Antigua, scheme A (cm/sec).

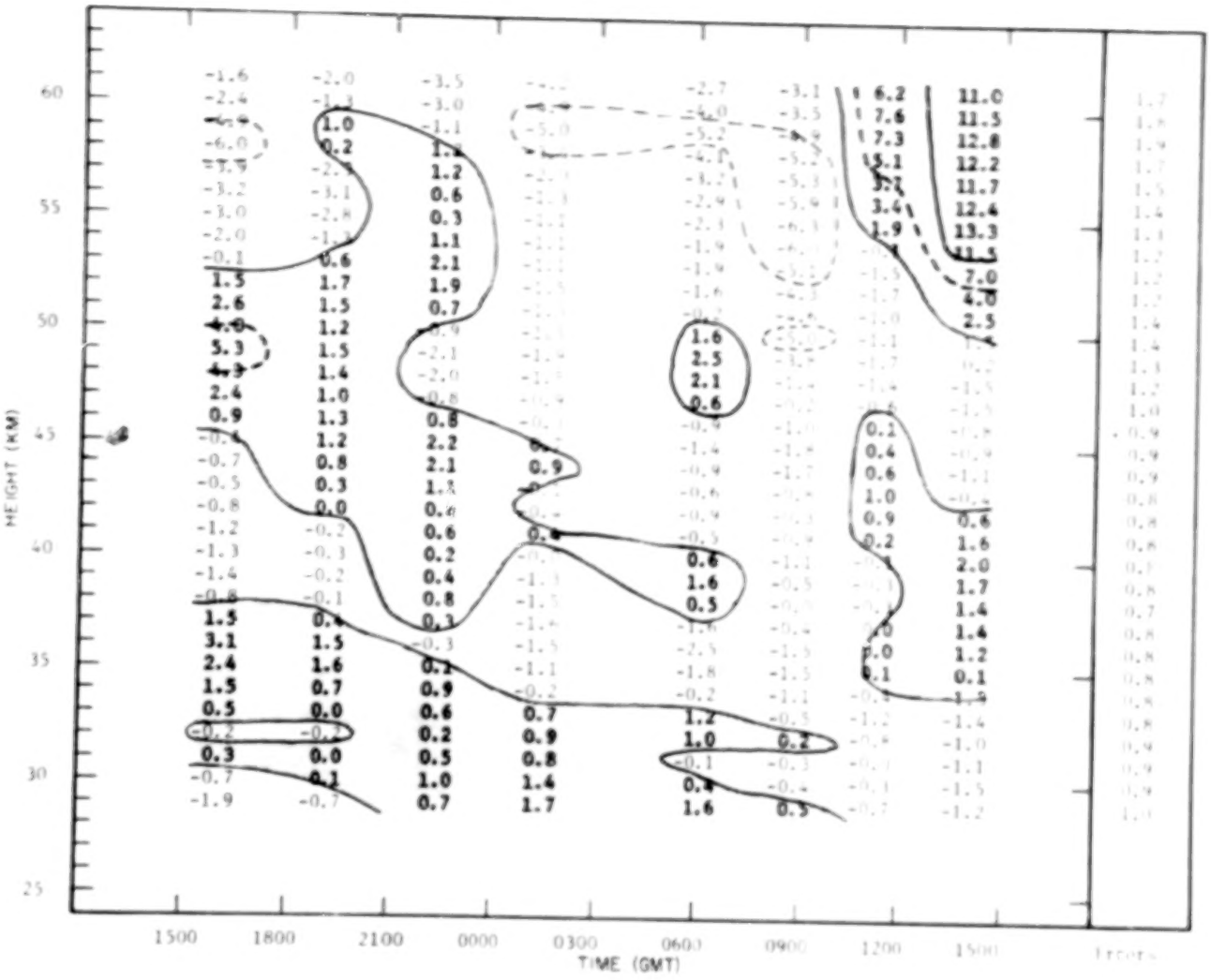

FIGURE 108. Vertical velocities and error estimates for Antigua, scheme B (cm/sec).

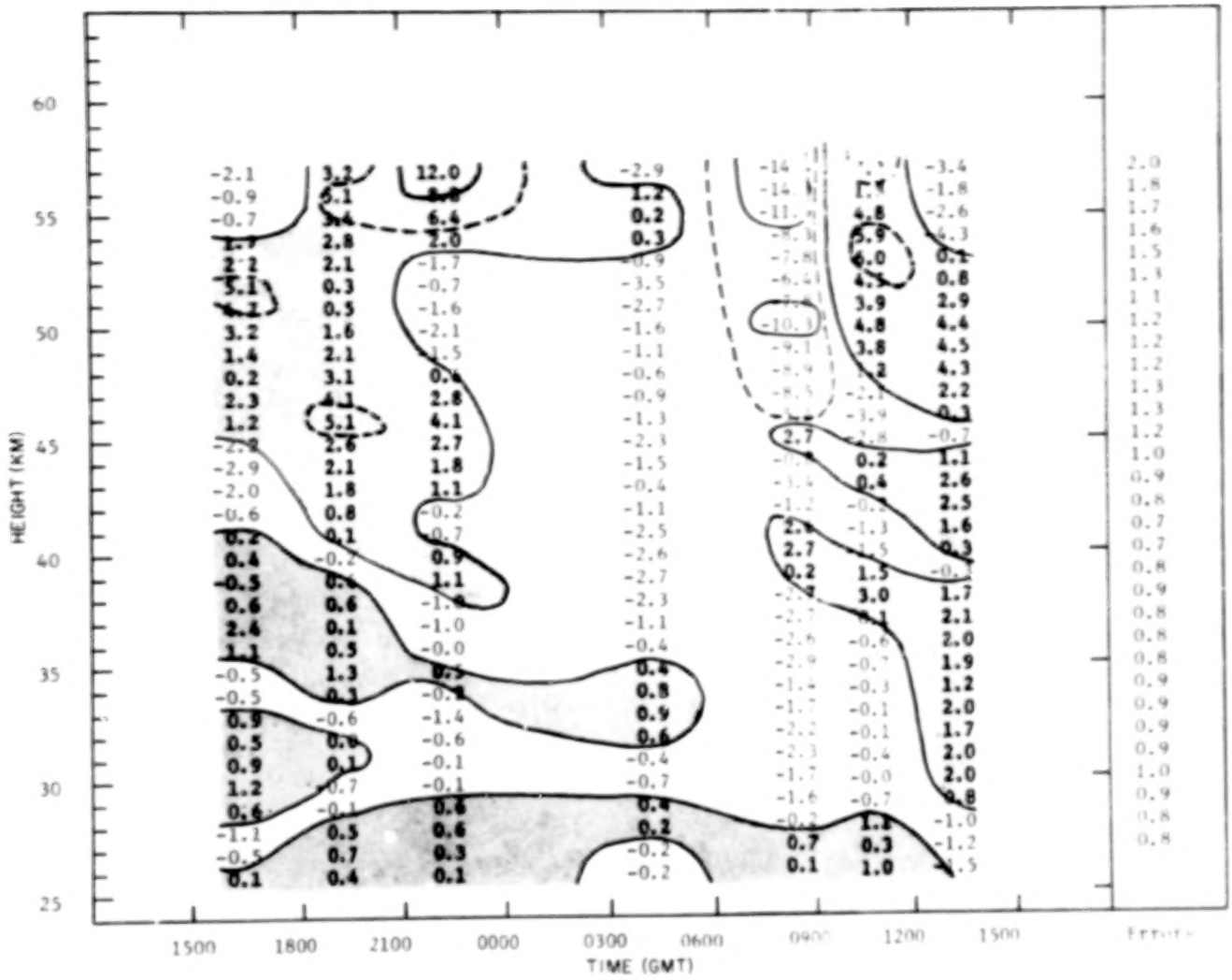

FIGURE 11A. Vertical velocities and error estimates for Natal, scheme A (cm/sec).

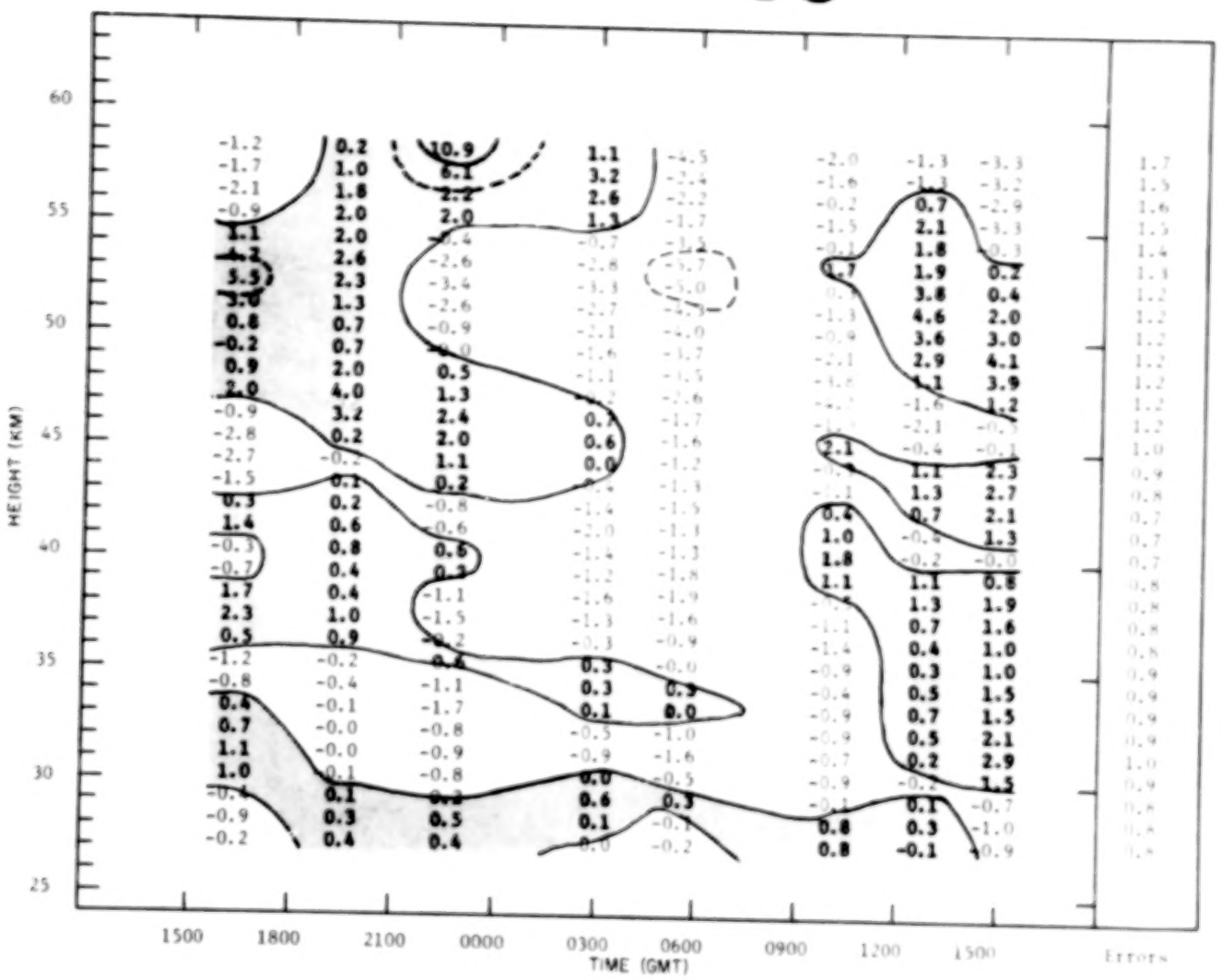

FIGURE 11B. Vertical velocities and error estimates for Natal, scheme B (cm/sec).

As indicated in the previous chapter, none of the results can be accepted unless they are first shown to be significant with respect to the numerical error estimates. To check this, vertical profiles of the root mean square as calculated from equations (3.9) and (3.7) have been included to the right of each cross section in figures 7 through 11. One will note that the relative error is quite small in all but perhaps the lower third of the altitude range (< 40 km). Even in this lower range, though, the error estimates are small compared to the maxima and minima of the vertical velocity patterns. Thus, upon consideration of this one criteria, it is felt that the general magnitudes and patterns of vertical velocities depicted in the cross sections can be accepted with little hesitation.

It has also been suggested in the previous chapter that for the results to be acceptable, they should be relatively insensitive to changes in the calculation scheme. This criteria will now be checked by comparing the results obtained using scheme A and scheme B. Inspection of the cross sections shows that the magnitudes of the vertical velocities calculated using scheme B are slightly smaller than those of scheme A. Also, some of the smaller time and space scale features appear slightly smoothed out in the scheme B cross sections. This smoothing effect, however, is exactly what one would expect if the observed motions were composed of semidiurnal or even smaller period waves along with the diurnal waves, or if the data contained significant amounts of high frequency noise. The increased finite differencing interval used in scheme B decreases the magnitudes of the derivatives for the smaller period motions. But since the

differences between the two schemes is generally small, it is felt that the results can be accepted relative to the sensitivity criteria.

Another question which must be considered when comparing the cross sections among the different stations is how the several cases of missing data affect the calculations. While most of the calculations have been done with a three hour interval between observation times, Ascension, Antigua, and Natal each have one observation period missing. For this particular time period, the calculations proceed as usual around the missing data by adding the additional three hours onto the time differencing interval. To see how this affects the results, a test calculation has been made for Kourou with the 0000Z data left out. The results for scheme A and scheme B are presented in figures 12A and 12B respectively. Comparing these with figures 7A and 7B, one notes that the actual magnitudes of the vertical velocities have changed over the affected time periods but the overall difference is a general smoothing out of the smaller time scale features. Since smaller time scale features cannot be depicted well by the present data set in any case, this type of induced error will be considered acceptable for this analysis.

4.2 INTERNAL CONSISTENCY

The next step in the analysis is to check the internal consistency between the calculated magnitudes of the terms comprising equation (2.18) and the estimated magnitudes suggested in equation (2.16A). Since the scaling arguments used characteristic values from about the 45 km level, the comparison should likewise be made with calculated

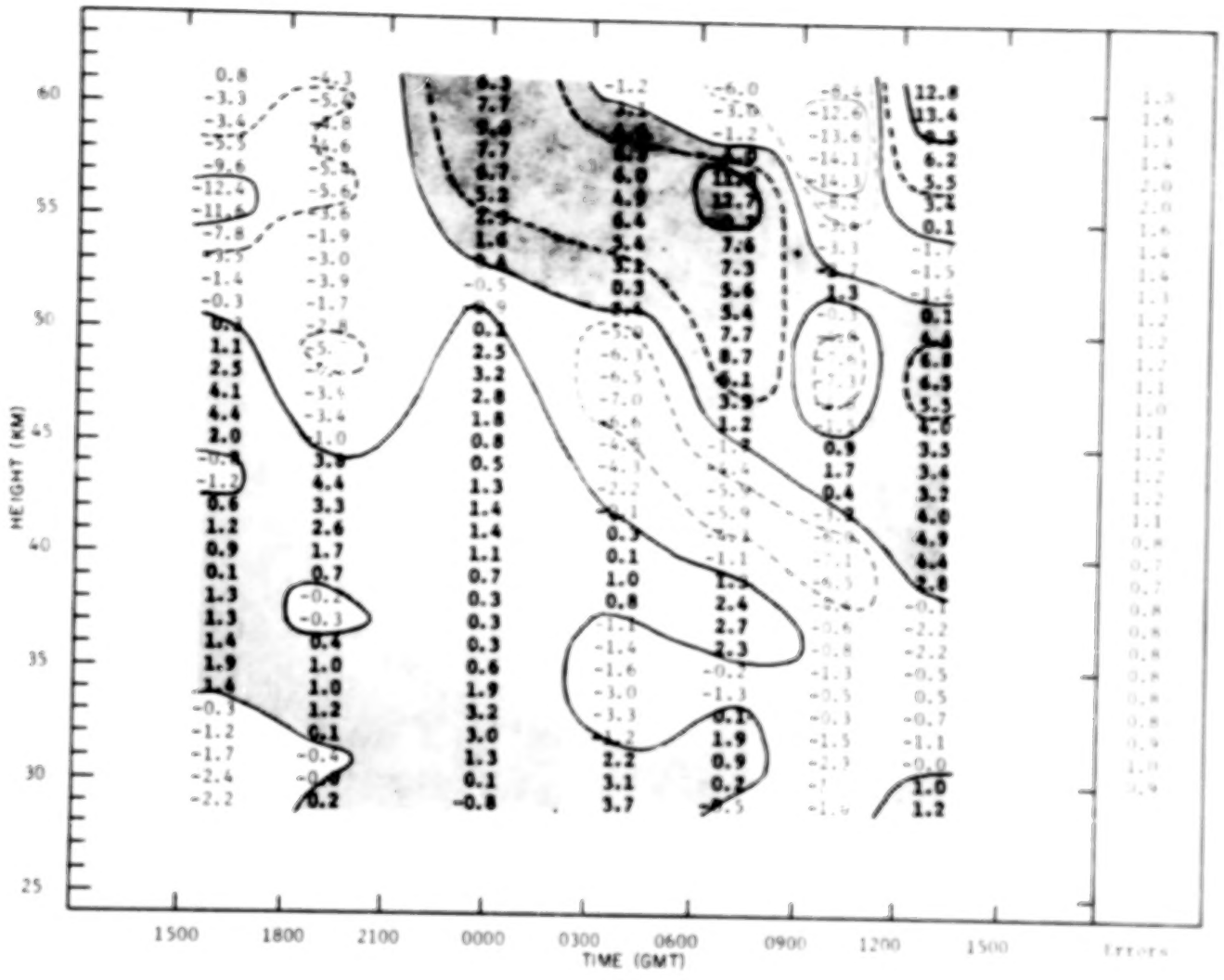

FIGURE 12A. Vertical velocities and error estimates for Kourou, 0000Z data left out, scheme A (cm/sec).

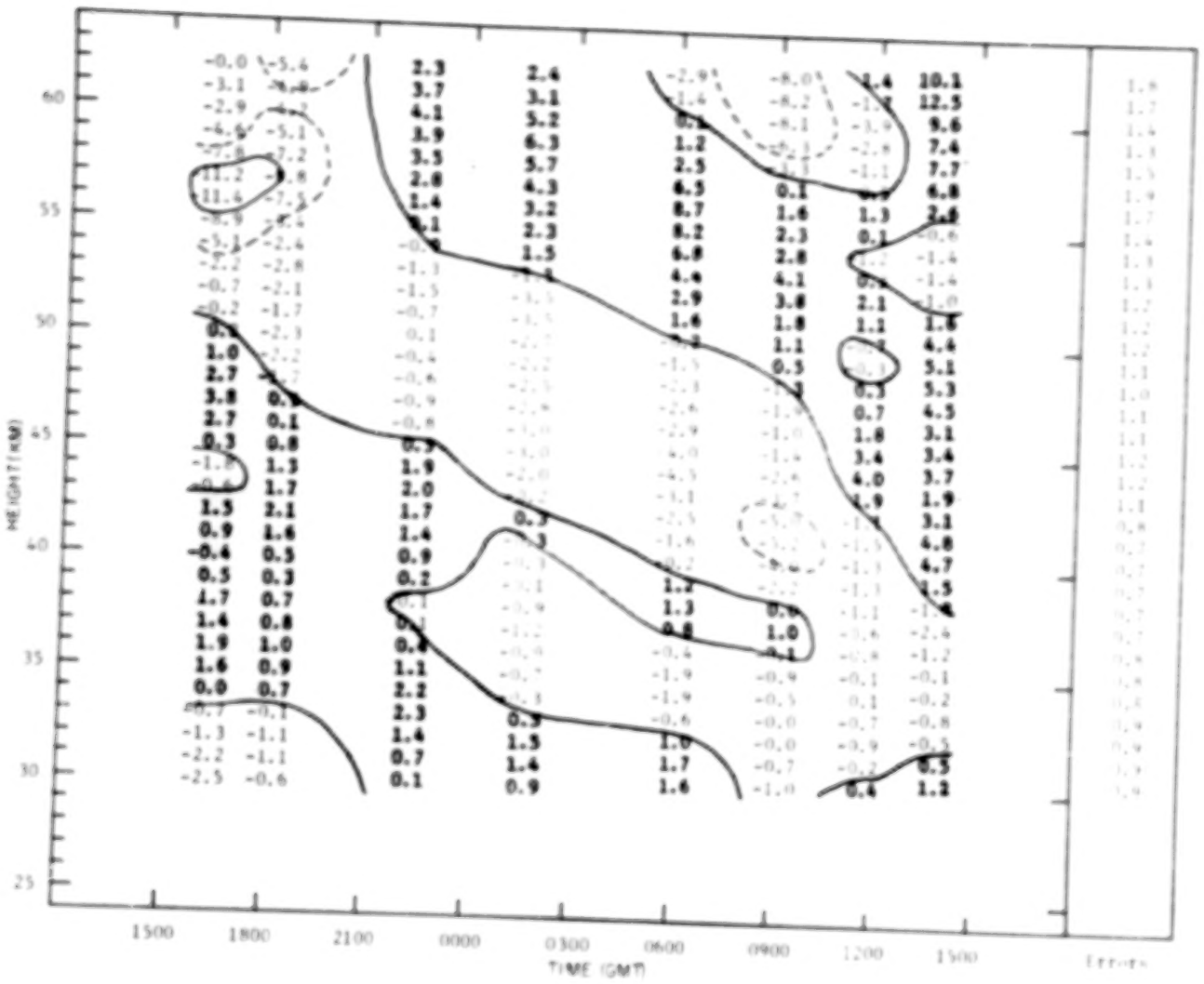

FIGURE 12B. Vertical velocities and error estimates for Kourou, 0000A data left out, scheme B (cm/sec).

magnitudes from this altitude range. However, it would also be useful to see how the calculated magnitudes vary with height. Considering this, the following approach has been taken.

The range of height at each station has been divided into three equal (~ 10 km) sections. Since the calculations generally run between 30 and 60 km, these divisions can be thought of as representing the mid-stratosphere (30-40 km), upper stratosphere (40-50 km), and lower mesosphere (50-60 km). To obtain a characteristic magnitude of the various terms for each of the three divisions, the absolute value of the terms were averaged over time and height for each 10 km layer. The results for scheme A and scheme B are presented in Tables 4 through 6. The terms have been designated as in equation (3.4) with the exception that the horizontal advection of temperature has been split into its geostrophic and ageostrophic parts.

$$(ADVT)_G \equiv \frac{fT}{g} (\underset{\sim}{V}_H \times \frac{\partial \underset{\sim}{V}_H}{\partial z}) \cdot \hat{k}$$

$$(ADVT)_{AG} \equiv \frac{T}{g} V_H \frac{\partial}{\partial z} \frac{\partial V_H}{\partial t} \qquad (4.2)$$

For consistency and ease of analysis, the terms in the numerator have been divided by the stability term. This puts all the terms into units of cm/sec as in equation (2.16A). In this procedure, the characteristic magnitudes from the upper stratosphere division will be the ones used for comparison with the scaling magnitudes.

First, it will be useful to check the scaling consistency criteria. Referring to Table 5, it appears as if the heirarchy of contributing terms is as suggested in the scaling arguments with DTDT being

TABLE 4A. Mean Magnitudes for Middle Stratosphere, Scheme A (cm/sec).

	DTDT	DIAB	$(ADVT)_{Ag}$	$(ADVT)_{g}$	W
Kourou	1.3	0.4	0.3	0.1	1.5
Ft. Sherman	0.7	0.5	0.7	0.2	1.2
Ascension	1.6	0.5	0.7	0.2	1.5
Natal	0.8	0.5	0..	0.1	0.8
Antigua	0.8	0.4	0.5	0.3	1.1
Average	1.0	0.5	0.5	0.2	1.2

TABLE 4B. Mean Magnitudes for Middle Stratosphere, Scheme B (cm/sec).

	DTDT	DIAB	$(ADVT)_{Ag}$	$(ADVT)_{g}$	W
Kourou	1.0	0.5	0.2	0.1	0.9
Ft. Sherman	0.6	0.5	0.6	0.1	0.7
Ascension	1.2	0.5	0.4	0.2	1.0
Natal	0.7	0.5	0.3	0.1	0.6
Antigua	0.7	0.5	0.3	0.3	0.8
Average	0.8	0.5	0.4	0.2	0.8

TABLE OF CONTENTS

TABLE 5A. Mean Magnitudes for Upper Stratosphere, Scheme A (cm/sec).

	DTDT	DIAB	$(ADVT)_{ag}$	$(ADVT)_{g}$	W
Kourou	2.8	0.8	0.4	0.1	3.6
Ft. Sherman	1.9	0.7	0.3	0.1	1.8
Ascension	2.2	0.7	0.7	0.2	2.4
Natal	1.3	0.7	0.4	0.1	1.8
Antigua	1.2	0.8	0.4	0.2	1.6
Average	1.9	0.7	0.4	0.1	2.2
Scaling	10.0	1.0	1.0	0.1	10.0

TABLE 5B. Mean Magnitudes for Upper Stratosphere, Scheme B (cm/sec).

	DTDT	DIAB	$(ADVT)_{ag}$	$(ADVT)_{g}$	W
Kourou	1.6	0.8	0.2	0.1	1.7
Ft. Sherman	1.4	0.7	0.2	0.1	1.7
Ascension	1.8	0.7	0.5	0.2	1.9
Natal	1.0	0.7	0.3	0.1	1.3
Antigua	0.9	0.8	0.2	0.2	1.1
Average	1.3	0.7	0.3	0.1	1.5
Scaling	10.0	1.0	1.0	0.1	10.0

TABLE 6A. Mean Magnitudes for Lower Mesosphere, Scheme A (cm/sec).

	DTDT	DIAB	$(ADVT)_{ag}$	$(ADVT)_{g}$	W
Kourou	5.0	1.1	0.8	0.2	5.7
Ft. Sherman	2.6	0.9	0.2	0.1	3.6
Ascension	3.7	1.0	1.6	0.4	5.1
Natal	2.9	1.0	1.0	1.0	4.2
Antigua	2.7	1.1	1.0	1.1	3.9
Average	3.4	1.0	0.9	0.6	4.5

TABLE 6B. Mean Magnitudes for Lower Mesosphere, Scheme B (cm/sec).

	DTDT	DIAB	$(ADVT)_{ag}$	$(ADVT)_{g}$	W
Kourou	3.7	1.0	0.7	0.2	4.5
Ft. Sherman	2.1	0.9	0.1	0.1	2.8
Ascension	2.4	1.0	1.0	0.4	2.9
Natal	2.0	1.0	0.6	0.2	2.5
Antigua	2.4	1.1	0.7	0.5	3.9
Average	2.5	1.0	0.4	0.3	3.3

the major contributor, but the calculated mean magnitudes appear to be smaller than those suggested by scaling. This can be explained somewhat by accounting for negative contributions among the various terms in the actual calculations, but not entirely. Another possibility is that the scaling values are wrong and upon reviewing the scaling arguments, one particular value becomes chief suspect, namely, the time scale. It was assumed in section 2.3 that a mean observable time scale would be 12 hours. If a 24 hour period had been used instead, the scaled magnitudes for DTDT, $(ADVT)_{Ag}$, and subsequently, w, all would be decreased by a factor of 2. This would now bring the scaled and calculated magnitudes all within the same range. This would suggest that a diurnal period wave is being depicted in the data as well as semidiurnal or shorter period waves. Indeed, this is what the cross sections seem to suggest. Thus, by using the larger time scale, the calculations and scaling arguments become internally consistent with each other.

For the lower mesosphere region (Table 6), one finds the same hierarchy of terms with DTDT clearly dominating the calculations. The magnitudes of all the terms are larger than for the upper stratosphere, but this is merely consistent with the theory of atmospheric waves which suggests that amplitudes should increase with height as $\rho^{-1/2}$, ρ being the density. In much the same way, the magnitudes of the terms for the middle stratosphere (Table 4) are found to be smaller than those for the upper stratosphere. Here again, the calculations are dominated by the DTDT term, but not by as great a margin as in the previous cases.

The apparent dominance of the calculations by the DTDT term suggests a shortcut in the vertical velocity calculations by neglecting all the terms in the numerator of equation (2.18) except for DTDT. To see how such a scheme would work, a test calculation was made for Kourou, the results of which are presented in figure 13A and 13B. A comparison with figures 7A and 7B demonstrates that while the magnitudes of the vertical velocities have changed slightly, the major features have remained well intact. This technique may thus prove to be quite useful in short time scale high altitude studies where wind measurements are inaccurate or missing entirely.

4.3 COMPARISON WITH ATMOSPHERIC WAVE THEORY

So far, the results have been demonstrated to be acceptable with respect to the numerical stability, error estimates, and internal consistency criteria. This, along with the continuous periodic features evident in the cross sections suggests that the derived vertical motions are real and are of the tidal or other internal gravity wave type. The goal of this section is to discuss these results in the context of atmospheric wave theory.

An often stated postulate of atmospheric wave theory is that the amplitude of an upward propagating gravity wave should increase with height as $\rho^{-1/2}$, ρ being the ambient density. This condition is necessary to ensure the conservation of kinetic energy. The first step in this analysis will be to test this relationship for the current results. For this purpose, a plot has been made of the maximum amplitude of the vertical velocity for the diurnal period versus height for each of the cross sections in figures 7A through 11A. The

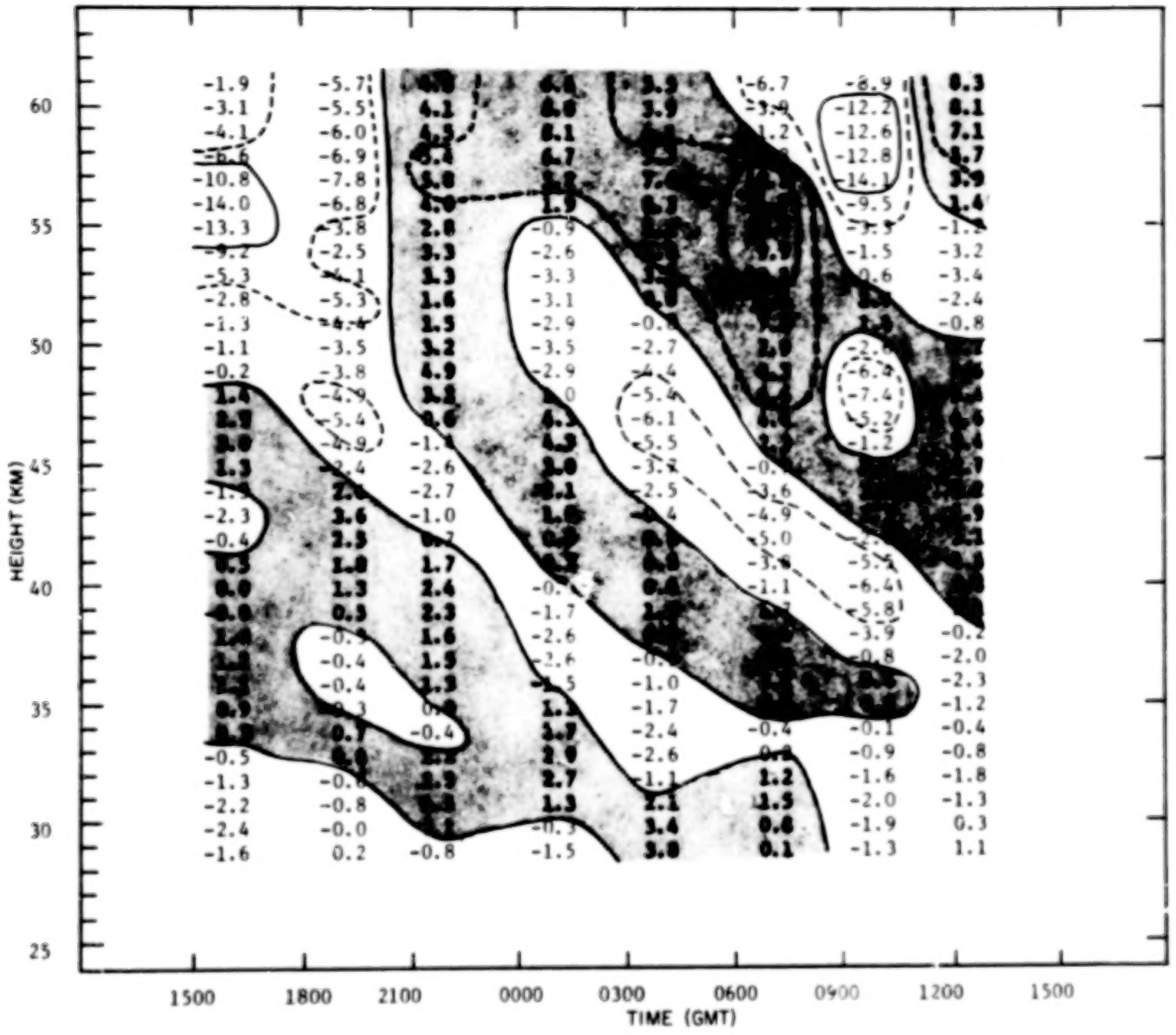

FIGURE 13A. Vertical velocities for Kourou as calculated with only local temperature change term, scheme A (cm/sec).

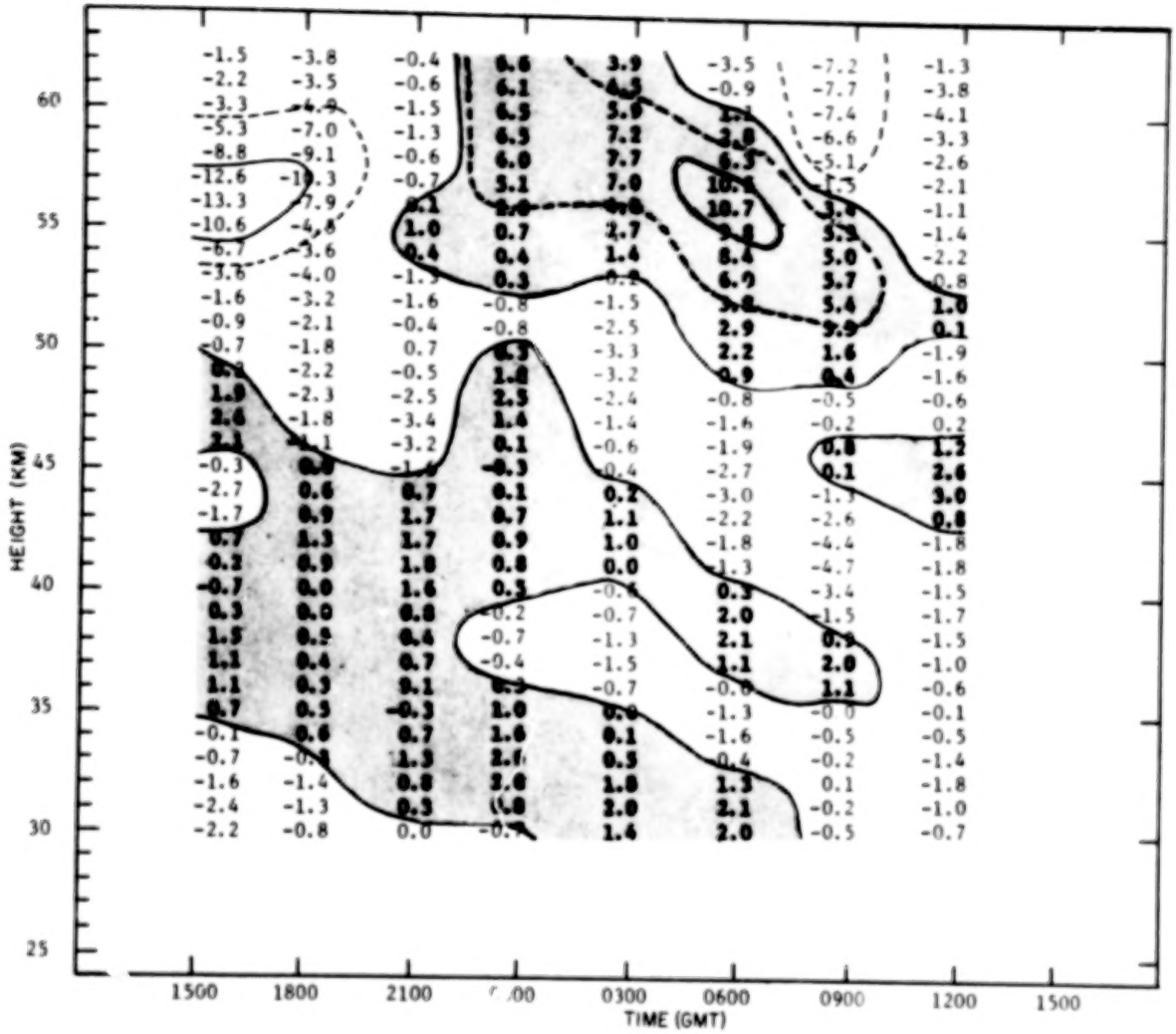

FIGURE 13B. Vertical velocities for Kourou as calculated with only local temperature change term, scheme B (cm/sec).

results for the Group I and Group II stations are shown in figures 14 and 15 respectively. Only the calculations from scheme A have been used to ensure that the maximum amount of information concerning the shorter period waves is included in the analysis. On each of the above figures a scaled plot of $\rho^{-1/2}$ has been included for easy reference (see Appendix D for details).

First, for figure 14, one will note that the amplitude variation with height of the derived vertical motions is similar for all three stations. The variation follows the $\rho^{-1/2}$ curve, but does so in a sinusoidal fashion. In figure 15, however, both Natal and Antigua display little amplitude variation below 45 km followed by a sharp increase in amplitude above this altitude. The net tendency, though, is to follow the $\rho^{-1/2}$ curve quite closely.

It thus appears as if the $\rho^{-1/2}$ condition is confirmed, at least in general, for all five stations in the study. But as with the cross sections, distinct differences appear between the Group I and Group II stations. These distinctions could be indicating that other types of motion are interacting significantly with what appear to be internal gravity waves or tidal motions. Before this conjecture is discussed further, it would prove useful to see to what extent the current results can be explained via tidal theory.

Unfortunately, any attempt to compare real data to tidal theory is at best a difficult task. One reason for this is the relatively early stage of the theoretical calculations. In order to obtain solutions to the tidal equations, many approximations must be made. Some of the more important ones are listed below:

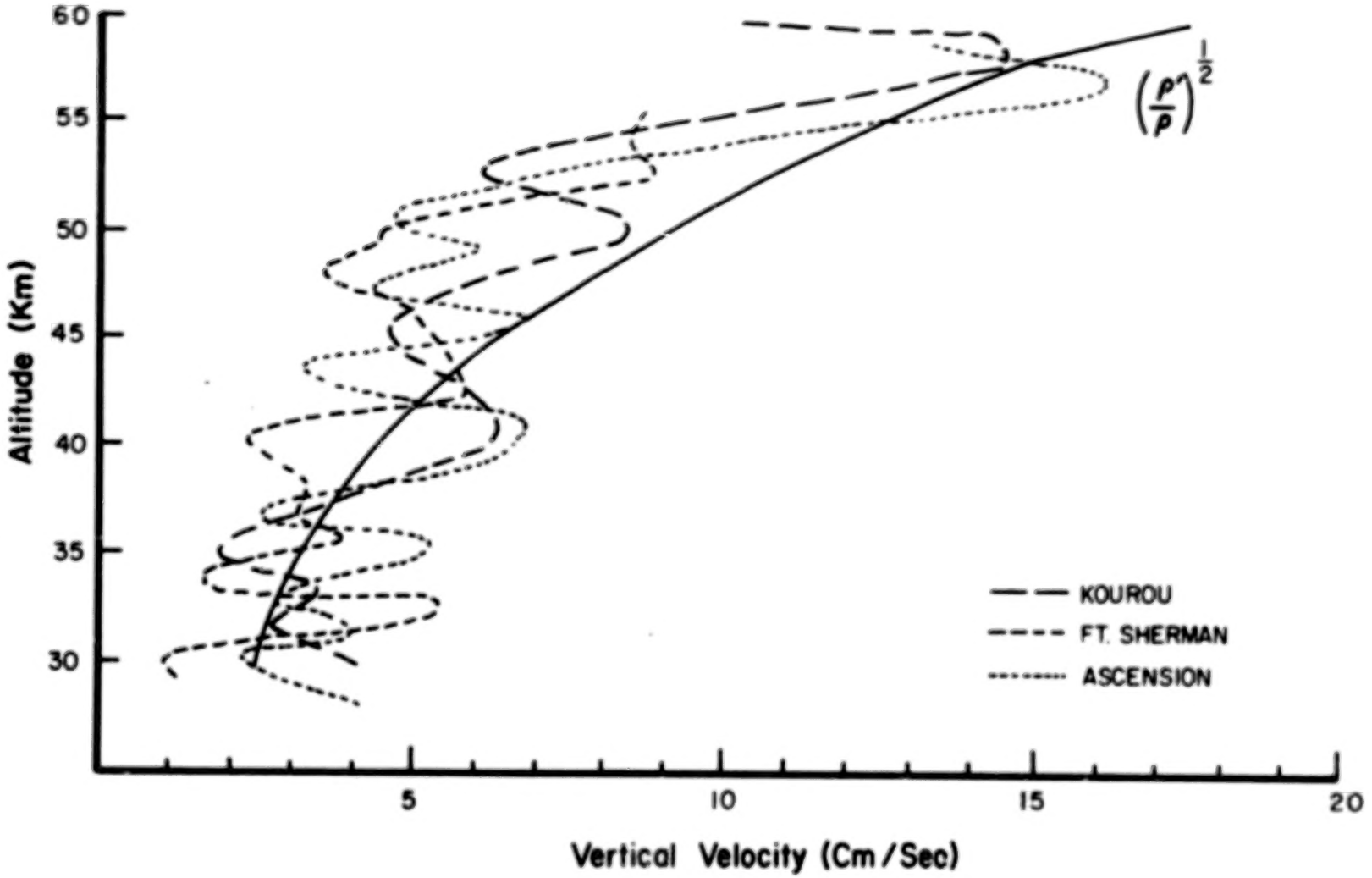

Figure 14. Maximum Magnitude of Vertical Velocity at Kourou, Ft. Sherman, and Ascension.

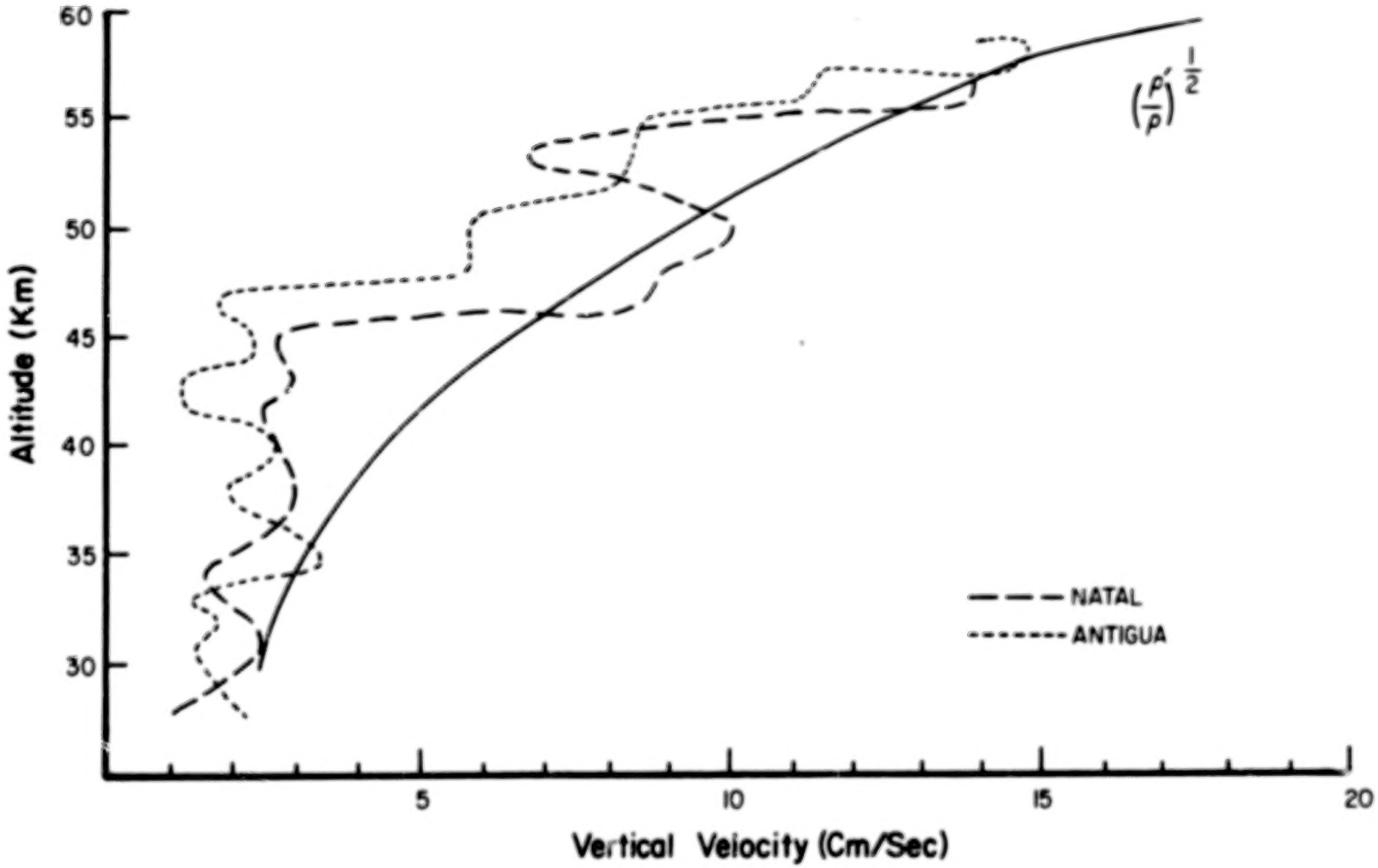

Figure 15. Maximum Magnitude of Vertical Velocity at Natal and Antigua.

1) The earth's surface topography is ignored.

2) Dissipative processes are ignored.

3) Any longitudinal dependence on the distribution of absorbing gases is ignored.

4) Tidal motions are considered to be linear perturbations on a basic state.

5) Horizontal temperature gradients are considered to be zero, implying that the mean flow is zero.

The last approximation has been relaxed recently for calculations of the semidiurnal tidal component by Lindzen and Hong (1974), but overall, the results from tidal theory apply to a highly idealized atmospheric state. For a fairly complete review of the theory, one should refer to the book, "Atmospheric Tides" by Chapman and Lindzen (1970).

Despite these limitations, many of the general features of the theory are found to match observations quite well. (See, for example, Groves (1975), Schmidlin (1976), Kao and Lordi (1977)). Good agreement is found with the amplitudes of the various components but a few differences still exist between the predicted and observed phases of some of the components.

To some extent, these differences can also be blamed on the deficient amounts and quality of atmospheric data sets available for studying tidal motions. Results from tidal theory are presented in terms of the various diurnal, semidiurnal, terdiurnal, and even smaller time period modes. Thus, in order to compare observations to the theory, the data must be decomposed into its diurnal, semidiurnal, etc., components. Through techniques of Fourier analysis, this can

be done with a good degree of accuracy for sufficiently large data sets. It is generally accepted that a sufficiently large data set should have at least 8 data points representing the particular mode being studied and should also include several complete periods of that particular mode. Upper atmospheric data sets which satisfy this criterion are virtually non-existent. Perhaps the best data set for studying upper atmospheric tides to date is the Diurnal Experiment, but even here, eight points make up the diurnal period, 4 points make up a semidiurnal period, and only one diurnal period makes up the entire sequence. One would therefore not normally consider even the present data set suitable for tidal analysis. However, since the Fourier analysis procedure is the best means at our disposal for comparing the derived vertical motions to tidal theory, this is the approach which will be taken. But considering the limitations of this procedure, the results must be analyzed in the context that tidal theory should be able to explain many but not necessarily all the features in the derived vertical motion field.

An additional requirement for use of the standard Fourier analysis routines is the necessity of having evenly spaced data points. For the Diurnal Experiment data, this condition is met only at Kourou and Ft. Sherman as the other three stations each have one calculation period missing. One could conceivably interpolate the vertical velocities for these time periods but it is felt that this would unduly add more possible errors on to an already heavily strained analysis. Thus, the procedure has been carried out only for Kourou and Ft. Sherman. Also, in order to get an even 8 points for the analysis, scheme B data

had to be used for Ft. Sherman while scheme A data could be used for Kourou.

The particular scheme used is described in Appendix E and includes a fast Fourier transform with mean removal. At this point, one would also want to remove any linear trends from the data but as shown in Appendix E, the identification of proper linear trends with this limited number of data points proves to be a difficult if not impossible task. Even though the results with and without linear trend removal were quite similar, it is felt that those without linear trend removal are the most believable. These are the results presented below.

First, referring to figure 16, one will note that the amplitude of the calculated diurnal component oscillates about the theoretical curve quite closely up to 50 km. Between 50 and 60 km, though, the calculated amplitudes are almost an order of magnitude larger than the theoretical values. Referring to figure 17, the calculated amplitudes of the semidiurnal component are found to be larger than the theoretical values by about an order of magnitude over the entire altitude range. Also, while theory suggests that the terdiurnal component should be smaller than the above two components, calculations for Kourou suggest that in many cases the terdiurnal component is as large as the above two components. These results are consistent with Kao and Lordi's (1977) calculations of the semi- and terdiurnal components of the horizontal winds and temperature. Thus, there seems to be some significant differences between the present results and theoretical predictions.

To shed some more light on this, the Fourier analysis technique has been used to derive some information concerning the vertical

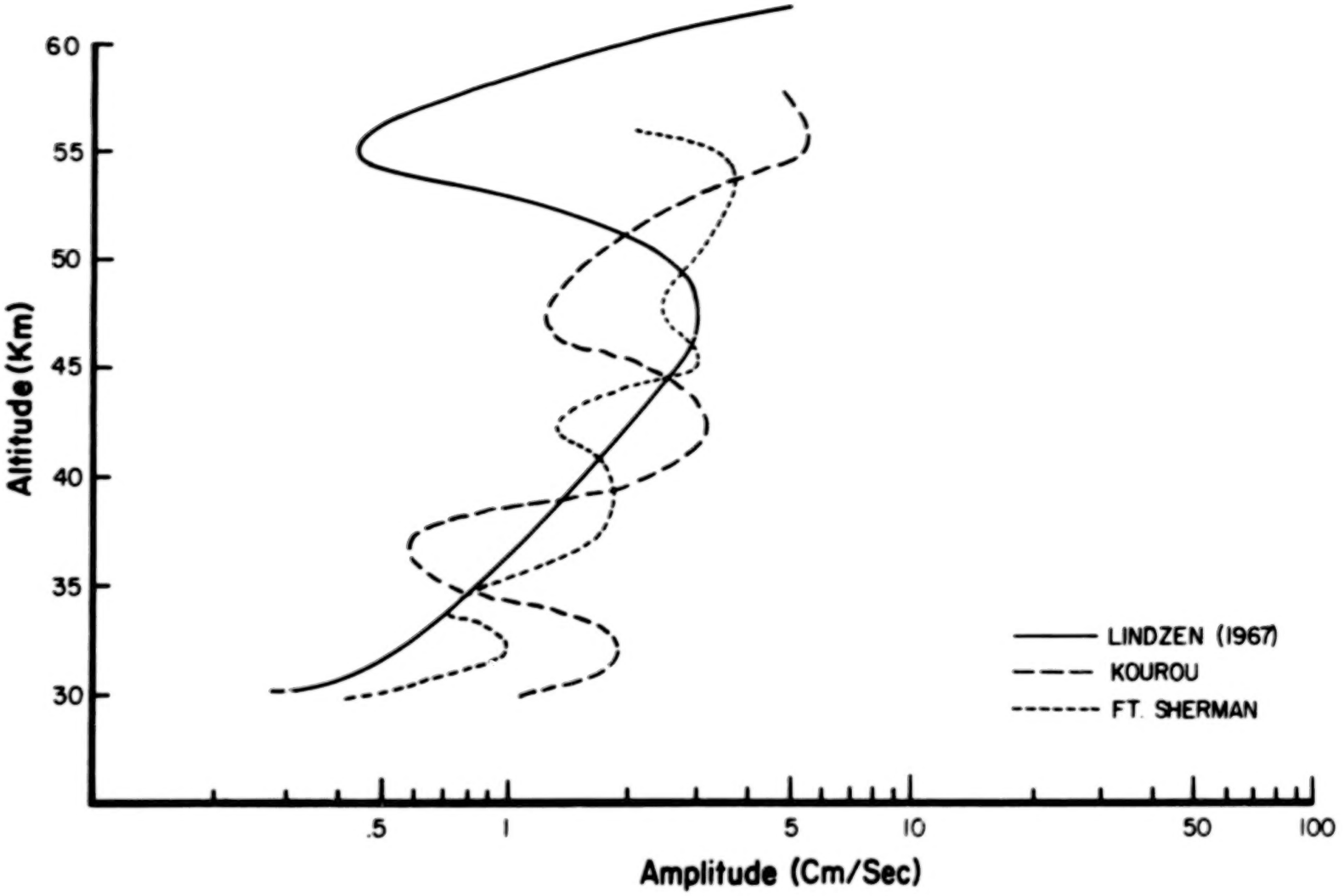

Figure 16. Amplitude of Diurnal Component of Vertical Velocity at Kourou and Ft. Sherman.

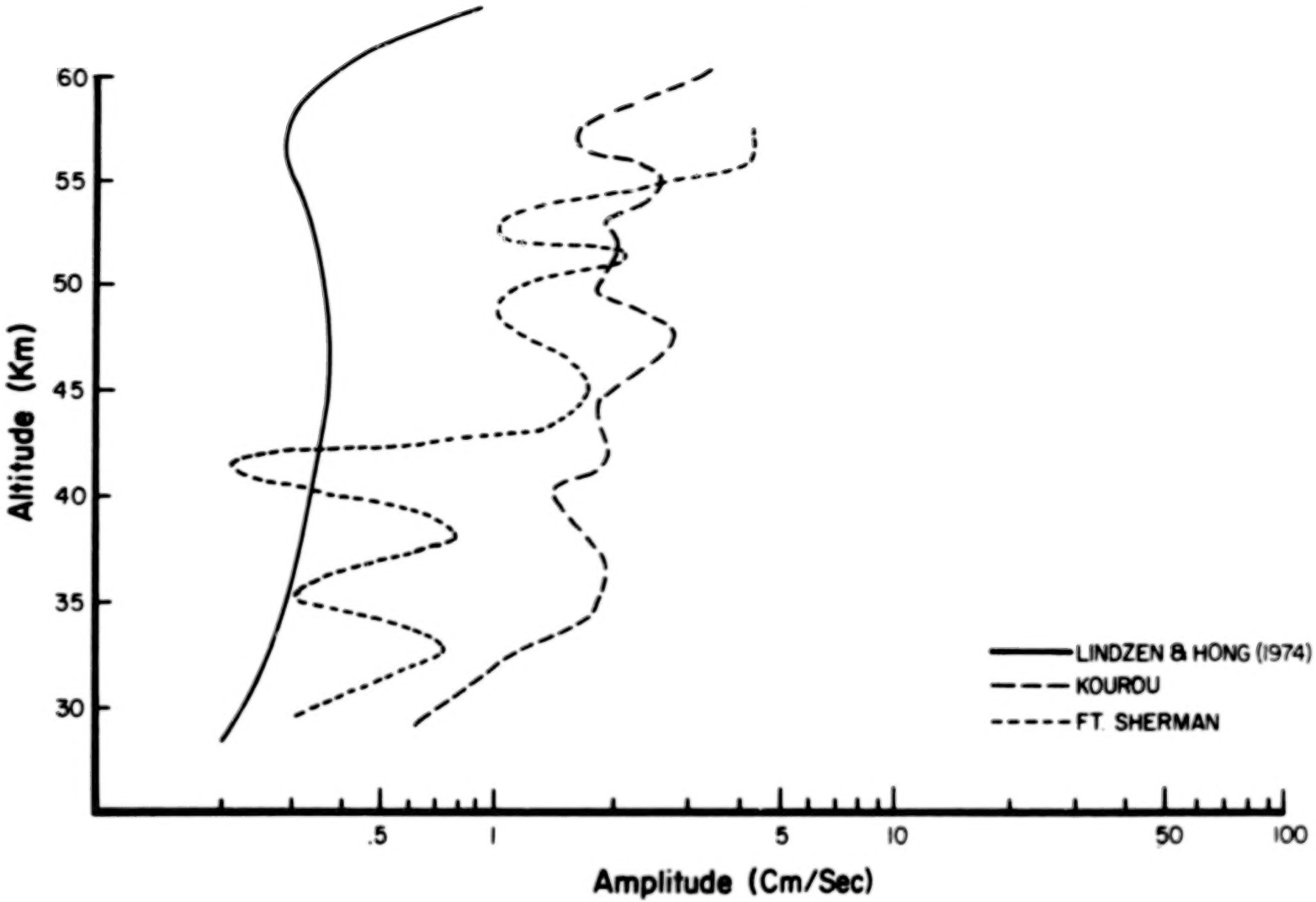

Figure 17. Amplitude of Semidiurnal Component of Vertical Velocity at Kourou and Ft. Sherman.

wavelengths of the observed wave features. With an average of 32 evenly spaced data points in height for each of the five stations, these results should be more numerically significant than the time analysis. The details of the calculation are given in Appendix E. The results, plotted as the spectral estimate vs. vertical wavelength are presented in figure 18. Again, the calculations have been made only for the scheme A results.

One will note that the majority of the spectral energy at each station appears within the 20-30 km vertical wavelength range. (The lines have been dashed on this portion of the curve to stress that only one spectral estimate covers the entire 16-32 km vertical wavelength range). The only exception to this tendency is the generally small magnitudes found at Ft. Sherman, but this is merely consistent with the overall smaller magnitudes depicted at this station in the cross sections. Theoretical results assign a vertical wavelength of 28 km to the dominant diurnal tidal component. The above results thus suggest that the derived vertical motion fields could be predominantly the result of the diurnal tide.

It is interesting to note that distinctions between the Group I and Group II stations again arise. For Group I, Ascension and Kourou both display relatively large spectral energies at the 16-32 km vertical wavelengths followed by a secondary maximum at 8 or 9 km. Ft. Sherman does not display as much energy at the higher vertical wavelengths but does display a similar maximum as Ascension at about 6 km. For Group II, not as much spectral energy is displayed at the higher vertical wavelengths and the energy generally decreases with decreasing wavelength without any apparent local maxima.

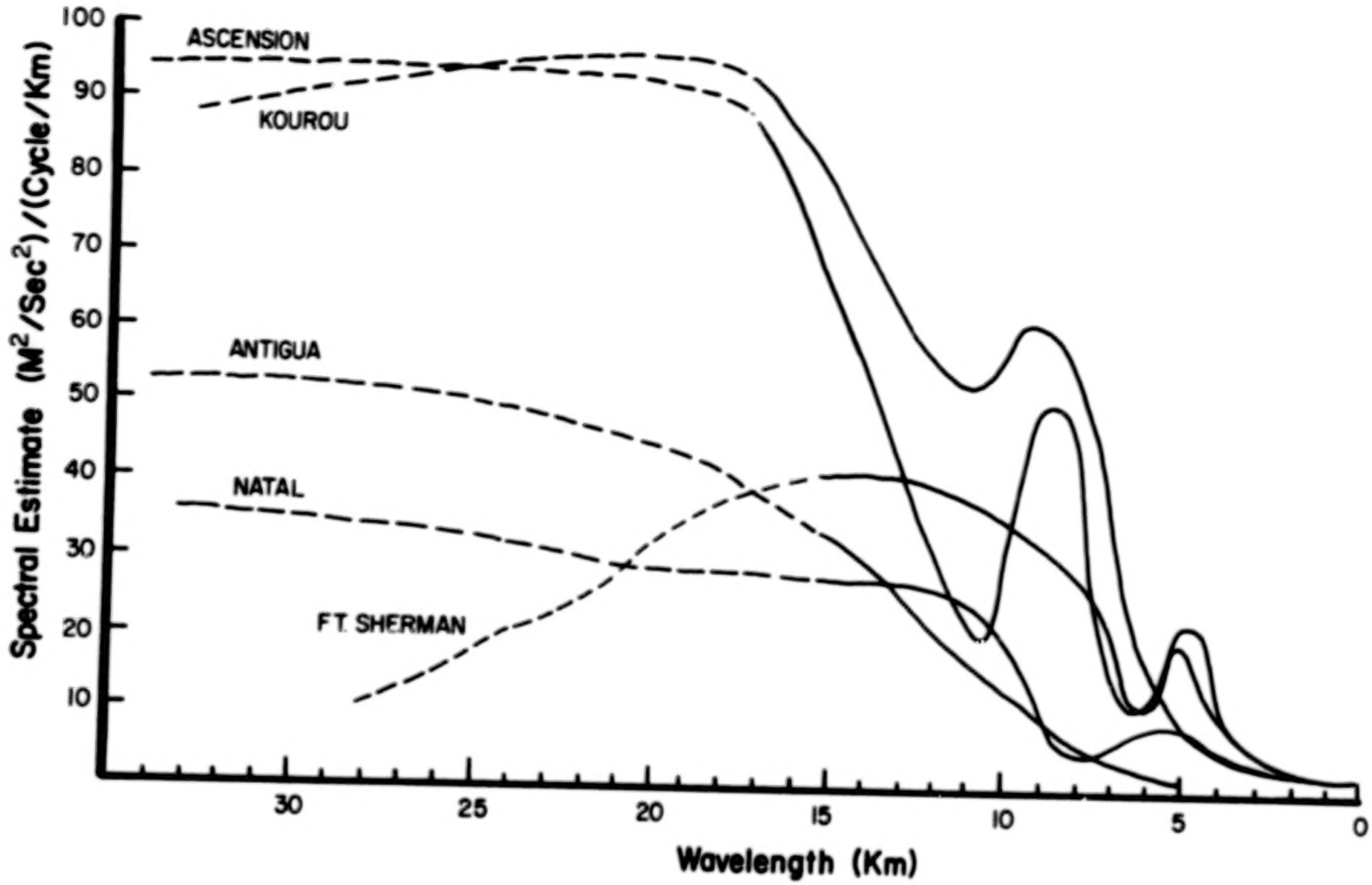

Figure 18. Spectral Estimates per Vertical Wavelengths.

One final form of analysis which could help delineate the types of motion being observed is to compare the observed phases of the dominant wave features to the phases predicted by tidal theory. This type of information can also be obtained through Fourier analysis techniques but would be quite unreliable with so few points with which to work. Upon careful inspection of the cross sections, however, one can subjectively pick out a dominant diurnal wave form and follow its phase progression with time. (In this case, phase has been defined to be the hour of maximum vertical velocity at a given height.) This has been done for the Group I stations (recall that the Group II stations were characterized by little or no phase progression with height) and the results, plotted versus local time, are presented in figure 19. Also included are the theoretical predictions of Lindzen (1967).

The phases at Kourou follow Lindzen's predictions quite closely. However, the phases for Ft. Sherman and Ascension, while similar to each other, differ from the theoretical predictions by up to 12 hours. Again, discrepancies arise between Lindzen's theoretical calculations and the present results for the Diurnal Experiment.

There are many possible explanations for the aforementioned discrepencies. One could attribute them to the induced errors involved in using a Fourier analysis scheme with such few data points. The expected effect of this type of error, however, would be a decrease rather than the observed enhancement of amplitudes for the smallest period motions. One could put the blame on the inadequacies of the present theoretical tidal calculations which are overburdened by approximations and similar shortcomings, but such an analysis is beyond

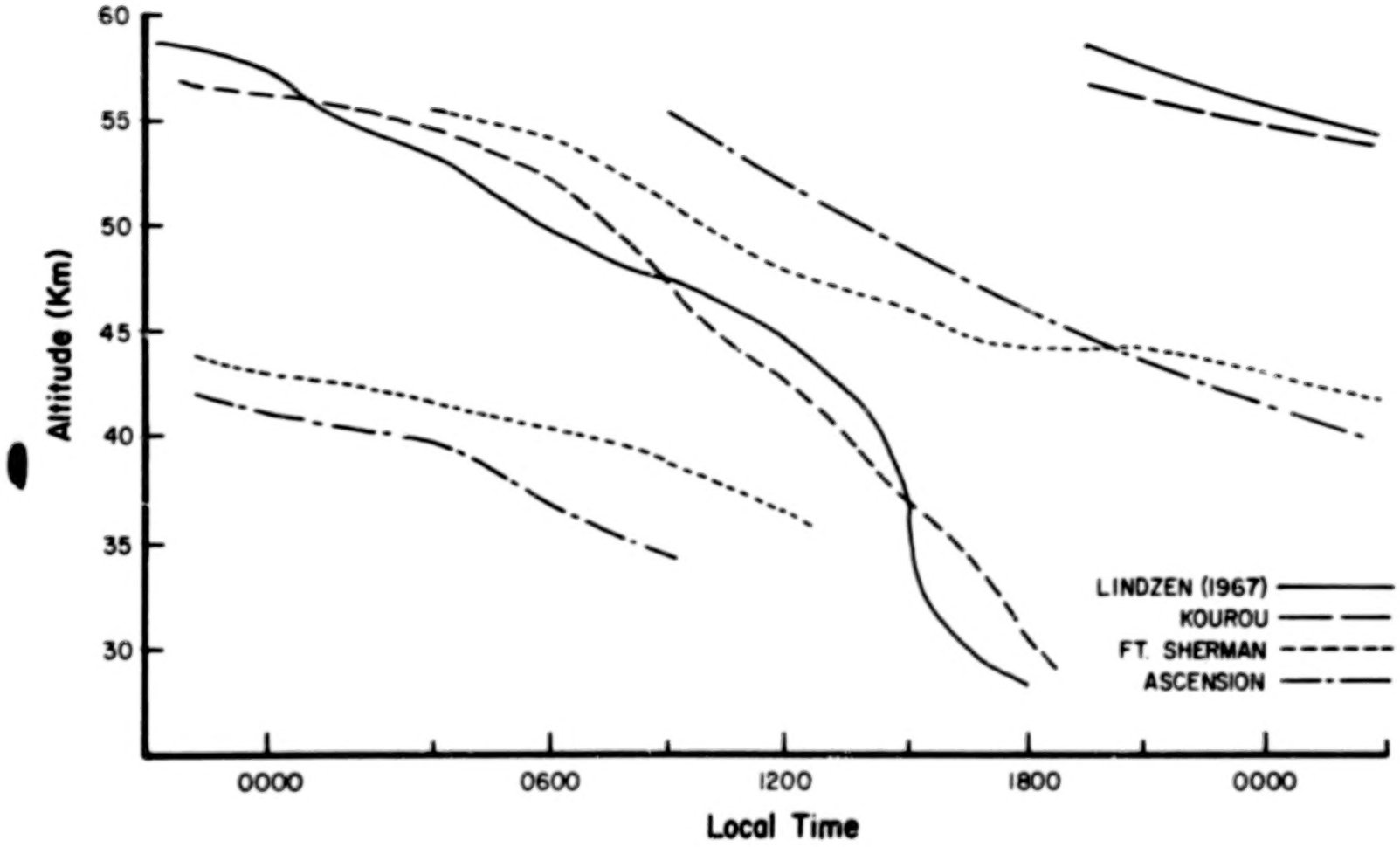

Figure 19. Phase (Hour of Maximum) of the Diurnal Component of Vertical Velocity at Kourou, Ft. Sherman, and Ascension.

the scope of this study. Another possibility would be that other types of motion are interacting significantly with the tidal fields to produce the apparent discrepencies. For example, internal gravity waves of periods less than 4 hours could be aliasing their energy back into the eight and twelve hour tidal components. Indeed, recent evidence supports the existence of such features in the middle and upper atmosphere. One must not forget the Group I - Group II designations which seemed to be present in almost every form of analysis. These effects could easily be attributed to larger time scale, perhaps synoptic scale motions.

At this point, it is felt that the evidence leans towards the hypothesis that types of motion other than just tidal contribute significantly to the day to day circulation of the equatorial middle atmosphere. Complete justification and clarification of this hypothesis, however, would require the analysis of a much more complete data set than is presently available. The next and final step in the thesis will thus be to review and summarize the progress which has been made in the vertical motion study and suggest how this information can be used in further studies of this region of the atmosphere.

5.0 SUMMARY, CONCLUSIONS AND RECOMMENDATIONS FOR FUTURE WORK

A single station technique for calculating vertical velocities in the equatorial middle atmosphere has been derived via the first law of thermodynamics and a generalized thermal wind relation (see Chapter 2). This equation has then been used to calculate vertical velocities using data supplied by the Diurnal Experiment of March 19, 20, 1974. The results have been analyzed to determine their numerical as well as physical significance by checking the following criteria:

1) Are the results significant with respect to error estimates?
2) Are the results numerically stable with respect to the calculation schemes used?
3) Are the results internally consistent with scaling arguments?
4) Does the derived vertical motion field show features which are continuous in time?
5) Do the features resemble internal gravity waves or tidal motions as suggested in the scaling arguments?
6) If so, do the wave forms confirm the $\rho^{-1/2}$ amplitude-height relationship?
7) How do the observed features compare to results from tidal theory?

By answering the above questions, the following conclusions have been drawn concerning the observed vertical motion field for the Diurnal Experiment and for vertical velocity calculations in equatorial regions in general:

1) Vertical velocities which are reasonable from both a numerical and physical point of view can be calculated for the equatorial middle atmosphere for time scales from 6 to 24 hours.

2) These vertical motions range in magnitude from 1 or 2 cm/sec near 30 km to as much as 15 cm/sec at 60 km.

3) The vertical motion field is generally periodic with characteristic periods including diurnal, semidiurnal, and even shorter time modes.

4) The apparent wave forms are characterized by a downward phase progression of 20-50 km/day and a $\rho^{-1/2}$ amplitude increase with height, suggesting that the motion is of the internal gravity wave type.

5) General features of the derived vertical motion field match results from tidal theory but particular features suggest that other internal gravity waves may be interacting significantly with the tidal fields.

6) It was found that the results for the five stations in the study could be classified into two distinct groups suggesting that even larger time scale motions, perhaps synoptic scale, could also be interacting significantly with the tidal fields.

These results suggest several implications for middle atmospheric research. First of all, the fact that short time period vertical motions can be derived from single station data sets suggests an alternate, more direct approach to the vertical transport problem than has previously been taken. Secondly, the relatively large magnitudes of the vertical motions derived, especially above 45 km, suggest that at least for time periods less than a day, they must be considered a significant part of the overall motion. This could especially effect radiative transfer type problems for now it appears as if short time scale temperature structure, at least in the equatorial middle

atmosphere, is predominantly a function of the vertical motion field. Finally, the discrepencies between the current results and tidal theory suggest that more research is needed to clarify the importance of other types of motion in this region such as internal gravity waves or synoptic type waves.

The only major drawback to the above results is that they can only be as good as the data from which they came. As has been pointed out several times, the current data set has many limitations associated with it, perhaps the biggest being its insufficient size. The lack of data points in time limits the use of Fourier analysis techniques while the lack of sufficient observing stations makes the identification of possible synoptic scale features nearly impossible.

Even with these limitations, though, there seems to be sufficient evidence to support the above conclusions, at least enough to warrant further study into all of these matters. A major recommendation of this thesis, then, is that additional data sets for equatorial regions preferably more extensive than the diurnal experiment be obtained so that the above results can be both confirmed and extended. Considering the limitations of Fourier analysis and other means of scale identification, it is felt that the following minimum specifications should be adhered to for such experiments. For the identification of diurnal and/or synoptic scale motions, observations should be taken at least every six hours (evenly spaced) for a period of eight days (32 observations). For the identification of semidiurnal scale motions, observations should be taken at least every three hours (evenly spaced) for a period of four days (32 observations).

Finally, the versatility of the present vertical velocity calculation and analysis technique offers a unique opportunity never before considered feasible, namely, the identification of the vertical motion field from equator to pole and from the surface to the thermosphere. Whether in helping to identify the important scales of motion or even vertical transport properties, such information would be an invaluable asset towards our eventual understanding of the coupling between the lower, middle, and upper atmosphere. Thus, an additional recommendation of this thesis is that observations as suggested above be extended to include as wide a range of latitudes and longitudes as possible.

APPENDIX A: APPROXIMATION OF $\frac{\partial}{\partial z}\left(-\frac{1}{\rho}\nabla_H p\right)$ TERM

To derive the expression,

$$\frac{\partial}{\partial z}\left(-\frac{1}{\rho}\nabla_H p\right) \simeq \frac{-g}{T}\nabla_H T \quad , \tag{A.1}$$

one must make use of the hydrostatic approximation,

$$\frac{\partial p}{\partial z} = -\rho g \quad , \tag{A.2}$$

and the equation of state in the following two differentiated forms:

$$\frac{1}{p}\nabla_H p = \frac{1}{\rho}\nabla_H \rho + \frac{1}{T}\nabla_H T \tag{A.3A}$$

$$\frac{1}{p}\frac{\partial p}{\partial z} = \frac{1}{\rho}\frac{\partial \rho}{\partial z} + \frac{1}{T}\frac{\partial T}{\partial z} \quad . \tag{A.3B}$$

First, one expands the left side of Eq. (A.1)

$$\frac{\partial}{\partial z}\left(-\frac{1}{\rho}\nabla_H p\right) = \frac{-1}{\rho}\nabla_H \frac{\partial p}{\partial z} + \frac{\nabla_H p}{\rho^2}\frac{\partial \rho}{\partial z} \quad . \tag{A.4}$$

Now, using Eq. (A.2), (A.3A), and (A.3B), Eq. (A.4) becomes

$$\frac{\partial}{\partial z}\left(\frac{-1}{\rho}\nabla_H p\right) = \frac{-g}{T}\nabla_H T - \frac{1}{\rho T}\frac{\partial T}{\partial z}\nabla_H p \quad . \tag{A.5}$$

The next step is to compare the magnitudes of the terms on the right. For this purpose, the following values have been chosen as being characteristic of the 30-40 km altitude range over the equatorial regions:

$|g| \sim 10 \text{ m/sec}^2$

$|\rho| \sim 8 \text{ gm/m}^3$

$\left|\frac{\partial T}{\partial z}\right| \sim 5° \text{ K}/10^3\text{m}$ (range from 0-10 °k/10^3m)

$|\nabla_H T| \sim 3° \text{ K}/10^6\text{m}$

$|\nabla_H p| \sim .05 \text{ mb}/10^6\text{m} = 5 \times 10^{-3} \text{ gm/m}^2 \text{ sec}^2$ (This term could be estimated even smaller).

By taking the ratio of the two terms on the right of Eq. (A.5), one finds:

$$\frac{\frac{1}{\rho T} \nabla_H p \frac{\partial T}{\partial z}}{\frac{g}{T} \nabla_H T} = \frac{|\nabla_H p| \left|\frac{\partial T}{\partial z}\right|}{|\rho||g||\nabla_H T|} \simeq \frac{(5 \times 10^{-3})(5 \times 10^{-3})}{(8)(10)(3 \times 10^{-6})} \simeq \frac{1}{10} \quad \text{(A.6)}$$

Thus, it seems reasonably safe to ignore the second term on the right of Eq. (A.5) leaving the following desired expression as in Eq. (A.1):

$$\frac{\partial}{\partial z}\left(-\frac{1}{\rho} \nabla_H p\right) \simeq \frac{-g}{T} \nabla_H T \quad . \qquad \text{(A.7)}$$

APPENDIX B: SCALING

In order to perform a scale analysis on a particular equation, one must be able to assign characteristic magnitudes to the various terms comprising the equation. For an arbitrary variable, ϕ, this can simply be done by choosing a characteristic magnitude from the given data set. To approximate the derivative of a variable, however, another approach is usually taken which considers the characteristic time and space scales of the motion being studied.

If the motion being studied is considered to be wavelike, one can expand the variable ϕ in the neighborhood of a point x^* as a function of wavelength, L:

$$\phi \simeq B \cos \left[\frac{2\pi}{L} (x - x^*)\right] , \tag{B.1}$$

where B represents the amplitude of the given wave. Taking the derivative of this expression, one obtains

$$\frac{\partial \phi}{\partial x} = \left[\frac{-2\pi}{L} B \sin \frac{2\pi}{L} (x - x^*)\right] . \tag{B.2}$$

If this derivative is approximated at a point halfway between the value of 0 and $\frac{-2\pi B}{L}$, the magnitude of the above expression becomes

$$\left|\frac{\partial \phi}{\partial x}\right| = \frac{2\pi}{L} B \frac{\sqrt{2}}{2} \simeq \frac{4B}{L} . \tag{B.3}$$

If the variable, x, represents a distance coordinate, then L represents a characteristic wavelength of the motion. If x represents a time coordinate, then L represents a characteristic time period of the motion. Again, B represents a characteristic amplitude of the waveform.

The representation in equation (B.3) has been used to scale the derivatives in equation (2.11). For the various derivatives, one obtains the following:

$$\left|\frac{\partial T}{\partial t}\right| \simeq \frac{|\Delta T|4}{\tau} \quad , \tag{B.4A}$$

$$\left|\frac{\partial V_H}{\partial z}\right| \simeq \frac{|\Delta V_3|4}{L_3} \quad , \tag{B.4B}$$

and

$$|\nabla_H V_H| \simeq \frac{|\Delta V_1|4}{L_1} \quad . \tag{B.4C}$$

τ, L_1, and L_3 represent respectively the time scales, horizontal length scale and vertical length scale previously defined. $|\Delta T|$, $|\Delta V_3|$, and $|\Delta V_1|$ represent the characteristic amplitudes of the particular variable in the derivatives. For this case, these values were assigned by taking characteristic values from time or space cross sections of each particular variable. Multiple derivatives are approximated by using the magnitude of one of the derivatives as the characteristic amplitude for the second derivative.

$$\frac{\partial}{\partial t}\frac{\partial V_H}{\partial z} \simeq \frac{\partial\left|\frac{\partial V_H}{\partial z}\right|}{\partial t} \simeq \frac{|\Delta V_3|16}{\tau L_3} \tag{B.4D}$$

$$\frac{\partial}{\partial z}\left[\underset{\sim}{V} \cdot \nabla_H V_H\right] \simeq \frac{V|\Delta V_1|16}{L_1 L_3} \qquad \text{(B.4E)}$$

APPENDIX C: ERROR ESTIMATES

An expression for estimating the errors in the vertical velocity calculations has been derived in section 3.3.

$$\delta w = \left[\frac{(\delta DTDT)^2 + (\delta ADVT)^2 + (\delta DIAB)^2}{(STAB)^2} + \frac{(\delta STAB)^2 (DTDT + ADVT + DIAB)^2}{(STAB)^4} \right]^{1/2} \qquad (C.1)$$

The goal of this appendix is now to assign the proper magnitudes to the various error terms in this expression, namely, δDTDT, δADVT, δDIAB, and δSTAB. For this purpose, use will be made of the $\pm$ 1°k and $\pm$ 3 m/sec accuracy estimates previously suggested for the measured temperature and winds.

This proves to be no problem for the non-composite terms such as δDTDT and δSTAB. Here, only one variable is involved in the error estimate. For δDTDT, the variable is the temperature difference as measured over a set time period, roughly 3 hours. Thus, a conservative estimate for δDTDT would be $\pm$ 1°k/3hours. For δSTAB, the uncertain variable is again temperature and its difference is measured over a set height interval, roughly 1 km. Thus, a conservative estimate for δSTAB would be $\pm$ 1°k/km. But in addition, the values of T were smoothed in height, an operation which tends to decrease random errors. Thus, a better estimate for δSTAB would be $\pm$ 0.5°k/km.

For composite terms such as δADVT, however, the process is not as simple for now one must consider cumulative affects. To see how to

approach this problem, consider the complete advection term.

$$ADVT = \frac{fT}{g}\left(\underset{\sim}{V}_H \times \frac{\partial \underset{\sim}{V}_H}{\partial z}\right) - \frac{T}{g} V_H \frac{\partial}{\partial z}\left(\frac{\partial \underset{\sim}{V}_H}{\partial t} - \underset{\sim}{V} \cdot \nabla V_H\right) \qquad (C.2)$$

The first term on the right may be rewritten as follows:

$$(ADVT)_1 = \frac{fT}{g} V_H \left|\frac{\partial \underset{\sim}{V}_H}{\partial z}\right| |\sin\theta| \qquad (C.3)$$

where θ is the angle between $\underset{\sim}{V}_H$ and $\frac{\partial \underset{\sim}{V}_H}{\partial z}$. Expanding this into an expression for relative error as in section 3.2, one obtains

$$\frac{\delta (ADVT)_1}{(ADVT)_1} = \frac{\delta T}{T} + \frac{\delta V_H}{V_H} + \frac{\delta\left|\frac{\partial \underset{\sim}{V}_H}{\partial z}\right|}{\left|\frac{\partial \underset{\sim}{V}_H}{\partial z}\right|} + \frac{\delta|\sin\theta|}{\sin\theta} \qquad (C.4)$$

This form suggests the use of a percentage error for the various terms. Physically, this would portray the situation where the magnitude of the error increases as the magnitude of the various terms increase. In fact, this is normally the case when calculating horizontal advection terms. The percentage error approach will thus be followed for the advection terms.

The accuracy estimate for wind measurements was given as $\pm$ 3 m/sec which is roughly 10% of the mean magnitude of the wind for this case. Using this value, a conservative estimate for δV_H and $\delta\left|\frac{\partial \underset{\sim}{V}_H}{\partial z}\right|$ would be (0.1) V_H and (0.1) $\frac{\partial \underset{\sim}{V}_H}{\partial z}$ respectively. One can again use $\pm$ 1°k for δT, but with a mean magnitude for T of 250°k, the percentage error becomes negligible. Finally, a 10% error estimate will be chosen for $\delta|\sin\theta|$.

Adding all of this up in equation (C.4), one obtains

$$\delta\ (\mathrm{ADVT})_1 \simeq 0.3\ (\mathrm{ADVT})_1 \qquad (C.5)$$

A similar estimate as above would be obtained for the second term on the right of equation (C.2). The third term on the right was neglected via scaling arguments as being an order of magnitude smaller than the other terms. Its contribution to the error should thus not exceed 10%. Considering all of the above estimates along with the fact that the individual errors may contribute negatively to each other, it is felt that 30% represents a reasonable estimate of the percentage error in the advection term.

Finally, one must assign a proper magnitude for δDIAB. This term has already been discussed in section 2.2 where it was suggested that the diabatic term should be accurate within 20%. Therefore, the value for δDIAB will be taken as 0.2 (DIAB).

All of the error terms in equation (C.1) have now been assigned. These values will be used to continue the discussion in section 3.2.

APPENDIX D: $\rho^{-1/2}$ CURVE

The goal of this Appendix is to construct a $\rho^{-1/2}$ density profile for inclusion in figures 14 and 15. Since such a curve is to be compared to the calculated magnitudes of w, one in essence must draw a $(\frac{\rho'}{\rho})^{1/2}$ curve where ρ' represents a scaling factor. The value of ρ' is assigned by using the magnitudes of w in figure 14 along with standard atmospheric values of ρ to solve the following expression:

$$(\frac{\rho'}{\rho})^{1/2} = w \qquad (D.1)$$

Three values of ρ' were calculated in this manner representing the 30, 40, and 50 km altitudes. The results are given below in Table 7.

TABLE 7: Values of ρ'

Height (km)	ρ (gm/cm^3)	w (cm/sec)	ρ' (gm/cm sec^2)
30	1.84×10^{-5}	3	16.57×10^{-5}
40	4.00×10^{-6}	5	9.9×10^{-5}
50	1.03×10^{-6}	6.5	4.34×10^{-5}

A characteristic value of ρ' was obtained by taking an average of the above three calculated values.

$$\bar{\rho}' = 10.30 \times 10^{-5} \qquad (D.2)$$

This value of ρ' is then used in equation (D.1) along with the standard atmospheric values of ρ to draw the hypothetical profile of w in

figure 14. The same value of ρ' is also used in the construction of the curve for figure 15.

APPENDIX E: FOURIER ANALYSIS

The results from tidal theory are presented in terms of the diurnal, semidiurnal, etc., components and associated vertical wavelengths which make up the tidal solutions. Thus, in order to compare the current results to tidal predictions, the derived vertical motions must also be decomposed into their diurnal, semidiurnal, etc., components and associated vertical wavelengths. This will be accomplished through the techniques of Fourier analysis as applied to discrete data sets (see, for example, Panofsky and Brier, 1968).

In essence, the discrete data points are assumed to represent a continuous periodic function. Thus function is then approximated by a least squares fit in terms of a series of sines and cosines. For a function of an arbitrary variable, x, the series may be written as

$$f(x) = \overline{f} + \sum_{i=1}^{N/2} \left(a_i \sin \frac{2\pi i x}{L} + b_i \cos \frac{2\pi i x}{L}\right) \qquad (E.1)$$

where $\overline{f}$ represents the mean value of the function, N represents the size of the data set, L represents the wavelength or period of the data set (depending on whether one is referring to a time or space series), and i represents the number of the harmonic. The coefficients a_i and b_i are given by the following relationships:

$$a_i = \frac{2}{N} \sum_{j=1}^{N} \left[f(x)_j \sin \frac{2\pi i x}{L}\right] \qquad (E.2)$$

$$b_i = \frac{2}{N} \sum_{j=1}^{N} \left[f(x)_j \cos \frac{2\pi i x}{L}\right] \quad . \qquad (E.3)$$

The amplitude of each harmonic, C_i, is then given as follows:

$$C_i = (a_i^2 + b_i^2)^{1/2} \quad . \tag{E.4}$$

The above information is also commonly represented in terms of the spectral energy per unit frequency interval, S_i (also referred to as the spectral estimate).

$$S_i = \frac{\frac{1}{2}(a_i^2 + b_i^2)}{\gamma} \quad , \tag{E.5}$$

where γ represents the unit frequency interval.

The particular computer routine which has been used for this analysis is the subroutine Fourt for the fast Fourier transform. The only major restriction to using this routine is that the data points must be evenly spaced. For the derived time series of vertical motions, this requirement is met only for Kourou and Ft. Sherman. Thus, time series analysis is limited to these two stations. For the derived height series of vertical motions, this requirement is met at all five stations comprising the study.

For the present case of 8 data points in time (N = 8), the above technique produces a maximum of 4 harmonics representing the diurnal (24 hour), semidiurnal (12 hour), terdiurnal (8 hour), and quadiurnal (6 hour) contributions to the vertical motion field. The amplitudes of the diurnal and semidiurnal components (C_1 and C_2) for Kourou and Ft. Sherman have been plotted versus height in figures 16 and 17.

For the present case of 32 data points in height (N = 32), the above technique produces 16 harmonics representing the variation of

vertical motion with height. The spectral energy per unit frequency interval for each of the 16 harmonics, S_i, is plotted versus vertical wavelength in figure 18 for each of the five stations comprising the present study. The spectral energies plotted represent averages over time for each individual station.

In using the above technique, the assumption is informally made that the discrete number of data points can be represented fully in terms of the N/2 harmonics. Unfortunately, in real life, this is not the case. Harmonics of number greater than N/2, whether noise or real signal, could be aliasing their energy back into the lower harmonics while harmonics too large to be defined by the data set could appear as trends in the data. If one is interested specifically in the N/2 harmonics identified in the Fourier analysis (as is the case when comparing the current results to tidal predictions), then both of these possible effects should be accounted for.

First considering the aliasing, this potential problem can be alleviated somewhat by smoothing the data. For the height series, the data has been smoothed over 2 km with a 1-2-1 filter. As discussed in section 3.1, however, smoothing of the time series is not a feasible option considering its small size. Thus, aliasing must be considered to be a potential contaminant to the time series results.

The problem of having trends in the data can be alleviated by removing the trends via regression techniques. For the height series of vertical velocities, a trend is quite evident and in fact approaches the expected $\rho^{-1/2}$ amplitude increase with height relationship. As a first approximation to removing this trend, a linear trend has been

removed from the vertical motions. The decomposition presented in figure 18 represent those results with the linear trend removed.

For the time series of vertical velocities, one must again deal with the small size of the data set. With only 8 points making up the diurnal period, an error of only one or two hours in the positioning of the end points of this series could produce significant apparent trends which would not be there if the data series were without these errors. Inspection of the derived vertical velocity series showed that this was indeed the case, with linear trends appearing due to the incomplete size of the series. Thus, it was felt advisable not to remove trends from the time series data. This decision is enhanced also by the fact that the larger time scale features for the equatorial middle atmosphere which could possibly affect 24 hour or less time periods (Kelvin waves, Rossby-gravity waves) have theoretical amplitudes at least an order of magnitude smaller than the derived vertical motions for the present study (see Holton, 1975). It is felt that such amplitudes could not possibly influence the present analysis. As a final check of this decision, a comparison was made between the results with and without the linear trend removal. The only differences found could be explained satisfactorily as being within the uncertainty of the analysis. Thus, the entire question of removing the linear trend from the vertical motion time series becomes merely one of academic interest for the present study and of no practical consequence.

REFERENCES

Chapman, Sydney, and R. S. Lindzen, 1970: Atmospheric Tides, Thermal and Gravitational. D. Reidel Publishing Co., Dordrecht, Holland, 200 pp.

Craig, Richard A., and M. A. Lateef, 1962: Vertical motion during the 1957 stratospheric warming. J. Geophys. Res., 67, 1839-1854.

Dutton, J. A., 1976: The Ceaseless Wind, An Introduction to the Theory of Atmospheric Motion. McGraw-Hill, Inc., 579 pp.

Forsythe, G. E., 1945: A generalization of the thermal wind equation to arbitrary horizontal flow. Bull. Amer. Meteor. Soc., 26, 371-375.

Groves, G. V., 1975: Diurnal and semidiurnal oscillations of the upper atmosphere derived from grenade experiments at Natal, Brazil. J. Atmos. Terr. Phys., 37, 1133-1138.

Holton, James R., 1975: The dynamic meteorology of the stratosphere and mesosphere. Meteorological Monographs, American Meteorological Society, Boston, 15, 216 pp.

Kao, S. K., and N. J. Lordi, 1977: Characteristics of the Motions, Turbulence Intensity, Diffusivity, Flux of Momentum and Sensible Heat in the Upper Atmosphere. Contractor Report, NASA CR-2782, National Aeronautics and Space Administration, Washington, D.C., 56 pp.

Kays, Marvin D., and Richard A. Craig, 1965: On the order of magnitude of large-scale vertical motions in the upper stratosphere. J. Geophys. Res., 70, 4453-4461.

Lindzen, R. S., 1967: Thermally driven diurnal tide in the atmosphere. Quart. J. Roy. Meteor. Soc., 93, 18-42.

Lindzen, R. S., and Siu-Shung Hong, 1974: Effects of mean winds and horizontal temperature gradients on solar and lunar semidiurnal tides in the atmosphere. J. Atmos. Sci., 31, 1421-1446.

Miller, Alvin J., 1970: A note on vertical motion analysis for the upper stratosphere. Mon. Wea. Rev., 98, 616-620.

Murgatroyd, R. J., and R. M. Goody, 1958: Sources and sinks of radiative energy from 30 to 90 km. Quart. J. Roy. Meteor. Soc., 84, 225-234.

Panofsky, H. A., 1946: Methods of computing vertical motion in the atmosphere. J. Meteor., 3, 45-49.

Panofsky, Hans A., and Glen W. Brier, 1968: Some Applications of Statistics to Meteorology. Earth and Mineral Sciences Continuing Education, College of Earth and Mineral Sciences, The Pennsylvania State University, University Park, Pennsylvania, 224 pp.

Quiroz, Roderick S., 1969: The warming of the upper stratosphere in February 1966 and the associated structure of the mesosphere. Mon. Wea. Rev., 97, 541-552.

Schmidlin, F. J., 1976: Diurnal Tidal Analysis in the Equatorial Stratosphere and Mesosphere. Paper presented at nineteenth meeting of COSPAR, Philadelphia.

Schmidlin, F. J., Y. Yamasaki, A. Motta, and S. Brynsztein, 1975: Diurnal Experiment Data Report, March 19-20, 1974. NASA SP-3095, National Aeronautics and Space Administration, Washington, D.C., 150 pp.

Staff, Upper Air Branch, National Weather Service, 1976: Synoptic Analysis, 5, 2, and 0.4 mb Surfaces for July 1973 Through June 1974. NASA SP-3102, Joint NASA-NOAA Publication, National Aeronautics and Space Administration, Washington, D.C., 140 pp.

The following references were also found to be quite useful, but were not specifically noted in the text.

Dopplick, T. G., 1971: The energetics of the lower stratosphere including radiative effects. Quart. J. Roy. Meteor. Soc., 97, 209-237.

Groves, G. V., 1976: Review lecture, rocket studies of atmospheric tides. Proc. R. Soc. Lond. A., 351, 437-469.

Kreitzberg, Carl W., 1964: The Structure of Occlusions as Determined From Serial Ascents and Vertically Directed Radar. AFCRL-64-26, Meteorology Laboratory Project 8641, Air Force Cambridge Research Laboratories, Office of Aerospace Research, U. S. Air Force, 121 pp.

Miller, Alvin J., 1967: Note on vertical motion in the lower stratosphere. Beiträge Zur Physik der Atmosphäre, 40, 29-48.

Nastrom, G. D., and A. D. Belmont, 1976: Diurnal stratospheric tide in meridional wind, 30 to 60 km, by season. J. Atmos. Sci., 33, 315-320.

1. Report No.	2. Government Accession No.	3. Recipient's Catalog No.
NASA CR-3096		

4. Title and Subtitle	5. Report Date
Vertical Motions in the Equatorial Middle Atmosphere	April 1979
	6. Performing Organization Code

7. Author(s)	8. Performing Organization Report No.
Morris Larry Weisman	
	10. Work Unit No.

9. Performing Organization Name and Address	11. Contract or Grant No.
The Pennsylvania State University Department of Meteorology University Park, PA 16802	NAS6-2726
	13. Type of Report and Period Covered
12. Sponsoring Agency Name and Address	Final Report
National Aeronautics and Space Administration Wallops Flight Center Wallops Island, VA 23337	14. Sponsoring Agency Code

15. Supplementary Notes

16. Abstract

The stratospheric and mesospheric diurnal experiment of March 19, 20, 1974 offers a unique opportunity to calculate and study small time scale vertical motions in the equatorial middle atmosphere. Since, however, the constraints of working in this region (data sparsity, lack of geostrophy, etc.) do not permit the use of standard vertical velocity calculation and analysis techniques, alternate techniques must be developed. As such, a single station vertical velocity equation which considers ageostrophic and diabatic effects is derived from the first law of thermodynamics and a generalized thermal wind relation. In addition, an analysis and verification procedure is developed which accounts for measurement and calculation errors as well as time and space continuity arguments and theoretical predictions.

This scheme is used to calculate vertical velocities at every kilometer between 25 and 60 km and for approximately every three hours for the above diurnal period at Kourou (French Guiana), Fort Sherman (Panama Canal Zone), Ascension Island, Antigua (British West Indies) and Natal (Brazil). The results, plotted as time series cross sections, suggest vertical motions ranging in magnitude from 1 or 2 cm/sec at 30 km to as much as 15 cm/sec at 60 km. The patterns depicted in the cross sections suggest the existence of internal gravity type waves in the motion field with diurnal, semidiurnal, and terdiurnal periods and vertical wavelengths between 10 and 30 km. There is also evidence of a 20-50 km/day downward phase progression and a $(\text{density})^{-1/2}$ amplitude increase with height relationship as is often suggested for such motions.

It is found that many of the general features of the results agree well with atmospheric tidal predictions (Lindzen, 1967, Lindzen and Hong, 1974) but many particular features suggest that both smaller time scale gravity waves (periods < 6 hours) and synoptic type waves (periods > 1 day) may be interacting significantly with the tidal fields. This suggests that more research is needed to help delineate the types and scales of motion which make up this region of the atmosphere.

Overall, the results suggest that vertical motions can be calculated for the equatorial middle atmosphere and must be considered a significant part of the motion for time scales from 8 to 24 hours.

17. Key Words (Suggested by Author(s))	18. Distribution Statement
Sounding Rockets Atmospheric Tides Meteorology Wind (Meteorology) Vertical Motion Stratosphere Tidal Oscillation	Unclassified - Unlimited STAR Category 47

19. Security Classif. (of this report)	20. Security Classif. (of this page)	21. No. of Pages	22. Price*
Unclassified	Unclassified	111	$6.50

*For sale by the National Technical Information Service, Springfield, Virginia 22151

NASA-Langley, 1979

END

June 12, 1981